

ISTANBUL TECHNICAL UNIVERSITY ★ GRADUATE SCHOOL OF SCIENCE
ENGINEERING AND TECHNOLOGY

**EXPERIMENTAL INVESTIGATION OF THE EFFECTS OF A CYLINDER
HEAD POST-VALVE GEOMETRY ON IN-FLOWING SWIRL MOTION IN A
FOUR-CYLINDER DIESEL ENGINE**

M.Sc. THESIS

Mihantarivelo Tahiry RABETY

Department of Mechanical Engineering

Automotive Engineering Programme

MAY 2014

ISTANBUL TECHNICAL UNIVERSITY ★ GRADUATE SCHOOL OF SCIENCE
ENGINEERING AND TECHNOLOGY

**EXPERIMENTAL INVESTIGATION OF THE EFFECTS OF A CYLINDER
HEAD POST-VALVE GEOMETRY ON IN-FLOWING SWIRL MOTION IN A
FOUR-CYLINDER DIESEL ENGINE**

M.Sc. THESIS

Mihantarivelo Tahiry RABETY
(503101723)

Department of Mechanical Engineering

Automotive Engineering Programme

Thesis Advisor: Prof. Dr. Cem SORUŞBAY

MAY 2014

İSTANBUL TEKNİK ÜNİVERSİTESİ ★ FEN BİLİMLERİ ENSTİTÜSÜ

**DÖRT SİLİNDİRLİ DİZEL MOTOR KAFASI SUPAP SONRASI
GEOMETRİSİNİN EMME HAVASI ÇEVRE HAREKETİ ÜZERİNDEKİ
ETKİSİNİN DENEYSEL OLARAK İNCELENMESİ**

YÜKSEK LİSANS TEZİ

**Mihantarivelo Tahiry RABETY
(503101723)**

Makina Mühendisliği Anabilim Dalı

Otomotiv Mühendisliği Programı

Tez Danışmanı: Prof. Dr. Cem SORUŞBAY

MAYIS 2014

Mihantarivelo Tahiry RABETY, a M.Sc. student of ITU Graduate School of Science Engineering and Technology student ID 503101723, successfully defended the thesis entitled “EXPERIMENTAL INVESTIGATION OF THE EFFECTS OF A CLINDER HEAD POST-VALVE GEOMETRY ON IN-FLOWING SWIRL MOTION IN A FOUR-CYLINDER DIESEL ENGINE”, which he/she prepared after fulfilling the requirements specified in the associated legislations, before the jury whose signatures are below.

Thesis Advisor : **Prof. Dr. Cem SORUŞBAY**

İstanbul Technical University

Jury Members : **Prof. Dr. İlyas Bedii ÖZDEMİR**

İstanbul Technical University

Doç. Dr. Muammer ÖZKAN

Yıldız Technical University

Date of Submission : 22 April 2014

Date of Defense : 28 May 2014

To my spouse and children,

“Ataovy tsara ny anionao mba tsy handatsa anao ny ampitso”...

FOREWORD

I have come across so many valuable people throughout this research, who have been of great help to me, and without whom my discovery of the world of research would not have been the same. Two pages dedicated to those people are very few compared to the support they have brought. I apologize for the length, but it seems essential for me to underline the importance of being well surrounded.

“True teachers are those who use themselves as bridges over which they invite their students to cross; then, having facilitated their crossing, joyfully collapse, encouraging them to create their own.” – Nikos Kazantzakis.

I would like to express my gratitude to Prof. Dr. Cem SORUSBAY for accepting to coach me through this journey and also for his encouraging assistance during the whole phases of the research. I would also like to thank all of the academic staff of Istanbul Technical University especially those of the faculty of Mechanical Engineering for sharing their knowledge and also bringing their valuable guidance and support to me.

“Coming together is a beginning; keeping together is progress; working together is success.” – Henry Ford.

I want to borrow the citation of the well-known icon in the automotive engineering sector Henry Ford to extend my appreciations to the Research & Development Section at one of the leading automotive company Ford Otomotiv Sanayi A.Ş. for entrusting me with this research. Furthermore, I would like to give a special acknowledgement to Ford Otosan’s Base Engine Casting team leader Demirhan MANAV along with the Mechanical Engineers Korkut KARAGOZ and Deniz Can UNAL for their precious moral and also material contributions.

“It's not because things are difficult that we don't dare; it's because we don't dare that things are difficult.” – Seneca.

I want to express my deep thankfulness especially my beloved wife Mialitiana Angela and our children starting with our dearest firstborn son Manantsoa Eren who have most gone through the hazards of my research works. I do not forget the RABETY and RASOLONJATOVO families too, for continuously encouraging me to keep progressing despite all kind of contradictions I have encountered and then allowing me to shift paradigms for the sake of academic research. I appreciate their kindness and interest on giving a part of their time so that I continuously felt their presence and support.

“Every now and then go away, have a little relaxation, for when you come back to your work your judgment will be surer. Go some distance away because then the work appears smaller and more of it can be taken in at a glance and a lack of harmony and proportion is more readily seen.” – Leonardo da Vinci.

A big part of the thesis work was also developed off the work desk, in front of a cup of hot chocolate, during some social events, travel times, etc.... I want to grab this opportunity to thank every single person with whom I have passed incredibly wonderful times; including my close friends, my colleagues, the esteemed members of the Union of Malagasy Students in Turkey (AUMT / F2MT), respectively the

GEZEN family and the ZAFERA family for considering me as an intimate member and allowing me to feel home in their families, hence easing my stay in Turkey. It is difficult to find the right words to express my gratitude to every people that supported me throughout this journey, so I would better leave the stage to those who might be able to find the correct sentences for that purpose.

“Where there is no guidance, a people falls, but in an abundance of counselors there is safety.”

Last but not the least; quoting the words above, I want to give thanks to every entity for guiding every physical, moral or spiritual step that I have taken through life and bringing me to this actual stage of conducting a thesis research. I could not have carried out this journey if I would have wanted to do everything on my own. This thesis is the fruit of unconditional blessings throughout my research works.

April 2014

Mihantarivelo Tahiry RABETY
(Mechanical Engineer)

TABLE OF CONTENTS

	<u>Page</u>
FOREWORD	ix
TABLE OF CONTENTS	xi
ABBREVIATIONS	xiii
LIST OF TABLES	xv
LIST OF FIGURES	xvii
NOMENCLATURE	xix
SUMMARY	xxi
ÖZET	xxiii
1. INTRODUCTION	1
1.1 Background	1
1.2 Statement of the Problem	2
1.3 Literature Review	4
1.4 Objectives and Scope	6
1.5 Outline of the Thesis	7
2. EXPERIMENTAL PROCEDURE OF INVESTIGATION	9
2.1 Nature of Steady Port-valve-cylinder Flows	9
2.2 Experimental Approach.....	10
2.2.1 Objectives of experiments.....	11
2.2.2 Experimental set-up	11
2.2.3 Notions about measurement repeatability and reproducibility	14
2.2.4 Measurement outputs	15
2.3 In-cylinder Flow Measurements.....	15
2.3.1 Measuring conditions and positions.....	16
2.3.2 Data processing	17
2.3.2.1 Derivation of the integrated swirl ratio formula:	17
2.3.2.2 Derivation of integrated mean flow coefficient formula:	20
2.3.2.3 Layout of the simpson’s rule for numerical integration:.....	23
2.3.3 Outcomes of the repeatability and reproducibility checks.....	23
3. CYLINDER HEAD SPECIFICATIONS	27
3.1 Basic Engine Properties	27
3.2 Intake Port Models	27
3.3 Intake Seat Angles.....	31
3.4 Additional Chamfers (c-chamfer & s-chamfer)	32
4. EXPERIMENTAL RESULTS	35
4.1 Specific Swirl Generation of the Intake Ports	37
4.1.1 Straight (long) intake port swirl generation	37
4.1.2 Helical (short) intake port swirl generation	40
4.1.3 Swirl generation resulting from simultaneous actuation of the intake valves	42
4.2 Effects of the Depth of the Concentric Chamfer	46

4.3 Effects of the Angle of the Concentric Chamfer	50
4.4 Effects of the Swirl Chamfer Offset	55
5. CONCLUDING DISCUSSIONS	61
5.1 Combined Effects of the C-chamfer Depth, Angle and Swirl Chamfer Offset	61
5.2 Limitations of the Experimental Investigation	64
5.3 Recommendations for Future Studies	64
REFERENCES	67
APPENDICES	71
APPENDIX A	72
APPENDIX B.....	79
APPENDIX C.....	81
CURRICULUM VITAE.....	87

ABBREVIATIONS

BDC	: Engine bottom dead center
CA	: Crankshaft angle
CFD	: Computational Fluid Dynamics
CR	: Crankshaft Ratio
FCM	: Overall Flow Coefficient per one cylinder
OEM	: Original Equipment Manufacturer
SRM	: Mean swirl ratio (integrated value)
SRMR	: Reduced mean swirl ratio (integrated value)
SRR	: Reduced swirl ratio (per valve lift)
TDC	: Engine top dead center

LIST OF TABLES

	<u>Page</u>
Table 2. 1: Swirl ratio and flow coefficient values for the reference cylinder head. .	14
Table 2. 2: Flow and induced swirl measurements.	24
Table 3. 1: Engine layout property.	27
Table 4. 1: Layout of the experimental operating conditions.	36
Table 4. 2: Measurement results on long ports from Head # 1.	39
Table 4. 3: Measurement results on short ports from Head # 1.	41
Table 4. 4: Measurement results on both ports from Head # 1.	43
Table 4. 5: Measurement results on two different c-chamfer depths.	48
Table 4. 6: Cylinder head configurations illustrating c-chamfer angle variations.	51
Table 4. 7: Measurement results on two different c-chamfer angles.	52
Table 4. 8: Cylinder head configurations illustrating s-chamfer offset variations.	56
Table 4. 9: Measurement results on two different s-chamfer offsets.	57
Table B. 1: Overall swirl ratio and integrated mean flow coefficient response.	79
Table C. 1: Intake valve lift displacement.	81

LIST OF FIGURES

	<u>Page</u>
Figure 1. 1: Technology improvements delivering the greatest impact on fuel economy and CO ₂ emission reductions.	2
Figure 1. 2: European emission standard for passenger cars (category M), [g/km]. ...	3
Figure 2. 1: Flow test rig schematic diagram.	13
Figure 2. 2: Flow test rig components' layout.	13
Figure 2. 3: Experimental measurement rig.	15
Figure 2. 4: Basic working principle of the swirl paddle measurement.	16
Figure 2. 5: Geometrical representation of the con rod length crank radius.	20
Figure 3. 1: Long port isometric view.	29
Figure 3. 2: Short port isometric view.	29
Figure 3. 3: Combustion chamber representation.	30
Figure 3. 4: Orientation of the intake airflow path into the combustion chamber.	31
Figure 3. 5: Seat angle geometrical details.	32
Figure 3. 6: Additional chamfers obtained through machining.	33
Figure 4. 1: Swirl generation of the long intake ports.	38
Figure 4. 2: Flow performance of the long intake ports.	38
Figure 4. 3: Swirl generation of the short intake ports.	40
Figure 4. 4: Flow performance of the short intake ports.	41
Figure 4. 5: Swirl generation of the both of intake ports.	43
Figure 4. 6: Flow performance of the both of intake ports.	44
Figure 4. 7: Synopsis of the swirl generation between short and long ports.	45
Figure 4. 8: Synopsis of the flow performance between short and long ports.	45
Figure 4. 9: Swirl generation of two different chamfer depths.	47
Figure 4. 10: Flow performance induced by two different chamfer depths.	47
Figure 4. 11: Synopsis of swirl production through different c-chamfer depths.	49
Figure 4. 12: Synopsis of flow performance through different c-chamfer depths.	49
Figure 4. 13: Swirl generation of two different chamfer angles.	53
Figure 4. 14: Flow performance induced by two different chamfer angles.	53
Figure 4. 15: Synopsis of c-chamfer angle effects on swirl generation.	54
Figure 4. 16: Synopsis of c-chamfer angle effects on flow performance.	55
Figure 4. 17: Swirl generation of two different s-chamfer offsets.	58
Figure 4. 18: Flow performance induced by two different s-chamfer offsets.	58
Figure 4. 19: Synopsis of s-chamfer offset effects on swirl generation.	59
Figure 4. 20: Synopsis of s-chamfer offset effects on flow performance.	60
Figure 5. 1: Interaction graph between the chamfers - effects on swirl generation. ..	62
Figure 5. 2: Interaction graph between the chamfers - effects on flow performance. ..	63
Figure C. 1: Intake valve opening cycle.	82
Figure D. 1: European emission standards for light commercial vehicles ≤ 1305 kg (category N ₁ -I), [g/km].	83

Figure D. 2: European emission standards for light commercial vehicles 1305 kg- 1760 kg (category N ₁ -II), [g/km].	84
Figure D. 3: European emission standards for light commercial vehicles > 1760 kg max 3500 kg (category N ₁ -III & N ₂), [g/km].	84
Figure D. 4: Data collection excell sheet.	85
Figure D. 5: Data output sheet.	86

NOMENCLATURE

A_o	: Area of the orifice
B	: Cylinder bore diameter
C	: Instantaneous piston speed
c_1	: Orifice flow coefficient of the measuring device
C_a	: Mean axial flow velocity
c-chamfer	: Concentric chamfer
C_d	: Discharge coefficient of the measuring pipe
C_F	: Flow Coefficient per valve lift
C_{Fm}	: Mean Flow Coefficient
C_m	: Mean piston velocity
D_o	: Orifice diameter
D_p	: Pipe diameter
dV	: Element of volume
dv	: Inner seat diameter for a single valve
dz	: Instantaneous piston stroke displacement
F_k	: Cross-sectional area of the piston
g	: Attraction of gravity
h	: Valve displacement on an interval spanning of 15 degrees CA
h_v	: Valve lift displacement considered in measurement
isd	: Effective Inner Seat diameter (as a function of number of valves)
\dot{m}	: air mass flow induced into the combustion chamber
\dot{m}_{theo}	: Theoretical mass flow
n	: Fictitious engine speed
n_D	: Paddle speed
P_{atm}	: Pressure of atmospheric air
R_{air}	: Specific gas constant for air
rm	: Ratio of the orifice diameter over pipe diameter
s	: Engine piston stroke
s-chamfer	: Swirl chamfer
T_{atm}	: Atmospheric air temperature
V_h	: Cylinder displacement
W	: Instantaneous velocity in the intake valve gap induced by the instantaneous piston velocity
\overline{W}_m	: Mean gas velocity in the reference cross-sectional area
\overline{W}_m	: Experimentally assessed gas velocity in the reference cross-sectional area
α	: Crank Angle
ΔP	: Pressure drop across intake ports
$\overline{\Delta P}_m$: Mean pressure drop through the suction stroke
ρ	: Density of air
$\overline{\rho}$: mean density of air
ρ_a	: air density in front of the port

ω : Angular velocity of the piston

EXPERIMENTAL INVESTIGATION OF THE EFFECTS OF A CYLINDER HEAD POST-VALVE GEOMETRY ON IN-FLOWING SWIRL MOTION IN A FOUR-CYLINDER DIESEL ENGINE

SUMMARY

The desire to change position has always animated and encouraged human beings to develop methods of transportation. The discovery of internal combustion engines figures surely amongst one of the most important inventions achieved in this field within the last two centuries. Since then, with continual advances in technology, scientists and researchers contribute to obtain higher power and torque outputs from the same or downsized volume internal combustion engines.

Driven by the increasing fuel prices on one hand and the narrowing specifications of the exhaust gases ejection into the environment on the other hand, the importance of the combustion efficiency optimization has aroused. However, due to the complexity of the combustion process (turbulent air flow, mixture formation, etc...), optimization of the combustion efficiency has become a research field that would need an in-depth and detailed consideration. There are indeed several research and development reports available in the literature.

Nevertheless, the combustion control strategy involves engine fluid dynamics which are characterized, in macro-scale, by the intake port geometries, the combustion chamber geometries and the mixture formation process. In a micro-scale, the fluid dynamics are characterized by the effect of mixture formation-induced kinetic energy on turbulent motion of the intake charge. Therefore, in combustion performance optimization performance perspectives, controlling the parameters affecting the mixture formation and altering them to fulfill the turbulent motion requirements appears to be a paramount control strategy suggestion.

In that context, the research summarized in this report addresses the experimental investigation of the effects of a cylinder head post-valve geometry on in-flowing swirl motion in a four-cylinder diesel engine. The cylinder head subjected to experimental measurements are provided by Ford Otomotiv Sanayi A.Ş. Numerical and Computational method limitations and the reasons behind opting for experimental assessment methods are also addressed through this report.

Experimental measurements are conducted using the paddle measurement method and measurements are taken on a stationary flow measurement bench. Parameters such as the concentric chamfer depth, concentric chamfer angle and the swirl chamfer offset and their respective effects on the overall swirl ratio and flow coefficient are assessed in detail. Furthermore, the combined effects of those parameters on the turbulent motion characteristics are investigated throughout the report.

Finally, the limitations of the experimental approach, the effects of manufacturing (casting) process on the swirl motion is considered and further investigation parameters and development fields are suggested.

To have a very brief summary on the thesis scope; concentric chamfer depth, its angle and the swirl chamfer offset change the nature of the induced turbulent air flow. This concept might be used to configure the cylinder head post-valve geometry so as to achieve a very specific swirl motion requirement in order to meet the exhaust gas emission regulations.

DÖRT SİLİNDİRLİ DİZEL MOTOR KAFASI SUPAP SONRASI GEOMETRİSİNİN EMME HAVASI ÇEVİRİ HAREKETİ ÜZERİNDEKİ ETKİSİNİN DENEYSEL OLARAK İNCELENMESİ

ÖZET

Bir yerden bir yere ulaşma arzusu, insanoğlunu çeşitli ulaşım yöntemine başvurmaya hep teşvik etmiştir. Son iki yüzyılda bu arzuya hizmet eden buluşlardan biri de şüphesiz içten yanmalı motorların imal edilmesiyle ortaya çıkmıştır. O günden bu yana teknolojik gelişmeler ile birlikte, dünyanın her tarafındaki bilim adamları ve araştırmacılar aynı veya daha küçük hacimdeki motorlardan hep daha fazla güç elde etmek için emek vermişlerdir.

Bir taraftan gün geçtikçe artan yakıt fiyatlarının etkisi ve alternatif enerji kaynakları üzerinde yürütülen çalışmaların sonucunda halen fosil yakıtların içten yanmalı motorlara enerji sağlayıcı maddelerin arasından büyük bir paya sahip olmasının pekiştirilmesi, diğer taraftan otomotiv sektörünün gelişmiş olduğu ülkelerde başta olmak üzere dünyada kabul görmüş ve sürekli daralma eğilimi gösteren çevreye salınabilecek yanma sonrası atık gazların miktarı politikaları, içten yanmalı motorlarındaki yanma veriminin optimize edilmesinin önemini vurgulamıştır.

Ancak yanma olayının karmaşıklığı nedeniyle (türbülanslı hava akışı, karışım oluşumu, vs...) yanma verimi optimizasyonu da o denli derinlemesine ele alınması gereken geniş bir çalışma alanı haline gelmiştir. Bu alanda birçok araştırma ve geliştirme kayıtlarına rastlamak mümkündür.

Nitekim yanma kontrol stratejileri içten yanmalı motorlardaki akışkanlar mekaniği konusunu içermektedir. Bahsi geçen akışkanlar mekaniği makro ölçekte silindir kafası parçalarındaki hava emme portu, yanma odası geometrileri ve karışım oluşumunu kapsar iken mikro ölçekte ise karışımın oluşumu sırasında kinetik enerjinin etkisiyle oluşan girdap hareketleri ve bu türbüans hareketine bağlı olan yanma hızları ve yanma karakteristiği konularını içermektedir. Dolayısı ile karışım oluşumunu etkileyen parametreleri kontrol altında tutmak ve ihtiyaca göre değiştirmek yanma verimini optimize etmek için önerilen başlı başına bir kontrol stratejisi haline gelmiştir.

İçten yanmalı motorlar için, özellikle dizel motorlar için kullanılan yakıt yüksek sıkıştırma oranından kaynaklı basınç ve sıcaklığın tesiriyle kendiliğinden tuttuğundan dolayı iyi bir yanma verimini elde etmek hem daha fazla hava-yakıt miktarını yakmak hem de yanma odasındaki havanın yakıt demetlerini mümkün mertebede parçalayıp demetler ile karışmasından geçmektedir. Bu ilkeden esinlenerek dizel motora olması gerektiği gibi karışımın oluşmasını sağlamak üzere özellikle son iki yüzyılda hava akışı optimizasyonu üzerinde çalışmalar yapılmaktadır.

Bu bağlamda, konu çalışma çerçevesinde içten yanmalı dört silindirli dizel motora ait silindir kafası supap sonrası geometrisinin emme havası teğetsel girdap hareketinin üzerindeki etkisi deneysel olarak incelenmiştir. Deneye konu olan dizel motor dört silindirli olup 2,2 litrelik hacme sahiptir. Bunun yanında, motordaki her yanma odası

için (her silindir için) ikisi emme ikisi egzoz olmak üzere toplam dört adet supap bulunmaktadır. Bu supaplara karşılık profilleri birbirlerinden farklı olmak üzere ikişer hava yoluğu (veya hava portu) bulunmaktadır.

Yapılan deneyler için konu silindir kafaları Ford Otomotiv Sanayi A.Ş. tarafından temin edilmiştir. Silindir kafası geometrisi ve emme portlarının konfigürasyonu emme supapları sonrası geometrileri ile birlikte ayrıntılı bir şekilde ele alınarak bir bölümde incelenmiştir.

Karışım oluşumunu iyileştirme çalışmaları deneylerle gerçekleştirilebildiği gibi teknolojik gelişmelerle ve insan hayatında bilgisayar sisteminin gittikçe daha fazla yer almasından dolayı artık bilgisayar ortamında da incelemek mümkün hale gelmiştir. Bu sanal ortamdaki benzetimler fiziki bir olayı soyutlaştırarak matematiksel bağıntılara indirgeyerek ve oluşturulan matematiksel bağıntıları bilgisayarlara sanal ortamda çözdürerek gerçekleştirilmektedir. Doğal olarak fiziksel olayın matematiksel denklemlere dönüştürülmesi sırasında yapılan varsayım ve kabuller sanal ortamda yapılacak benzetimin sonuçlarını göreceli olarak gerçek olma durumundan uzaklaştırmaktadır. Ek olarak, sanal ortamda incelemeye konu olan parametrelerin boyutları (büyüklükleri) azaldıkça karmaşık indirgenmiş ve bir takım varsayımla sadeleştirilmiş matematiksel denklemleri hassas bir şekilde çözebilmek için bilgisayarlar tarafından ihtiyaç duyulan süre oldukça geniştir.

Sayısal analiz metodunun sınırları ve deneysel ölçüm metodunun avantajları da bu çalışma raporunda değerlendirilmiştir. İki analiz yöntemi (deneysel incelemeler ve sayısal incelemeler) karşılaştırılıp maliyetli olması ve daha fazla zaman ayrılması ihtiyacına sebebiyet vermesine rağmen deney yapılması tercihindeki etkenler detaylı bir şekilde anlatılmıştır. Konuyu daha ayrıntılı olarak ele almak gerekirse, incelemeye alınan parametrelerin mertebeleri itibarı ile (0 ila 0.7mm arasında değişkenlik gösteren boyutlar bahis konusudur) sayısal analiz yönteminin yakınsak çözüme ulaşmasının çok fazla zaman gerektirdiğinden dolayı deneysel ölçüm yöntemi yeğlenmiştir. Literatürde mevcut olan ve İngilizce kısaltmaları ile LDV (Laser Doppler Velocimetry), PIV (Particle Image Velocimetry) gibi birçok ölçüm arasından da sabit ölçüm tezgâhında teğetsel girdap ölçümünün alınmasına karar verilmesinin de sebeplerine değinilmiştir.

Deneysel ölçümler, kürek ölçüm metodunun kullanıldığı sabit teğetsel girdap ölçüm tezgâhı aracılığı ile gerçekleştirilmiştir. Bu ölçüm metoduna göre, silindir kafası yanma odası çapını temsil edecek şekilde tasarlanıp imal edilen bir boru yardımı ile tezgahın üzerine bağlanmaktadır. Emme sisteminden temsili yanma odasına doğru giren havanın debisi ve söz konusu havanın silindir kafasındaki emme portlarından geçişlerinde yarattığı teğetsel girdap hareketinin yanma odasını temsil eden boru aparatının altında aynı eksende olması koşuluyla yerleştirilen bir sensör tarafından algılanan emilen havanın dönüş hızları değerlendirilmek üzere kayıt altına alınmaktadır.

Daha önce belirlenmiş olan emme supaplarının açılma yüksekliği değerlerinde kayıt altına alınan basınç, debi gibi değerler, valf parkuru boyunca oluşturulan teğetsel girdap hareketini değerlendirmek amacıyla hizmet edecek şekilde geliştirilmiş uygun bir teğetsel girdap hesaplama metodu kullanılarak dönüştürülmüştür ve böylece her supap açılma yüksekliği için bir girdap katsayısı ve hava akımı katsayısı elde edilmiştir. Hesaplanan girdap ve hava akım katsayıları daha sonra sayısal entegrasyon yöntemi aracılığı ile motor pistonunun üst ölü noktadan alt ölü noktaya hareketi (emme stroku) boyunca oluşan toplam girdap oranı ve hava akımı katsayısı elde edilmiş bulunmaktadır.

Ölçüm sonuçları elde edilince, sırasıyla eş aksel pah açısının, eş aksel pah derinliğin ve girdap pahı eksen kaçıklığının karışım oluşumunu doğrudan tanımlayan teğetsel girdap oranına ve emme portu verimliliği ile doğrudan ilişkilendirilebilecek hava akımı katsayısına etkisi incelenmiştir.

Sonuçları özetlemek gerekirse, eş aksel pah açısının artan değeriyle teğetsel girdap oranının arttığı, eş aksel pah derinliği arttıkça da teğetsel girdap oranının azalma eğilimi gösterdiği ve son olarak girdap pahı eksen kaçıklığının artmasıyla toplam teğetsel girdap oranının artma eğiliminde bulunduğu; ölçüm sonuçları incelendiği zaman gözlemlenmiş bulunmaktadır. Ayrıca değerlendirmeye alınan her bir ölçüm sonucu için geçerli olmak üzere, teğetsel girdap oranı arttığı durumunda hava akımı katsayısının azaldığı da tespit edilmiştir.

Çevresel sınır şartlarının ölçüm hassasiyeti (tekrarlanabilirliği ve tekrar üretilebilirliği) üzerindeki etkilerine daha önce tanımlanmış olan belirli koşullar altında teğetsel girdap ve akış performansı ölçümleri alınarak yapılan değerlendirmelere değinilmiştir ve yukarıda bahsi geçen tüm parametrelerin (eş aksel pah derinliğinin, açısının ve teğetsel girdap pahı eksen kaçıklığının) birleşik olarak teğetsel girdap hareketinin üzerine etkisi ayrıntılı olarak incelenmiştir. Bunun için toplamında otuz dokuz adet kombinasyon örneği ele alınmıştır. Toplanan örnekler, Minitab adında bir istatistik hesaplama programı kullanılarak derlenmiş ve parametre kombinasyonlarının toplam girdap oranı ve hava akımı katsayısı üzerindeki etkisini incelemek mümkün hale gelmiştir.

En son olarak, deneyler için yapılmış olan kabuller doğrultusunda, örnek olması adına alınan ölçümlerin motor çalışma şartlarında gerçekleşen hava akımı hareketini tam olarak simüle edemeyeceği gibi, konu deneysel yaklaşımın sınırlarından, silindir kafası parçalarının imalat süreçlerinin (döküm yönteminin) teğetsel girdap üzerindeki etkisinden bahsedilmiş ve bundan sonra bu çalışma üzerinde yapılabilecek araştırma ve geliştirme çalışmaları için incelenebilecek parametreler için önerilerde bulunulmuştur.

Bir bütün olarak bu tez çalışması incelendiği zaman emme supabı sonrası geometrilerinin (ayrıntılı olarak eş aksel pah açısının, eş aksel pah derinliğin ve girdap pahı eksen kaçıklığının) teğetsel girdap (swirl) ve hava akımı (flow) katsayıları üzerindeki etkileri incelenmiştir. Böylece bu parametrelerin çeşitli konfigürasyonları ile istenilen girdap hareketi sağlanmış olacaktır. Günümüzde özellikle otomotiv sektöründe sürekli azalma meyilli olan egzoz gazları salınımları şartnamelerini sağlayabilmek adına bu tez kapsamında yürütülen çalışma, yanma prosesini şartlandırabilecek bir kontrol stratejisinin geliştirilmesinde kullanılabileceğinden literatüre kazandırılması şüphesiz faydalı olacaktır.

1. INTRODUCTION

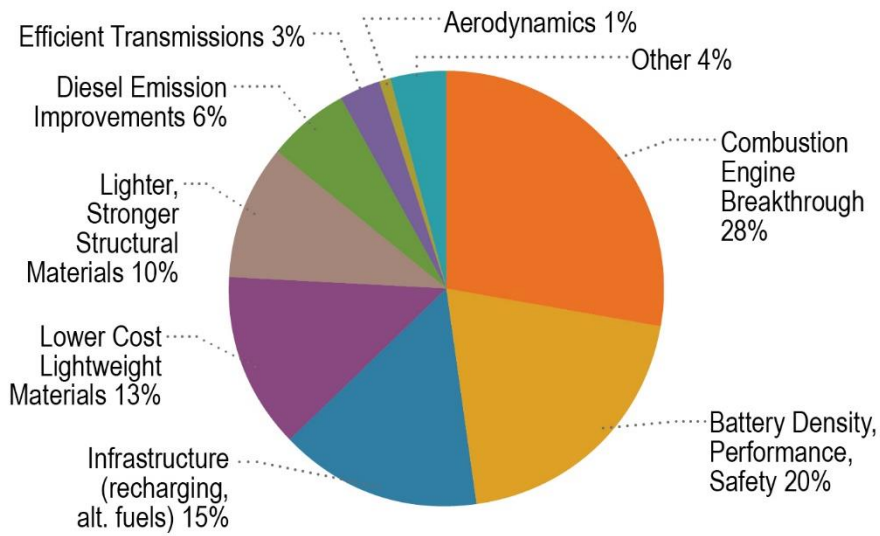
Movement is the act or process of moving people or things from one place or position to another [1]. This expression has driven the desire of humanity to explore his surroundings. That desire has been involved also with the actually frequently used tools such as vehicles, trains, airplanes etc.... Nowadays where mobility has become a driving factor of productivity and efficiency, several inventions and developments have marked the last few decades, especially in the automotive field. However, this high demand of mobility requires an increasing use of energy, inevitably affecting our environment in a negative way, in occurrence, with high level of pollutant generations.

As far as the automotive sector is concerned and despites the increasing amount of researches achieved in terms of using alternative energies, one has to note the dependency on the internal combustion engine in terms of powering up the vehicle [2]. This is illustrated through the insufficiency of the available alternative energies such as hydrogen, electrical energies etc.... The case of the electrical energy is special since electricity itself is often being produced by means of fossil resources etc... as stated by [3]. On the other hand, other alternative energies resources need some further developments to reach the level of usage in a modern vehicle.

1.1 Background

With the narrowing level of pollutants allowed into the nature with respect to time, engineers have to find another way to meet the target. According to a survey carried out in 2012 about the technology improvements delivering the greatest impact on fuel economy and CO₂ emission reductions on Figure 1. 1, one can point out to the outstanding opportunity available within the Combustion Engine Breakthrough category, representing 28% of the total improvement possibility [4].

TECHNOLOGY IMPROVEMENTS DELIVERING THE GREATEST IMPACT
ON FUEL ECONOMY AND CO₂ EMISSION REDUCTIONS



Source: 2012 WardsAuto survey sponsored by DuPont.



Figure 1. 1: Technology improvements delivering the greatest impact on fuel economy and CO₂ emission reductions [4].

1.2 Statement of the Problem

It has been aforementioned that the environmental impact of the mobility requirements has led researchers and engineers to deep-dive on further development works on the internal combustion engines. Figure 1. 2 [5] summarizes the evolution of the narrowing of pollutant levels emitted into the environment within the European zone for passenger cars. Respective trends for vehicles belonging to other classifications are provided in Figure D. 1, Figure D. 2 and Figure D. 3.

Tier	Date	CO	THC	NMHC	NO _x	HC+NO _x	PM	P***
Diesel								
Euro 1†	July 1992	2.72 (3.16)	-	-	-	0.97 (1.13)	0.14 (0.18)	-
Euro 2	January 1996	1.0	-	-	-	0.7	0.08	-
Euro 3	January 2000	0.64	-	-	0.50	0.56	0.05	-
Euro 4	January 2005	0.50	-	-	0.25	0.30	0.025	-
Euro 5	September 2009	0.50	-	-	0.180	0.230	0.005	-
Euro 6 (future)	September 2014	0.50	-	-	0.080	0.170	0.005	-
Petrol (Gasoline)								
Euro 1†	July 1992	2.72 (3.16)	-	-	-	0.97 (1.13)	-	-
Euro 2	January 1996	2.2	-	-	-	0.5	-	-
Euro 3	January 2000	2.3	0.20	-	0.15	-	-	-
Euro 4	January 2005	1.0	0.10	-	0.08	-	-	-
Euro 5	September 2009	1.0	0.10	0.068	0.060	-	0.005**	-
Euro 6 (future)	September 2014	1.0	0.10	0.068	0.060	-	0.005**	-
* Before Euro 5, passenger vehicles > 2500 kg were type approved as light commercial vehicles N ₁ -I								
** Applies only to vehicles with direct injection engines								
*** A number standard is to be defined as soon as possible and at the latest upon entry into force of Euro 6								
† Values in brackets are conformity of production (COP) limits								

Figure 1. 2: European emission standard for passenger cars (category M), [g/km] [5].

From the figures above, it can easily be spotted that whatever the category of the vehicle is, the emission level adopts a narrowing trend. On the other hand, there is a continuous demand on vehicle performance delivery, therefore engine performance delivery [6]. The key of achieving this high performance demand is without doubt the optimization of the combustion process. However, such kind of optimization is quite difficult to carry out because of its complexity. It is good to remember that the combustion process involves both a flow of air through the engine intake pipes and ports, the injection of fuel, the mixing of the charge, its ignition and combustion then the rejection of the burnt gases [7]. Many control strategies have also aroused, in occurrence the skip-cycle method, the stoichiometric Air-Fuel Ratio, etc..., thanks to this complexity.

Nevertheless, those control strategies basically involve engine fluid mechanics, which consist at a large scale of the intake port and combustion chamber (cylinder bore and piston bowl) geometries, the mixing of charges and the induced kinetic energy (generated by intake swirling and/or tumbling) during the intake process. This kinetic energy is driving at a smaller scale the turbulence fluctuation within the engine, primarily affecting the combustion speed.

Based on the afore-mentions, one can records that optimizing the combustion is the main factor to achieve the trade-off between high performance demand and narrowing environmental regulations. Having a look at a small scale, it would not be hard to spot the difficulty to improve the in-cylinder turbulence motion and fluctuation, considering the boundary conditions such as pressure and temperature applying within the combustion chamber after the closure of the intake valves [8]. On a larger scale, governing over the swirling and tumbling motion yield to containing the in-cylinder turbulence motion of the mixture too.

To summarize, it is possible to suggest a combustion control model by controlling the cylinder flow, although that combustion control is not universal but depends on the engine configuration. A capability to predict the behaviour of fluid dynamics within the combustion chamber would considerably ease the task of developing engines featuring both high performance and low pollutant emission.

1.3 Literature Review

Many are the scientific approaches that are put to service to understand the importance of engine fluid dynamics in reciprocating engines. Since a few decades, a considerable amount of progress has been recorded both in terms of computational and experimental technique in the field of prediction of in-cylinder flow behavior, as stated by Wilson, B. M. (2009) in his research paper [9].

Non-dimensional numbers of single characteristics are defined to give an insight about flow structures within the internal combustion engines. Due to the importance of breathing and air utilization in performance and efficiency perspectives, inlet flow characteristics for a given engine are crucial [10]. The more frequently used parameters are the swirl number and/or tumble number, which are quantitative numbers characterizing the angular momentum of the air (and/or mixture) about the combustion chamber axis and/or an axis normal to the combustion chamber axis.

Khalid, A. and Manshoor, B. (2012) claimed that he assessment of the swirl number and tumble number induced during the intake cycle of the combustion process gives an indication on the homogeneity of the mixture formation within the combustion chamber, thus enables prediction of the combustion performance [11].

When it comes to acquiring detailed informations about the in-cylinder flow, many techniques have been recorded in the literature. However, a complete review of each of these techniques will not be considered but the purpose of this section is rather to give a very basic overview on the most widely used techniques with respect to engine breathing performance assessment.

The need for extra power and combustion efficiency has driven researchers to investigate the basic components of the engine, in occurrence, valves, cylinder heads and manifolds in a more detailed way. Original equipment manufacturers have started to make the use of those airflow driven port performances on their engines. Nevertheless, the advantages of outsourcing flow measurements to commercially dedicated research and development companies resulted in a way that the OEMs learned to entrust those companies in favor of cost-effectiveness. Since then, starting with racing cylinder head tunings, research and developments of engines have included the usage of flow measurement data for many years.

Starting from the 1970's, flow measurement rigs were commercially available. For instance, Airflow Research, Chrysler and Donovan Engineering (n.d.) figure amongst the first pioneer companies in the field of airflow investigations by designing special cylinder heads [12]. Nowadays, there counts thousands of flow benches widely used for the purpose of port efficiency and this will not stop as technology developments keep advancing. In some cycle during the design development process of each successful OEM lays the usage of an airflow measurement data.

Actually, flow measurement devices and such systems have a very large application, based on their working principle. The most common of them is based on orifices, nozzles, Pitot tube systems, laminar flow elements, positive displacement measurements; hot-wire velocimetry, particle image velocimetry, laser-doppler anemometer, etc... [13]. In occurrence, hot-wire velocimetry (HWV); laser-doppler velocimetry (LDV) and particle image velocimetry (PIV) are the mainly used experimental methods to predict the flow behavior within the combustion chamber [14 - 17]. Hot-wire velocimetry consist of locally measuring the fluid velocity passing through a wire electrically heated, generating electrical potential difference. Laser-doppler velocimetry consist of determining the local fluid velocity with a constant measuring volume delimited by the crossing of two laser beams. The pre-defined measuring volume is tracked via the variation in frequency of emitted and

bouncing laser beam. Particle image velocimetry is a technique based on taking multiple pictures with short time delays of a fluid loaded with particles while it is passing through a laser sheet, followed by an evaluation of the particle displacements throughout the laser plane. Both of those two methods involve the measurement of the charge velocity within the combustion chamber, are both very complex measurement techniques and therefore have their own advantages and disadvantages over each other. Hence, they are selected according to the purpose of the experimental evaluation.

Numerical simulations have also been in the market for determining the nature and behavior of the in-cylinder flows [18- 21]. It consists of modelling the flow by means of mathematical approaches and then simulating the combustion process with the applied boundary conditions. Many Computational Fluid Dynamics (CFD) software are available in the market for researchers. Like the experimental techniques, the nature of the computational approach depends on the purpose of the parameter evaluation, being it of quasi-dimensional or zero-dimensional (involving simplified thermodynamical equations for a more macro-scale evaluation) category or multi-dimensional (involving more complex thermodynamical equations for a micro-scale evaluation) category. The more complex the equations system is, longer the time needed by the computer to simulate the flow process.

1.4 Objectives and Scope

Many publications and reports exist on the analysis of the impact of the swirl motion to the combustion process. Amongst them are present some detailed experimental and computational approaches. Moreover, the technological development has enhanced the evaluation and interpretation of the flow analysis results. Yet regardless to the approach, publications and reports about detailed flow investigations are very limited.

The investigation presented throughout this thesis aims to add more understanding to the influence of basic geometries of the engine cylinder head located after the intake valves, such as the swirl-chamfer offset distance and the concentric chamfer angle along with its depth to the induced flow structure during the intake phase of the combustion process. This will be carried out by means of detailed experimental measurements through intake ports of physical engine cylinder head workpieces. In

addition, the accuracy along with possible experimental error sources will also be evaluated in the scope of the research.

With the limited computer resources and the risk of incoherence between the derived mathematical model, which would be used for CFD study, and the physical flow model, computational approaches have not been adopted in the research.

The airflow generated during the intake stroke of an internal combustion engine has a high impact on the induced in-cylinder flow and turbulence motion during the compression stroke and the ignition phase. Therefore, the performance of the intake system is very significant. In the research carried out through this thesis. Because of the complexity of the nature of the in-cylinder flow at the end of the compression stroke of an engine due to the effects of piston and valve motions during the intake and compression phases, only analyzing the unsteady phenomena leads to realistic information about the boundary conditions towards the end of the compression stroke.

Considering the afore-mentioned reasons, with the lack of sophisticated experimental test benches, steady flows are analyzed at several realistic flow conditions and different valve lift heights, in contrast with the literature reporting several investigations mostly under a specific valve lift height.

1.5 Outline of the Thesis

The experimental procedure adopted throughout the investigation is being taken into consideration on Chapter 2. The nature of the steady flow occurring between the intake ports, valves and combustion chambers are assessed on the following sections, followed by a detailed illustration of the experimental set-up design and the measurement process. Further sections in Chapter 2. evaluate the data processing method and the possible experimental uncertainty throughout measurement sequences.

Chapter 3 deals with the particularities of the measurement specimens, with a detailed survey of the geometrical features, whose influences onto the combustion process will be assessed. These geometrical features consist of intake seat angles, concentric chamfer (C-chamfer) angle with its respective depth and the swirl chamfer (S-chamfer) offset.

The results of the experimental investigation are presented in Chapter 4 and their respective effects on the induced swirl number are interpreted.

Finally, limitations of the experimental investigation, conclusions and deductions are addressed in Chapter 5. Moreover, recommendations for future studies are discussed.

2. EXPERIMENTAL PROCEDURE OF INVESTIGATION

In fact, intake port efficiency can also be evaluated in a virtual environment. Several softwares have been developed to meet the engineering need of visualization and prediction of the in-cylinder flow. However, computational and numerical prediction methods presented some limitations in terms of analyzing the effects of the parameter variations throughout simulations [9 - 21]. In fact, the changes of which the effects on the swirl and flow generation were evaluated are in order of one tenth of a millimeter. The c-chamfer depths that underwent experimental measurements vary from 0mm to 0.7mm. Similarly, the swirl chamfer offset variations extended across 0.8mm through 1.6mm. Although one could clearly visualize the parameters' induced changes computationally, the main restriction would be in terms of refinement of the meshing size, compromising with the required CPU time for solving the numerical model.

Besides the meshing size restriction, the biggest constraints faced while computationally and/or numerically assessing the performance of a physical model lays in the adequacy and mostly the complexity of definition of the mathematical model and the operating parameters. These constraints yield uncertainty on the coherence of the physical and the numerical model [21 - 22].

Driven by the limitations of the computational approach in terms of assessing the effects of the design parameters such as c-chamfer and swirl chamfer offset variations, experimental approach is deemed adequate in order to evaluate the swirl generation performance of the intake ports of an internal combustion engine. This section deals with details regarding the experimental investigations carried out through this study.

2.1 Nature of Steady Port-valve-cylinder Flows

The airflow through intake port-valve-cylinder is complex. The nature of the flow generally depends on the configuration of the intake ports and the rotational motion requirement of the charge within the combustion chamber following intake valve

closure [23, 24]. During the intake stroke of each cylinder, the air sucked through the inlet manifolds passes through the intake ports, hit the valve stems and enters into the cylinder through the opening area between the intake valves and valve seats. Depending on the breathing demands of the engine, it is sometimes required to have a rotating flow well before the air mass enters the combustion chamber [25, 26]. In such conditions, the usage of a straight intake port along with a helical intake port insures a wide combination of the rotational flow of the charge once entering the cylinder. Through this breathing demand of the engine, it can be clearly noted that the intake port configuration, being straight or helical, plays a major role in determining the nature of the flow during the intake stroke of a cylinder.

Straight after the opening of the intake valve, at low valve lift height, the flow entering the combustion chamber is mainly restricted by the gap through which the air has to pass. Therefore, the induced flow structure is determined by the geometry of the post-valve region; more precisely the seat angle, c-chamfer angle and depth and finally the swirl chamfer offset. As the valve lift increases, straight towards the end of the intake stroke, the piston speed is the main restricting parameter determining the nature of the charge flow. Nevertheless, the characteristic of the intake port, valves and cylinder head post-valve geometries govern the nature of the flow remaining within the combustion chamber, during steady state flow measurement.

2.2 Experimental Approach

Experimental measurements were carried out under steady state conditions. Steady state conditions mean, in other words, that the piston motion of a real running engine is disregarded and a constant charge flow is pulled into the combustion chamber through intake valves [27], as this study aims to assess the performance of engine cylinder head intake ports in terms of airflow admittance throughout data collection.

Several swirl measurement techniques are now developed and provided for researches and development practices [14 -[17] such as paddle swirl meter, PIV metering, LDV metering and impulse & paddle swirl meter, just to cite a few of these measurement techniques. Many are also the report papers comparing the advantages and disadvantages of each of these experimental methods. For this study, the collections of experimental data have been kept as simple but accurate as possible.

Throughout comparison reports written about the context, it is decided that the usage of paddle swirl meter in order to track the airflow variation and the generated rotational motion of the charge inside the combustion chamber is adequate.

2.2.1 Objectives of experiments

Experiments are carried out in order to obtain quantitative data that will be used further to evaluate the changes on the generated swirl along with main parameters affecting the flow. The list of parameters affecting the inlet flow to the cylinder of an internal combustion chamber is very long, and the parameters are interacting with each other to characterize the outcoming flow from intake ports [28, 29]. For example, the swirl level generated by the straight intake port is quite different from the swirl level induced by the helical inlet port, while a very different swirl level is resulting from the mutual motion of the valves through straight and helical intake ports, as claimed by Ricardo Consulting Engineers Ltd. [30, 31]. It is therefore of crucial importance to accurately assess every respective effect of these parameters on the overall flow characteristics. Moreover, the machining process also induces some variations in the outcoming geometry of the inlet system of a cylinder head, which also requires a special attention. Those machining parameters are to be also investigated.

2.2.2 Experimental set-up

Measurements were carried out with a Superflow SF-600FC flow bench developed by Superflow Corporation. A schematic layout of the test rig is illustrated on Figure 2. 1.

The measurement set-up consists of an electrical air pump, a table bench onto which a dummy cylinder representing the combustion chamber is mounted, a valve actuator adaptor along with micrometer serving as an indicator, a paddle swirl meter and a pressure gauge.

Air is sucked into the flow measurement rig with a determined pressure drop across an attached test section ranging from 0.25 to 12 kPa (1 inch to 48 inch H₂O). Ambient temperature and humidity prior and following the data collections are

recorded with a hygro thermometer and these are used to calculate the air density. Likewise, the barometric pressure is also measured via a pressure gauge.

The cylinder head is placed at the top of an adaptor serving as a dummy cylinder mounted onto the flow bench. The dummy cylinder consists of a bore with the same diameter as that of the engine combustion chamber with two connecting flanges at each extremity. The length of the dummy cylinder should be at least equal to the bore diameter or a more. For this case, the length of the bore is set to be 1.75 times longer than its diameter. The dummy cylinder is then bolted to the flow bench at its bottom flange.

Another device is mounted onto the top of the cylinder head in order to be able to control the opening of intake valves in concordance with the test positions. There are several methods to position the inlet valve so that the corresponding lift displacement is easily set and controlled. As far as the flow measurement is concerned, this is achieved with the use of a fine pitch threaded bolt located at the top of the valve stem permitting its displacement along its shaft axis and a micrometer mounted at the top of the bolt serving as displacement indicator. Figure 2. 2 has been provided for a better understanding of the flow bench components.

Steady-flow swirl measurements are performed using the device mentioned above, fixed onto the top of the cylinder head and bolt tightened to the dummy cylinder using cylinder head bolts. Prior flow measurements, every opening orifice / hole that might affect the flow such as glow plug threaded hole, etc... is obstructed.

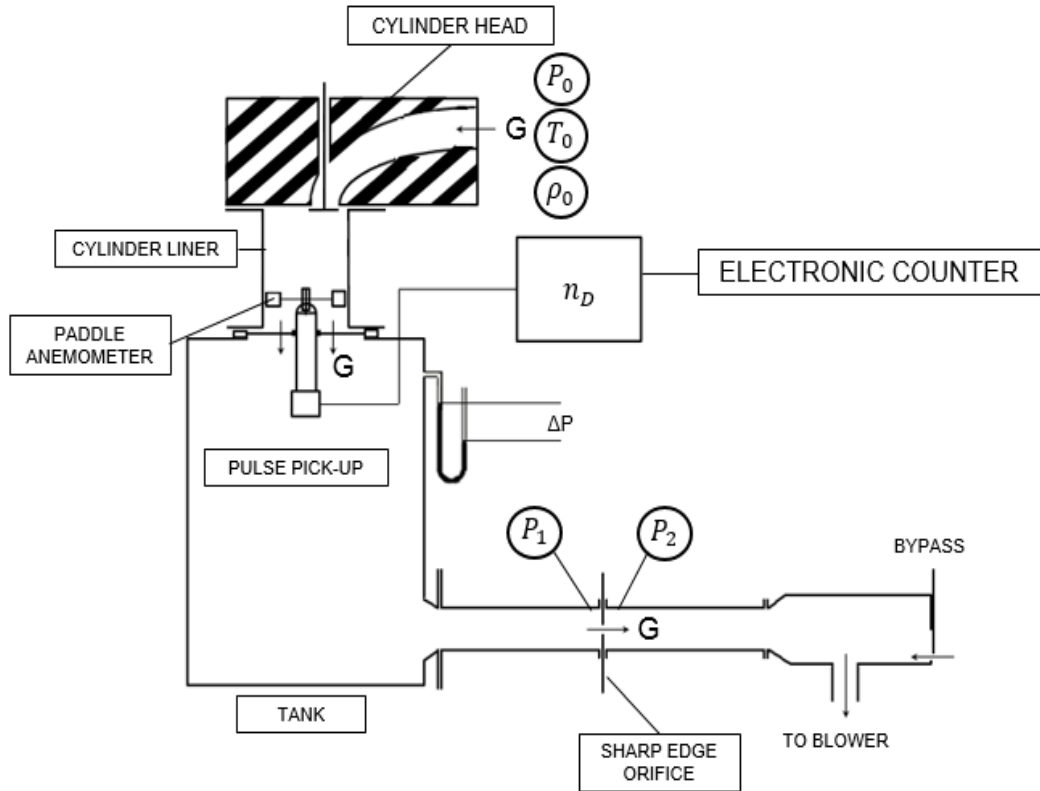


Figure 2. 1: Flow test rig schematic diagram.

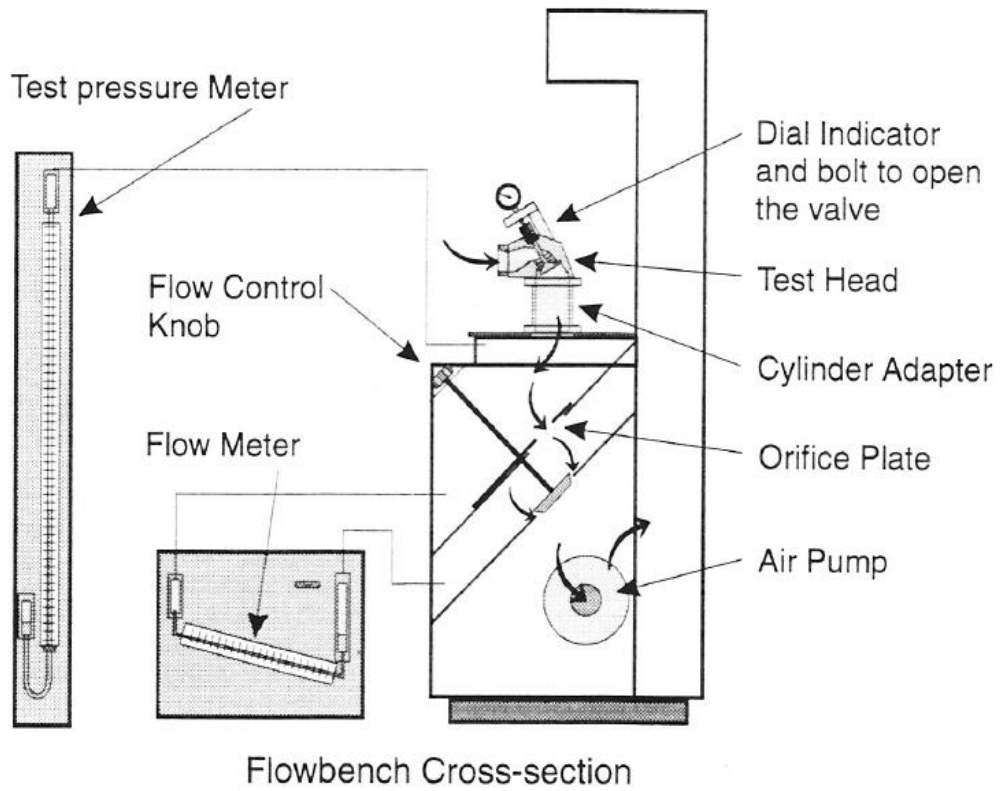


Figure 2. 2: Flow test rig components' layout.

2.2.3 Notions about measurement repeatability and reproducibility

As any type of experimental data collection, the flow measurement also induces errors . It is therefore important to clarify the accuracy and reproducibility of the swirl measurement technique for coherence point of view. For accuracy and reproducibility investigations, several measurements are conducted on a reference engine cylinder head assembly of known port efficiency performances as stated on Table 2. 1.

Table 2. 1: Swirl ratio and flow coefficient values for the reference cylinder head.

Reference cylinder head		
Overall measurement values	Swirl	1,5
	Flow	0,365

That cylinder head is configured as follow:

- Seat Angle: 45°,
- Concentric Chamfer Depth: 0.60 [mm],
- Concentric Chamfer Angle: 120 °,
- Swirl Chamfer Offset: 1,2 [mm].
- Swirl Chamfer Depth: 1.80 [mm],
- Concentric Chamfer Angle: 90 °.

The repeatability of experimental measurements are checked through a set of consecutive flow measurements conducted on the same reference cylinder head, while the initial conditions like ambient temperature and ambient humidity are varying. It aims to assess the ability of measurement duplication under the same conditions.

Reproducibility checks for the flow measurements are performed through a serie of measurement of several ports under the same pressure drop value while initial conditions are restored to a determined value prior each measurement.

A snapshot of the measurement rig is represented on Figure 2. 3.

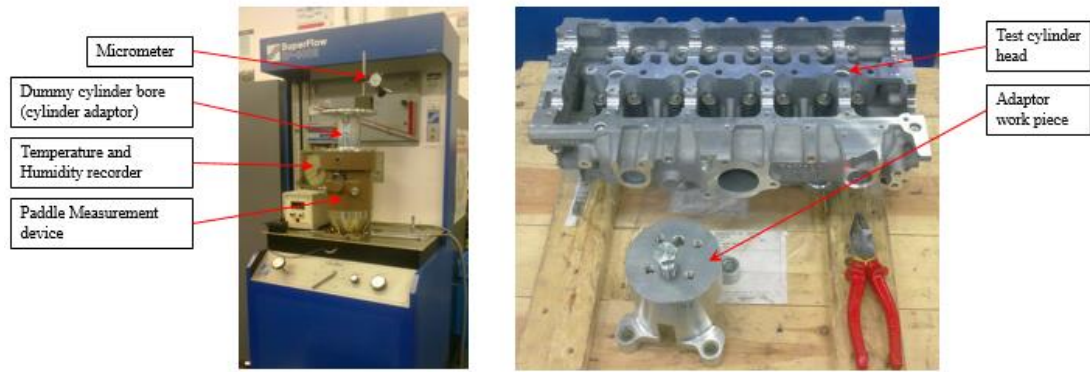


Figure 2. 3: Experimental measurement rig.

2.2.4 Measurement outputs

After the pressure drop reaches the steady-state condition following the incremental opening of the intake valves, the pressure drop through inlet ports and the pipe orifice is recorded automatically by the flow-measuring computer Flowcom and the generated swirl motion is recorded as a function of the rotating paddle. These two parameters (paddle speed and flow rate) will be used to calculate the main flow characteristics such as discharge coefficient, flow coefficient and generated swirl level with respect to specific valve lift displacements.

2.3 In-cylinder Flow Measurements

The inlet ports subjected to swirl flow measurements throughout this study belong to an internal combustion engine cylinder head. The engine is a four-cylinder diesel engine powering typical passenger cars. A basic scheme of the measurement principle is given in Figure 2. 4 below while a more detailed survey of the engine cylinder head to be investigated is addressed on Chapter 3.

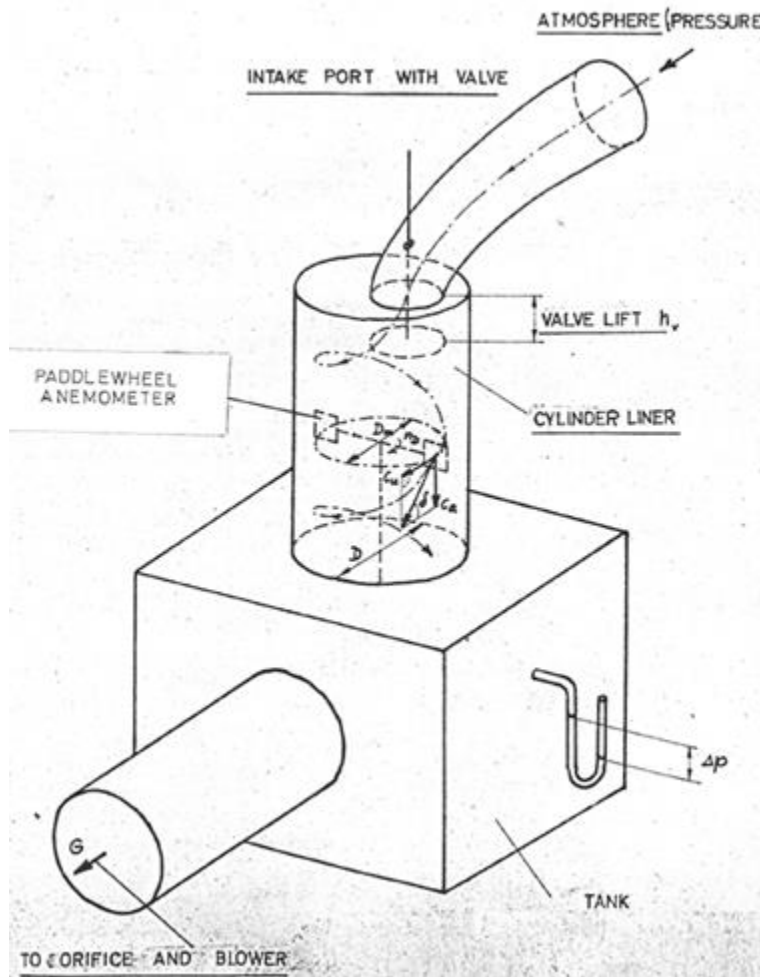


Figure 2. 4: Basic working principle of the swirl paddle measurement.

2.3.1 Measuring conditions and positions

With the usage of a micrometer as visual indicator for the valve lift value, restrictions might be observed in term of reading accuracy since the gauge steps of the micrometer are limited. Hence, in order to ensure a precise reading of the valve lift displacement, only integer values of the valve lift height have been set as measurement points.

An increment of 1 mm per valve lift displacement is taken through the process. Extrapolating the flow characteristics from its value at maximum valve lift is avoided by taking also further measurement point beyond the maximum valve lift value. Consequently, a total of 10 steps corresponding to a valve opening up to 10 mm is carried out, although the valve would not open that much in reality for the risk of hitting the engine piston.

As the intake valve is forced to open, instancial vacuum within the system (cylinder head and dummy cylinder) fluctuates and pressure drop is also prone to decrease consequently. The fluctuation then fades out after stabilization of the flow passing through the defined area of the intake port. Following this flow stabilization, the pressure drop and a vane speed value representing the generated swirl motion is automatically recorded to the data log.

2.3.2 Data processing

Conversion of the flow rate and vane speed value into overall generated swirl ratio and flow coefficient with respect to the valve lift height is achieved with the help of formulas transcribed into a Matlab Code. Outcoming swirl coefficients and flow coefficients are computed by means of this matlab code for each combustion chamber, and the final result is obtained by averaging the overall integrated swirl ratio and flow coefficients between all the four cylinders.

The demonstration of swirl level calculation is described in the sections below.

It is assumed that the cylinder charge rotates within the intake system (intake manifold, intake ports and valves along with the combustion chamber) as a solid body. Therefore the moment of the momentum of the charge is equal to the sum of the momentums of sucked air. Moreover, in-flowing air is considered incompressible and the engine suction stroke occurs only between the piston TDC and BDC.

2.3.2.1 Derivation of the integrated swirl ratio formula:

The momentum generated in dt is then set to be equal to the rotational speed of a cylindrical disc corresponding to the volume flowing into the combustion chamber within the time increment dt.

The integral swirl ratio is defined as the ratio of the rotational complete cylinder charge to the engine speed, mathematically expressed by equation (2. 1).

$$\left(\frac{n_D}{n}\right)_m = \frac{1}{V_h} * \int_{TDC}^{BDC} \left(\frac{n_{D(\alpha)}}{n}\right) . dV \quad (2. 1)$$

$n_{D(\alpha)}$ is obtained by stationary (steady state) flow measurements under specific conditions such as constant pressure drop through the intake ports (pressure drop occurring between the atmosphere and the dummy cylinder). Through such

measurements, a relation between the paddle speed and the mass flow depending on the valve lift displacement is acquired. Expression of the ratio of the paddle speed n_D to the fictitious engine speed n results in the dimensionless steady-state swirl coefficient shown in equation (2. 2). In other words, equation (2. 2) gives the value of the swirl ratio per valve lift displacement.

$$\frac{n_D}{n} = \frac{n_D}{\dot{m}} \cdot \frac{\rho \cdot V_h}{30} \quad (2. 2)$$

The fictitious engine speed is calculated by equating the mean axial flow velocity C_a (equation (2.3. a)) to a mean piston velocity C_m (equation (2.3. b)).

$$C_a = \frac{\dot{m}}{\rho \cdot F_k} \quad (2.3. a)$$

and

$$C_m = \frac{s \cdot n}{30} \quad (2.3. b)$$

Therefore

$$n = \frac{30 \cdot \dot{m}}{s \cdot \rho \cdot F_k} \quad (2. 3)$$

where F_k describes the piston cross-sectional area for the related engine.

On the other hand, the element of volume dV can be defined as

$$dV = F_k \cdot s \cdot dz_{(\alpha)} = V_h * \frac{dz_{(\alpha)}}{d\alpha} * d\alpha \quad (2. 4)$$

The instantaneous rotational speed of the cylindrical disc triggered by the piston speed is expressed as:

$$n_{D(\alpha)} = n_D * \frac{C_{(\alpha)}}{C_m} \quad (2. 5)$$

where $C_{(\alpha)}$ describes the instantaneous piston speed.

$$C_{(\alpha)} = s * \frac{dz_{(\alpha)}}{dt} = s * \frac{dz_{(\alpha)}}{d\alpha} * \frac{d\alpha}{dt} \quad (2. 6)$$

Given the angular velocity of the piston (denoted as ω):

$$\omega = \frac{d\alpha}{dt} = \frac{n \cdot \pi}{30} \quad (2.7)$$

One can express the piston speed ratio as follow:

$$\frac{C_{(\alpha)}}{C_m} = \pi * \frac{dz_{(\alpha)}}{d\alpha} \quad (2.8)$$

Solving equation (1) with the help of the equations above yields:

$$\left(\frac{n_D}{n}\right)_m = \pi * \int_{\alpha=0}^{\pi} \frac{n_D}{n} * \left(\frac{dz_{(\alpha)}}{d\alpha}\right)^2 * d\alpha \quad (2.9)$$

Rearranging equation (2.9) leads to the following expression:

$$\left(\frac{n_D}{n}\right)_m = \frac{1}{\pi} * \int_{\alpha=0}^{\pi} \frac{n_D}{n} * \left(\frac{C_{(\alpha)}}{C_m}\right)^2 * d\alpha \quad (2.10)$$

where the values of $\frac{n_D}{n}$ are interpolated from the steady-state measurements that have been carried out for specific valve lift displacements (through 1mm increment in this case-study). Correlation between crankshaft angles α and valve lift displacements is given by the valve lift curve of the engine.

The following relation (equation (2.11)) illustrates the ratio of the instantaneous piston velocity over the mean piston velocity:

$$\frac{C_{(\alpha)}}{C_m} = \frac{\pi}{2} * \left(1 + \frac{\lambda \cdot \cos \alpha}{\sqrt{1 - \lambda^2 \sin^2 \alpha}}\right) * \sin \alpha \quad (2.11)$$

with λ describing the crank radius (R) and the connecting rod length (L) ratio as illustrated on Figure 2.5.

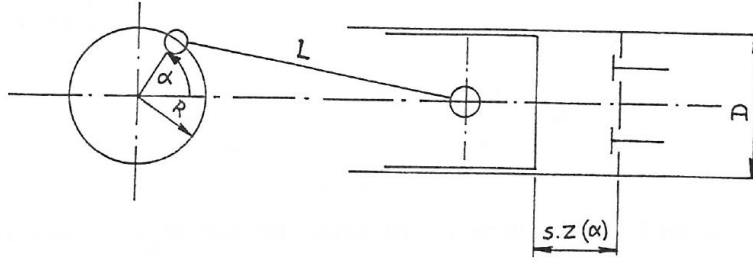


Figure 2. 5: Geometrical representation of the con rod length crank radius.

The swirl ratio defined in equation (2. 10) is still dependent on the engine stroke therefore would be different for each engine specification. To allow a more objective evaluation, a dimensionless parameter is defined so that the ratio of the engine stroke to its bore diameter is equal to unity. Hence, one has to multiply equation (2. 10) with $\frac{D}{s}$ for the sake of comparison. This parameter is then defined as reduced swirl ratio and expressed as follow:

$$\left(\frac{n_D}{n}\right)_{m_r} = \frac{D}{\pi \cdot s} * \int_{\alpha=0}^{\pi} \frac{n_D}{n} * \left(\frac{C_{(\alpha)}}{C_m}\right)^2 * d\alpha \quad (2. 12)$$

During the transcription of the formula into the Matlab codes, the reduced swirl ratio is denoted by SRMR.

2.3.2.2 Derivation of integrated mean flow coefficient formula:

The flow coefficient parameter (addressed as C_F) is defined as the ratio of the actual mass flow through the inlet valves at certain pressure drop over the theoretical mass flow at the same pressure drop through a reference cross-section and assuming no restriction.

$$C_F = \frac{\dot{m}}{\dot{m}_{th}} \quad (2. 13)$$

For the sake of calculation simplification, the reference cross-section area is set to be the inner valve seat diameter d_v .

Therefore,

$$\dot{m}_{th} = \frac{\pi \cdot d_v^2}{4} * \rho * \sqrt{\frac{2 \cdot \Delta P}{\rho}} \quad (2.14)$$

The values of C_F are calculated from the stationary (steady-state) measurements at different valve lifts and are plotted against these valve lift displacements. It is clearly deduced from the equation (2. 13) that the flow coefficient depends on the value of the reference cross-section thus on the inner seat diameter.

The mean gas velocity W_m in the cross-sectional area (in this case-study the inner seat diameter d_v) without a restriction (valve geometrical cross-section) at the mean piston velocity C_m is important and computed from the continuity equation assuming a constant density of the in-flowing air.

Therefore,

$$C_m * \frac{D^2 \cdot \pi}{4} = W_m * \frac{d_v^2 \cdot \pi}{4} \quad (2.15)$$

Solving for the mean gas velocity yields:

$$W_m = C_m * \frac{D^2}{d_v^2} \quad (2.16)$$

The value expressed in equation (2. 16) is based on theoretical assumptions. However, it is possible to define the mean gas velocity in a more realistic way as follow:

$$\overline{W_m} = \frac{W_m}{(C_F)_m} \quad (2.17)$$

W_m is computed by equating the in-flowing pressure drop to the pressure drop obtained with the development of the flow area over time throughout the suction stroke.

Hence, the Bernoulli equation is written as follow:

$$\overline{\Delta P_m} = \frac{\rho}{2} * \overline{W_m}^2 \quad (2.18)$$

Furthermore, the pressure drop obtained via the flow area development through engine suction stroke is written:

$$\overline{\Delta P}_m = \frac{1}{V_h} * \int_{v=0}^{v=V_h} \frac{\rho}{2} * W^2 . dV \quad (2.19)$$

where W describes the instantaneous velocity in the intake valve gap induced by the instantaneous piston velocity $C_{(\alpha)}$:

$$W = W_{(\alpha)} = W_m * \frac{C_{(\alpha)}}{C_m} * \frac{1}{C_F} \quad (2.20)$$

Substituting equation (2. 8) into equation (2. 20) yields:

$$W = W_m * \pi * \frac{dz_{(\alpha)}}{d\alpha} * \frac{1}{C_F} \quad (2.21)$$

Equating equation (2. 18) and equation (2. 19) with the help of equation (2. 4) and equation (2. 21) results in the following expression:

$$\frac{1}{(C_F)_m^2} = \pi^2 * \int_{\alpha=0}^{\alpha=\pi} \left(\frac{dz_{(\alpha)}}{d\alpha} \right)^3 * \left(\frac{1}{C_F} \right)^2 . d\alpha \quad (2.22)$$

Rearranging equation (2. 22) yields:

$$(C_F)_m = \frac{1}{\pi} * \frac{1}{\sqrt{\int_0^\pi \left(\frac{dz_{(\alpha)}}{d\alpha} \right)^3 * \left(\frac{1}{C_F} \right)^2 . d\alpha}} \quad (2.23)$$

or by considering equation (2. 23):

$$(C_F)_m = \frac{1}{\sqrt{\frac{1}{\pi} * \int_0^\pi \left(\frac{C_{(\alpha)}}{C_m} \right)^3 * \left(\frac{1}{C_F} \right)^2 . d\alpha}} \quad (2.24)$$

where $\frac{C(\alpha)}{C_m}$ is computed from equation (2. 11) for each valve lift displacement and C_F is obtained by measurements.

The ratio of the integrals is evaluated using the method of Simpson's numerical integration explained below.

2.3.2.3 Layout of the simpson's rule for numerical integration:

This method explains the principles in finding the area under a curve of a pre-defined function by approximating that curve with a series of parabolic segments lying above the intervals $[x_{k-1}, x_k]_{k=1}^{2m}$, assuming the utilization of several parabolic functions for the numerical integration [32].

Considering the function

$$y = f(x) \text{ over } [a, b] \quad (2. 25)$$

Supposing that the interval $[a, b]$ is divided into $2m$ segments $[x_{k-1}, x_k]_{k=1}^{2m}$ of equal width $h = \frac{b-a}{2m}$ utilizing the equally spaced sample points $x_k = x_0 + k.h$ for $k=0, 1, 2, \dots, 2m$. The numerical integration can be denoted with the following relation:

$$S_{(f,h)} = \left[\frac{h}{3} * (f_a + f_b) \right] + \frac{2h}{3} \sum_{k=1}^{m-1} f_{(x_{2k})} + \frac{4h}{3} \sum_{k=1}^m f_{(x_{2k-1})} \quad (2. 26)$$

It is however good to recall that such an integration method involves a remainder term E_s such as:

$$E_{S_{(f,h)}} = -\frac{(b-a) \cdot f^{(c)} * h^4}{180} \quad (2. 27)$$

where $a < c < b$ and $c \in [a, b]$.

2.3.3 Outcomes of the repeatability and reproducibility checks

In order to evaluate the repeatability and reproducibility of experimental measurements conducted throughout this investigation; several measurements are carried out.

One of the most important factors affecting the measurements is the level of humidity and temperature under which the test is proceeding. This can be explained through the variation of the ambient air's density according to the level of humidity and temperature.

Therefore, in order to assess the variation of these parameters, a set of three measurements of flow and induced vane speed (as an indicator of the swirl level) were conducted. Afterwards, another set of measurement has been carried out to evaluate the reproducibility of the experimental measurement under the same conditions, which mean, in other words, that the initial conditions such as temperature and relative humidity percentage are being restored to a reference value prior each measurement of flow rate and induced torque.

The measurements are summarized with Table 2. 2, where humidity and temperature level, measured flow coefficient and measured induced swirl ratio (defining the turbulence level) have been recorded. Measurements are taken at a constant pressure drop across the intake ports.

Table 2. 2: Flow and induced swirl measurements.

Measurements	Humidity [%]	Temperature [°C]	Measured Flow Coefficient [-]	Measured Induced Swirl Ratio [-]
SET 1	51,9	29,3	0.365	1.479
	51	29,8	0.363	1.485
	49,2	30,2	0.365	1.522
SET 2	50	30	0.365	1.492
			0.365	1.503
			0.365	1.512

As stated on Table 2. 2: Flow and induced swirl measurements. , the swirl generation of this cylinder head measured at 30°C and 50% of humidity is recalled as 1.5 swirl ratio and 0.365 flow coefficient. The numbers are well reproduced throughout the sets of measurements.

From Table 2.1, it can clearly be noted that the values of measured flow coefficient and induced swirl ratio do not change in function of humidity and temperature.

Although the measured values fluctuate around 1.5%, the measurement process is considered stable throughout the study and investigations, considering the same cylinder head.

3. CYLINDER HEAD SPECIFICATIONS

3.1 Basic Engine Properties

The volume displacement of the engine is 2.2 liters, and the engine falls in the TDCI (Turbo Diesel Common-rail Injection) engine classification. It is mentioned in the previous chapter that the engine is powering a typical passenger vehicle, of which the emission regulations and standards fall into the specifications illustrated on Figure 1. 2.

Layout properties of the engine are summarized in Table 3. 1 represented below.

Table 3. 1: Engine layout property.

ENGINE FEATURES	
Engine Architecture	In-line 4 Cylinder (2.2L) TDCI
Bore Diameter [mm]	86.015
Stroke Length [mm]	94.6
Valve Configuration	4 valves per cylinder (2 intake valves and 2 exhaust valves)
Maksimum Valve lift [mm]	7.645
Intake Valve Opening [°CA]	-325°
Intake Valve Closing [°CA]	-166°

3.2 Intake Port Models

Generally, the ports of the cylinder head should be as short as practicable [6, 33, 34]. Indeed, this requirement has emerged in order to avoid unnecessary heating transfer from the surrounding environments towards the air charge entering into the combustion chamber.

Restricted by packaging concerns, the internal combustion engines suitable for passenger cars and light commercial vehicles are limited in terms of volume of displacement. Consequently, a very limited number of fuel sprays are allowed for those small-size engines. This hence requires a higher mixture formation to achieve a good combustion performance. Such a configuration is hard to achieve with conventional intake port geometries. As a result, a combination of two different intake ports arouses.

The intake ports of the engine cylinder head consist of two different ports: one straight (or tangential) intake port, which is also addressed as long intake port in the following sections, and one helical intake port which is also referred as long intake port in the following sections per engine cylinder [35]. Those ports are simultaneously opening and closing as the engine carries on its cranking cycle.

However, by means of experimental set-up bench, it is possible to actuate only either the short port (and its corresponding valve), the long port (and its corresponding valve) or both of the two ports so simulate in a closer way the intake stroke of the engine.

Long port is represented on Figure 3. 1 and short port is represented on Figure 3. 2 while the geometrical configuration of the combustion chamber is illustrated through the Figure 3. 3.

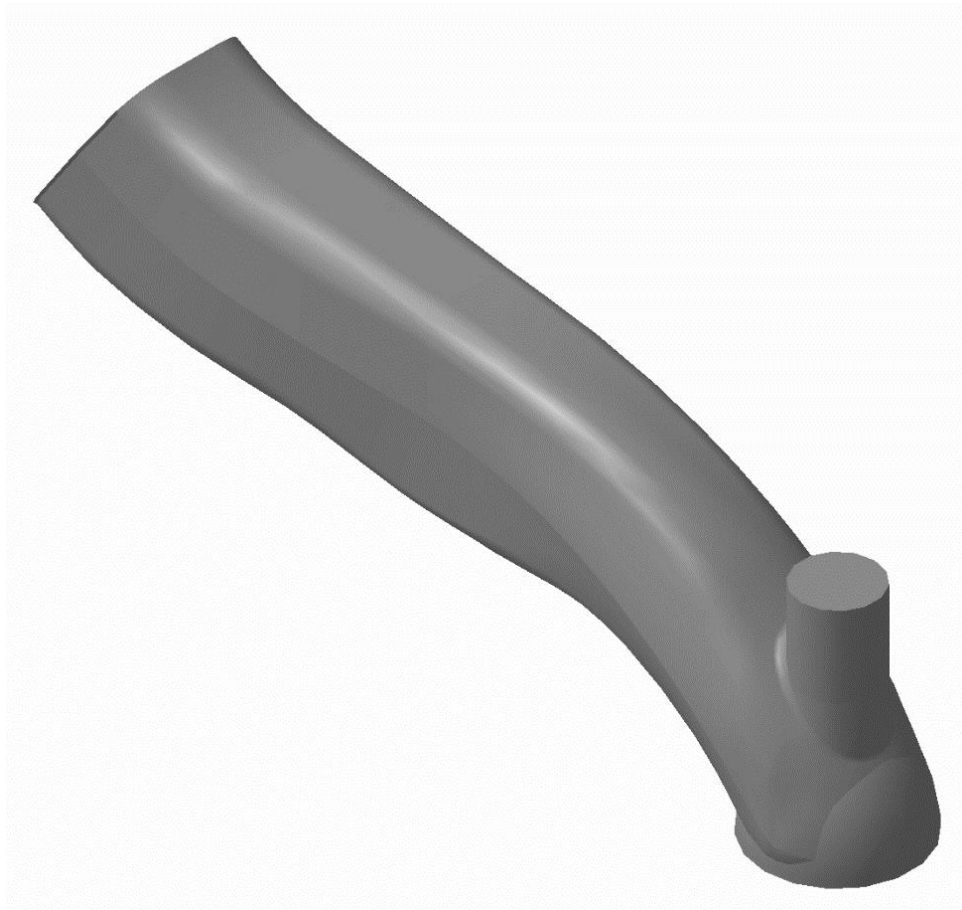


Figure 3. 1: Long port isometric view.

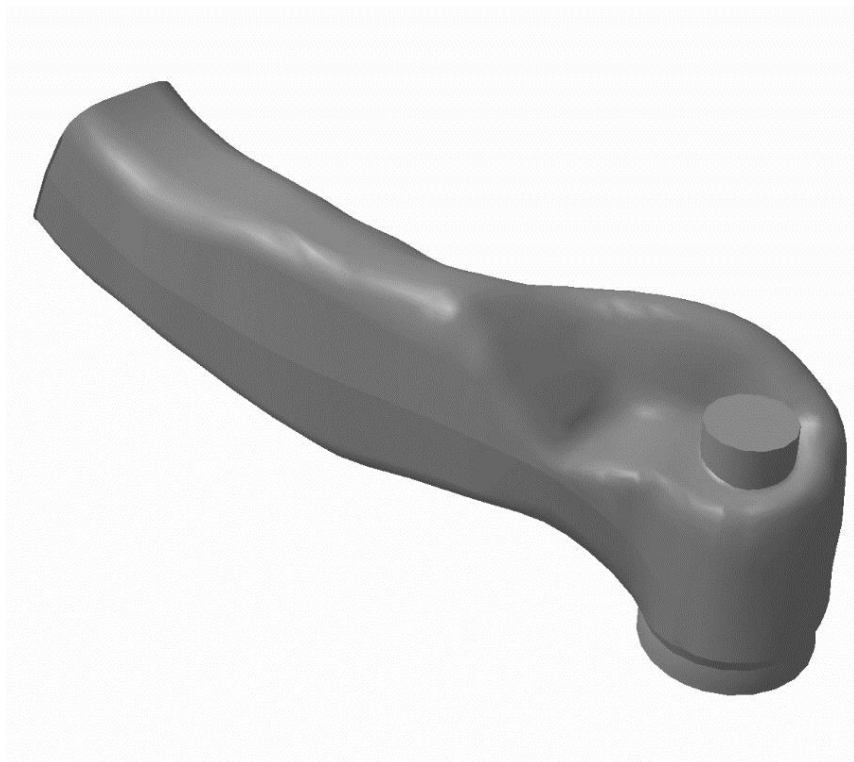


Figure 3. 2: Short port isometric view.



Figure 3. 3: Combustion chamber representation.

The main particularity of the straight port is that it allows a direct entrance of the air into the combustion chamber with smooth cross-sections and lowest flow restrictions. This functionality ensures that the airflow reaches the bottom boundary of the combustion chamber, which is delimited by the engine piston geometries. Otherwise, the helical intake port generates a rotary air motion as it enters the combustion chamber, resulting in a turbulent flux providing a better mixture of the fuel spray with the air imprisoned within the engine cylinder.

The design development of an engine cylinder head is a continuous compromise between having a rapid yet efficient mixture formation and increasing the engine performance [36]. It has been stated that the best way to achieve a rapid mixture is having a high level of turbulence however increasing the level of turbulence results inevitably to a loss of volumetric efficiency, which consequently decreases the power output of the engine through combustion. To overcome this issue, the air flux towards the combustion chamber must be kept as smooth as possible. Therefore, some more machining features have been added so as to better orientate the passage

of the air through the valves. Figure 3. 4 resumes the layout of the machining features while a detailed survey will be addressed a few sections later on this chapter.

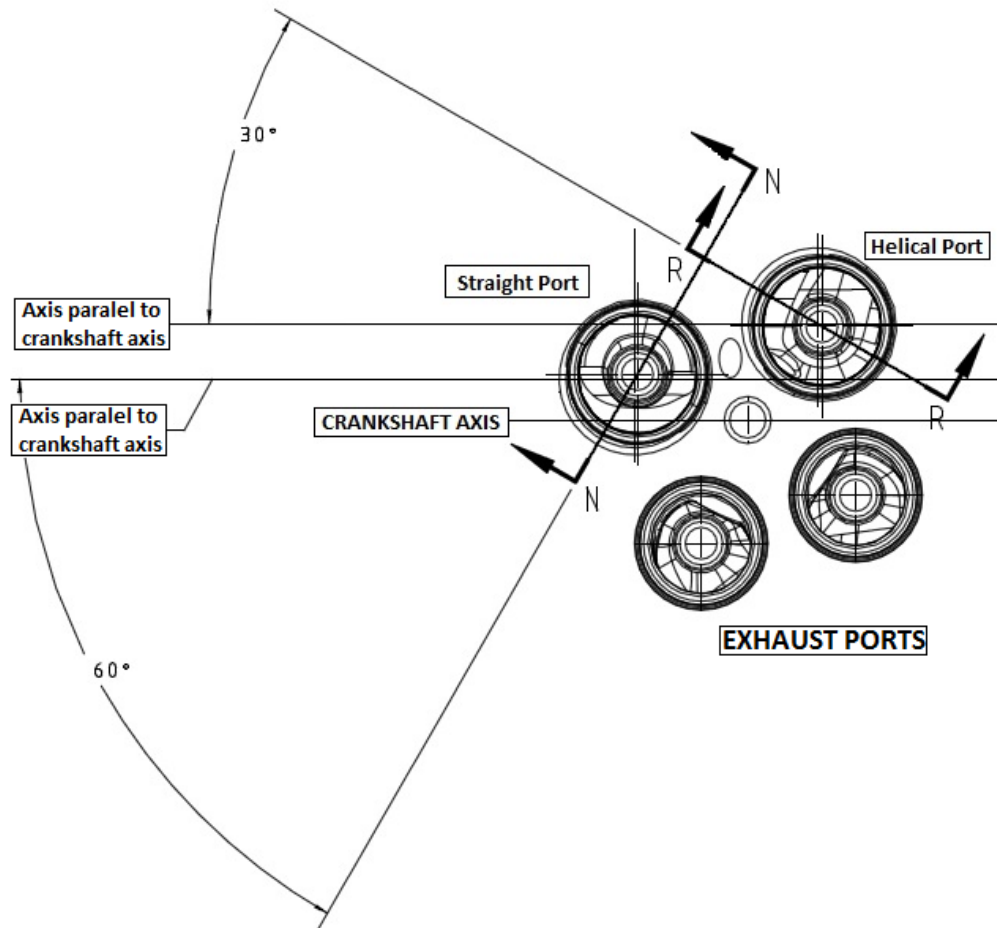


Figure 3. 4: Orientation of the intake airflow path into the combustion chamber.

3.3 Intake Seat Angles

The intake seat is the workpiece serving as an interface between the surface of the intake valve and the engine cylinder head. This workpiece is very important in terms of functionality since it supports the valve upon its closure, cools and also seals the valves. Basically, the design of an intake seat consists of three major sections: the throat, the seat and the top section of the intake seat component. The logic behind having three different sections over the intake seat geometry is to smoothen the passage of the air sucked into the combustion chamber as much as possible. Figure 3. 5 gives a better understanding of the different sections on the intake valve-seat. General practices and manufacturing considerations have defined the throating angle around 60 degrees, the seat angles around 60 degrees to 90 degrees and the topping

angle around 120 to 150 degrees [35]. Many more details about the design of intake valves and the intake seats are available but they are not the focus of this section, therefore the informations addressed throughout this survey are limited to basic notions.

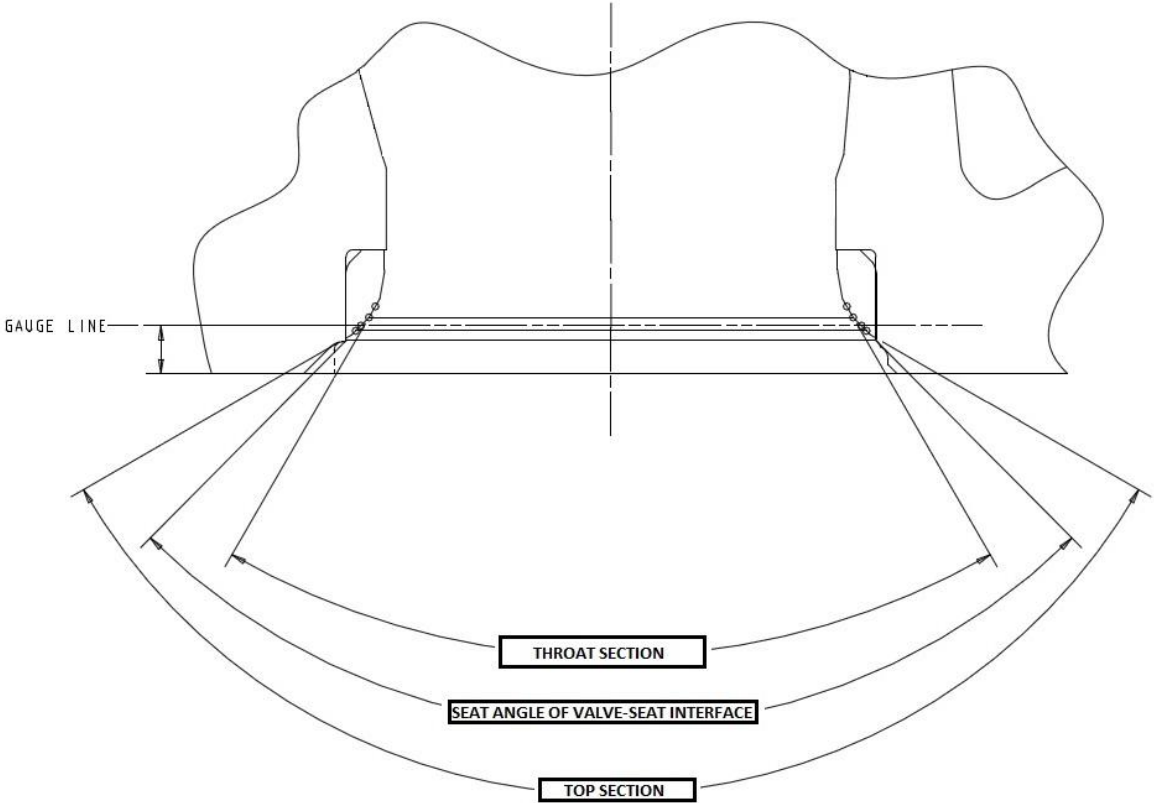


Figure 3. 5: Seat angle geometrical details.

3.4 Additional Chamfers (c-chamfer & s-chamfer)

To allow a more efficient orientation of the airflow past the valves and into the combustion chamber, some additional features can be implemented through accurate machining on some specific areas over the flame face of the cylinder head.

As overviewed on Figure 3. 4 through the section N-N or P-P, some additional features are easy to spot through the view from the valve flame faces. To give a better understanding on the issue, the section N-N of Figure 3. 4 is reproduced on Figure 3. 6 below; where half of the value of the respective angles were represented.

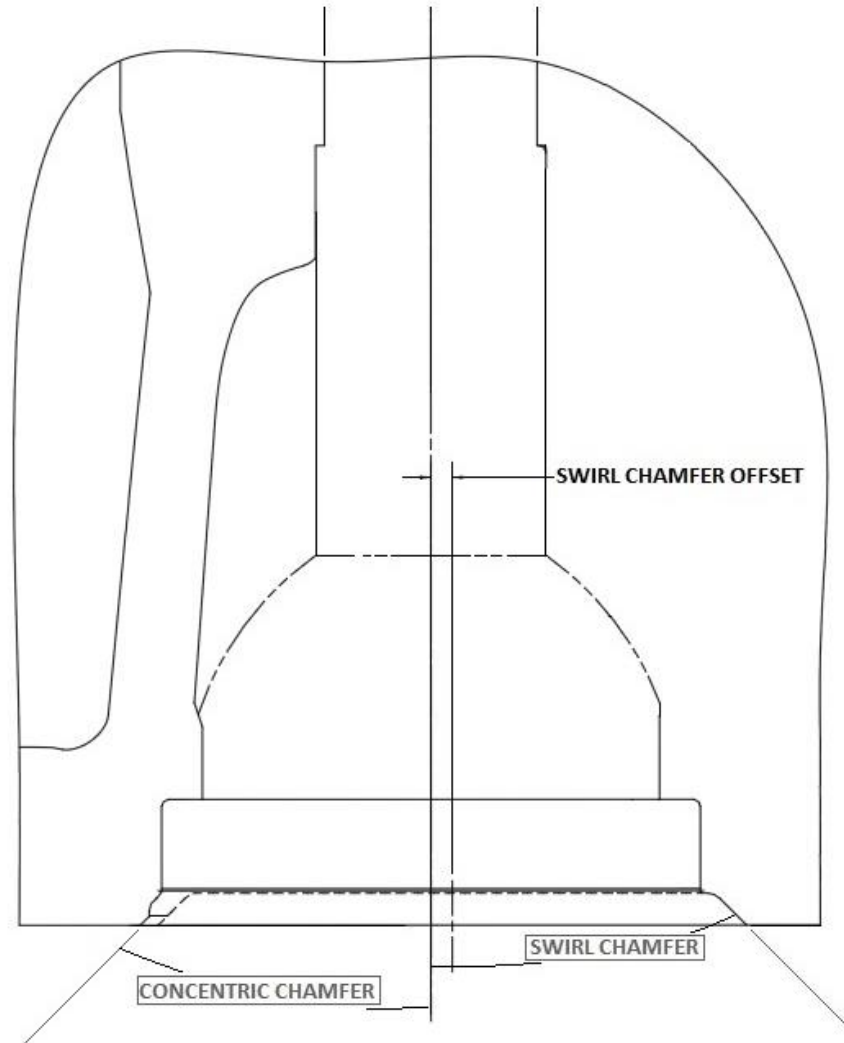


Figure 3. 6: Additional chamfers obtained through machining.

The additional machining aims to smoothen the airflow through inlet valves by imposing the minimum possible friction of the inducted air with the boundaries. A closer look at the chamfers reveals two different machining features: a concentric chamfer and an offset chamfer.

The concentric chamfer (which will be addressed as c-chamfer on the following sections) is implemented to the machined cylinder head. The purpose of such an action is to force the airflow passing through the valves to have a more tangential motion parallel to the combustion chamber axis. Meanwhile, the offset chamfer (which will be addressed as swirl chamfer or s-chamfer in the following sections) has been added to direct the flow to have a downstream pattern as tangential with the cylindrical wall as possible.

The effects of those additional chamfers on the induced swirl motion will be investigated through the further sections addressed on this report.

4. EXPERIMENTAL RESULTS

The physical and environmental boundaries were selected and tuned in order to define the basic properties of the turbulent flow in the combustion chamber. This is achieved with a simplified measurement under steady-state conditions as discussed at the former chapters.

Based on the test procedures detailed on Chapter 2. , several experimental measurements of the swirl numbers and flow coefficients have been conducted. A detailed calculation of the swirl ratio is available on Appendix A. Calculations were carried out using a software code written on Matlab Simulink and in terms of simplification perspectives, the calculated results are summarized through respective tables on this section.

The parameters; which are subjected of experimental measurements; are summarized on Table 4. 1, which shows the layout of the experimental operating conditions.

A separate study of the specific influence of the intake ports (respectively straight and helical intake port) on swirl generation is carried out. This is achieved on an incremental valve lift value. Through the same investigation, the intake port performance over the maximum valve lift value is analyzed.

The focus of the investigation will consist of analyzing the effect of the intake seat angle, the concentric chamfer angle, its depth and the swirl chamfer offset on the magnitude of the induced swirl. That investigation is conducted assuming the simultaneous actuation of both the straight intake valve and the helical intake valve, so as to efficiently approach and reproduce the engine breathing conditions.

Finally, the combination of the different machinings over the swirl generation will be investigated and analyzed.

Table 4. 1: Layout of the experimental operating conditions.

HEAD NUMBER	C-CHAMFER DEPTH	C-CHAMFER ANGLE	SWIRL CHAMFER OFFSET
1	0,6	120	1,2
2	0,4	90	1,2
3	0,65	120	1,2
4	0	0	1,2
5	0,65	120	1,2
6	0,65	120	1,2
7	0,65	120	1,2
8	0	0	1,2
9	0	0	1,2
10	0,6	90	1,2
11	0,45	90	1,2
12	0,5	90	1,2
13	0,5	90	1,2
14	0	0	1,2
14_bis	0,3	90	1,2
15	0,3	90	1,2
16	0,2	90	1,2
17	0,2	90	1,2
20	0,5	90	1,4
21	0,5	120	1,6
23	0,5	120	1,6
24	0,7	120	1,4
25	0,7	120	1,6
27	0,7	120	1,6
28	0,7	120	1,6
30	0,55	90	1,2
31	0,5	90	1,2
32	0,7	120	1,2
33	0,5	90	1,4
34	0,5	90	1,4
35	0,5	90	1,4
36	0,55	90	1,2
38	0,7	120	1,2
39	0,7	120	1,6
40	0,7	120	1,6
41	0	0	0,8
42	0	0	0,8
43	0,3	120	1,2
44	0,5	120	1,2

4.1 Specific Swirl Generation of the Intake Ports

A special cylinder head was used to measure the effect of the intake ports on the generated swirl magnitude. The configuration of that cylinder head is as follow:

- Seat Angle: 45°,
- Concentric Chamfer Depth: 0.60 [mm],
- Concentric Chamfer Angle: 120 °,
- Swirl Chamfer Offset: 1,2 [mm].

The swirl chamfer depth details are not given in this section since it is not an easy parameter to change, so the value of the other details of the swirl chamfer is kept constant as follow throughout the entire investigation:

- Swirl Chamfer Depth: 1.80 [mm],
- Concentric Chamfer Angle: 90 °.

4.1.1 Straight (long) intake port swirl generation

Figure 4. 1 shows the influence of the long (or straight or also tangential) intake port on swirl generation, based on measurements taken from the cylinder head, Figure 4. 2 otherwise, points out to the corresponding induced flow coefficient.

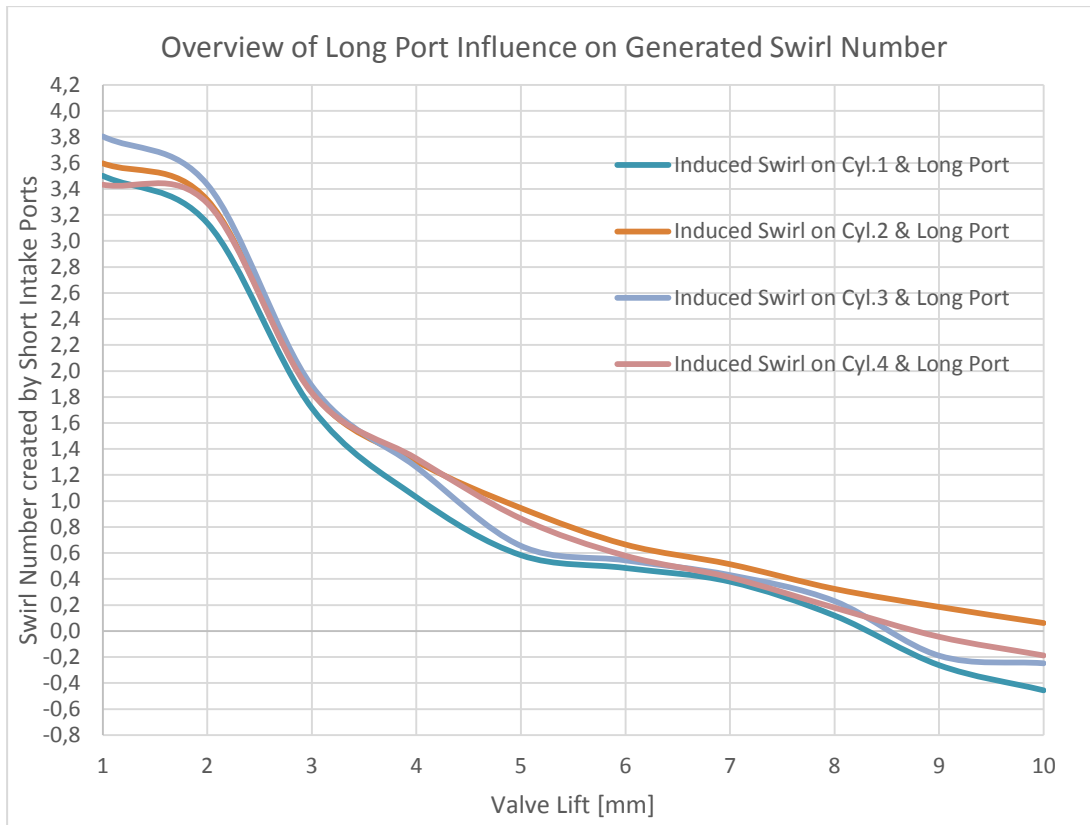


Figure 4. 1: Swirl generation of the long intake ports.

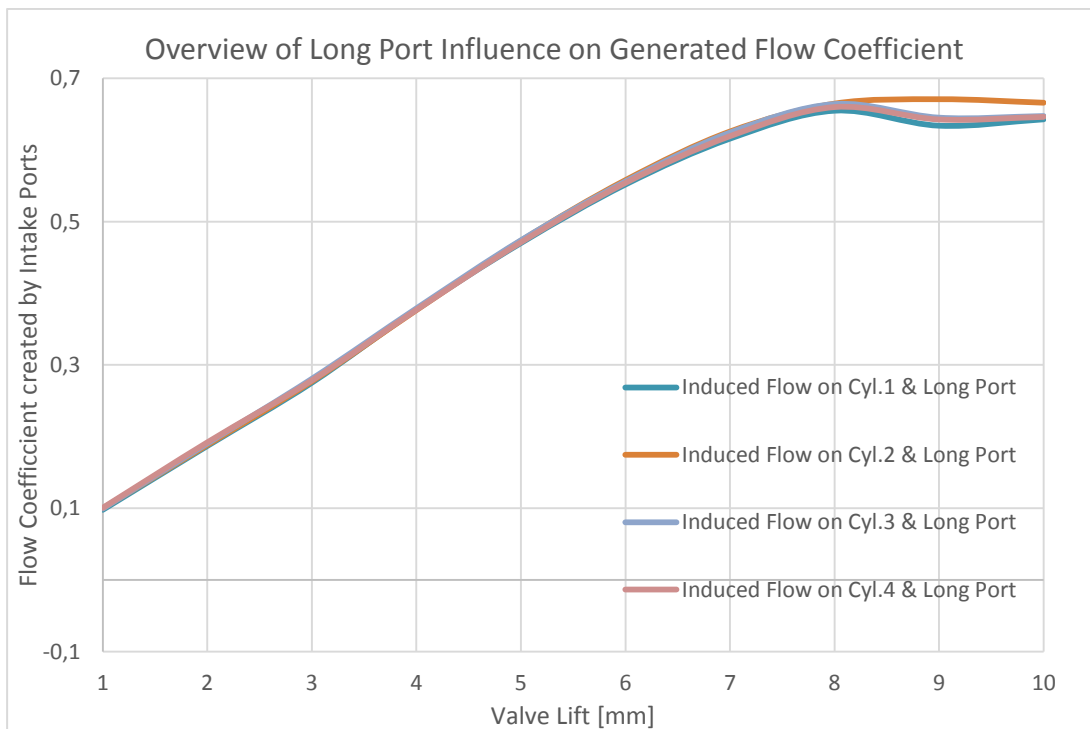


Figure 4. 2: Flow performance of the long intake ports.

The numerical values of the generated swirl numbers, the flow coefficient and the overall swirl ratio of Head#1 are summarized in Table 4. 2.

It can clearly be seen from Figure ... that high swirl number is produced at low valve lifts. One can observe a very sharp decrease in terms of swirl generation until the valve lift reaches 4mm depth, and then the decrease is a little slighter at bigger valve lifts. The decrease in terms of swirl generation is quite consistant with respect to each cylinder.

Table 4. 2: Measurement results on long ports from Head # 1.

LONG PORT ONLY	Head # 1							
	Swirl Number	Flow Coeff.	Swirl Number	Flow Coeff.	Swirl Number	Flow Coeff.	Swirl Number	Flow Coeff.
Valve Lift	Cyl.1		Cyl.2		Cyl.3		Cyl.4	
1	3,483	0,099	3,859	0,101	3,610	0,100	3,373	0,098
2	3,308	0,192	3,327	0,191	3,330	0,192	3,183	0,188
3	1,842	0,281	1,904	0,280	1,831	0,280	1,782	0,276
4	1,179	0,382	1,240	0,381	1,169	0,382	1,178	0,374
5	0,677	0,478	0,641	0,477	0,552	0,476	0,773	0,467
6	0,505	0,561	0,603	0,559	0,465	0,559	0,457	0,549
7	0,385	0,627	0,458	0,627	0,313	0,626	0,363	0,611
8	0,138	0,664	0,294	0,667	0,144	0,665	0,156	0,650
9	-0,288	0,640	-0,059	0,657	-0,165	0,641	-0,271	0,631
10	-0,276	0,649	-0,087	0,646	-0,210	0,648	-0,431	0,641
Swirl Ratio	0,692		0,763		0,613		0,681	
Overall Swirl Ratio	0,687							
Flow Coeff.	0,392		0,391		0,391		0,382	
Overall Flow Coeff.	0,389							

From Figure (swirl variation against valve lift), one can note that there is a fluctuation between each cylinder, due to the casting variation. Nevertheless, the overall generated swirl ratio is around 0.69 which is a low value. From the data shown on Table 4. 2, it can be then deducted that moderate level of swirl is generated at low valve lift values but this turbulent motion is cancelled out as the valve continues its opening. Moreover, a closer look at the swirl number values at high

valve lifts allows spotting that the generated swirl tends to be equal to zero and even turns out to be of a negative value at valve lifts beyond the maximum opening. This is interpreted as a reversing of the direction of the turbulent motion within the combustion chamber. This is not observed at real conditions since the intake valves do not exceed its maximum value of 7.645 mm but gives only notion about the flow behavior as the extension of the investigation.

A similar remark can be deduced with respect to the flow coefficient shown on Figure 4. 2, which increases with a more or less constant gradient until the maximum valve lift value, and stabilizes or slightly decreases beyond the maximum lift value.

4.1.2 Helical (short) intake port swirl generation

The influence of the helical (or short) intake ports on swirl generation and the corresponding flow coefficient are represented respectively on Figure 4. 3 and Figure 4. 4 . Numerical values extracted from experimental measurements are regrouped on Table 4. 3.

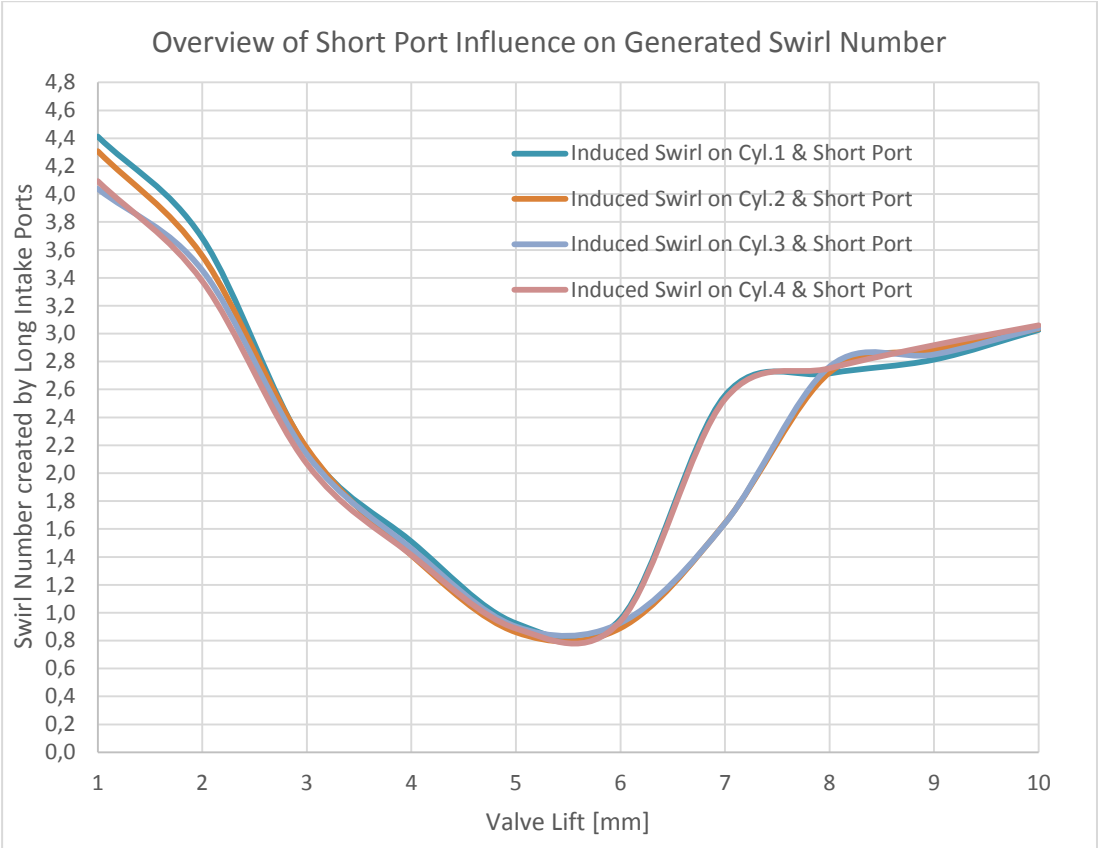


Figure 4. 3: Swirl generation of the short intake ports.

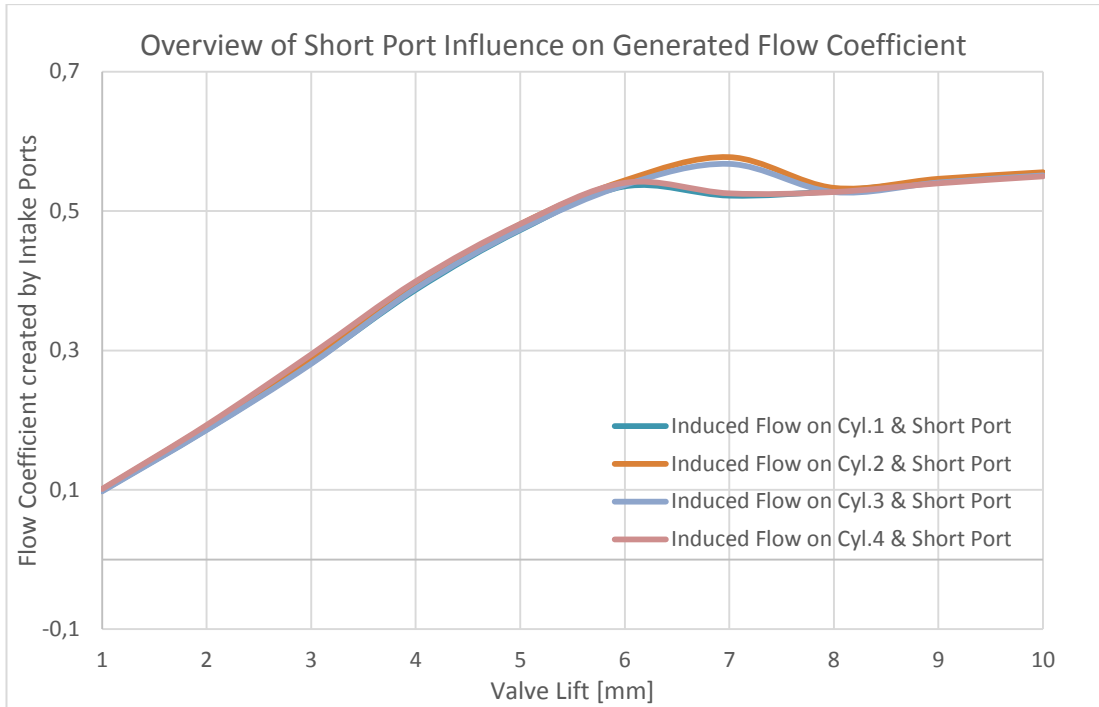


Figure 4. 4: Flow performance of the short intake ports.

Table 4. 3: Measurement results on short ports from Head # 1.

SHORT PORT ONLY	Head # 1							
	Swirl Number	Flow Coeff.	Swirl Number	Flow Coeff.	Swirl Number	Flow Coeff.	Swirl Number	Flow Coeff.
Valve Lift	Cyl.1		Cyl.2		Cyl.3		Cyl.4	
1	4,412	0,099	4,307	0,100	4,038	0,098	4,093	0,101
2	3,684	0,187	3,557	0,191	3,454	0,186	3,375	0,193
3	2,172	0,282	2,180	0,286	2,134	0,281	2,067	0,294
4	1,510	0,387	1,412	0,393	1,460	0,389	1,414	0,399
5	0,924	0,473	0,860	0,481	0,901	0,474	0,887	0,481
6	0,955	0,535	0,890	0,544	0,927	0,537	0,939	0,541
7	2,556	0,522	1,643	0,577	1,641	0,568	2,531	0,525
8	2,715	0,529	2,722	0,533	2,763	0,527	2,752	0,527
9	2,814	0,543	2,884	0,546	2,850	0,541	2,917	0,540
10	3,027	0,554	3,035	0,556	3,039	0,551	3,059	0,550
Swirl Ratio	2,742		1,895		1,893		2,693	
Overall Swirl Ratio	2,306							
Flow Coeff.	0,351		0,376		0,369		0,356	
Overall Flow Coeff.	0,363							

In contrast with the swirl generation of the short ports, the helical intake ports generate a higher swirl value than the straight ports. However, the decrease in swirl generation is sharper and it reaches a minimum value prior the maximum lift, around 5.7 mm of valve lift then starts to increase again with a sharper slope until around 7mm of valve lift then it continues to increase but with a slighter slope for valve lifts beyond its maximum displacement of 7.645 mm. Similarly, the flow coefficient also increases with a constant slope until a valve lift of around 7mm where it continues to increase with a slighter slope.

Those phenomena are reflecting the fact that for the helical port, the swirling flow decreases as the gap between the intake valve and the intake seat increases, but still, the valve and seat geometries are dominant in determining the nature of the flow, resulting in a high swirling motion at low valve - seat area and high transition velocity. As the valve continues its opening, the swirl production decreases with the increase of the area, until a value of lift around 7mm as the effect of the interface geometries fades out. Then the swirl number starts to rise again since at high valve lifts, the airflow adopt a behavior of a solid body turning around the valve axis.

Variations from one cylinder to another are observed on Figure 4. 3 and Figure 4. 4, affecting the specific value of swirl ratio at its respective valve lift. This is interpreted as the variation yield by the manufacturing processes such as casting surface qualities and locations.

4.1.3 Swirl generation resulting from simultaneous actuation of the intake valves

Based on the measurement datasets taken from a simultaneous actuation of the intake valves, one can see the consistency of the swirl and corresponding flow coefficient graphics against the valve displacement. Numerical data are represented on Table 4. 4 and the variations of induced swirl and flow coefficient with respect to the valve lifts are described through Figure 4. 5 and Figure 4. 6.

Table 4. 4: Measurement results on both ports from Head # 1.

BOTH PORTS	Head # 1							
	Swirl Number	Flow Coeff.	Swirl Number	Flow Coeff.	Swirl Number	Flow Coeff.	Swirl Number	Flow Coeff.
Valve Lift	Cyl.1		Cyl.2		Cyl.3		Cyl.4	
1	3,130	0,094	3,264	0,096	2,824	0,095	3,334	0,095
2	2,549	0,185	2,433	0,189	2,528	0,189	2,528	0,189
3	1,374	0,278	1,484	0,280	1,432	0,281	1,452	0,279
4	0,998	0,383	1,042	0,386	0,963	0,385	1,023	0,384
5	0,954	0,468	1,025	0,471	0,956	0,471	0,979	0,469
6	1,189	0,522	1,281	0,523	1,200	0,524	1,270	0,520
7	1,161	0,568	1,274	0,567	1,185	0,568	1,250	0,563
8	1,075	0,589	1,201	0,596	1,171	0,596	1,144	0,594
9	1,019	0,605	1,098	0,607	1,060	0,607	1,046	0,606
10	1,047	0,619	1,094	0,621	1,076	0,621	1,066	0,620
Swirl Ratio	1,356		1,473		1,373		1,445	
Overall Swirl Ratio	1,412							
Flow Coeff.	0,367		0,368		0,369		0,367	
Overall Flow Coeff.	0,368							

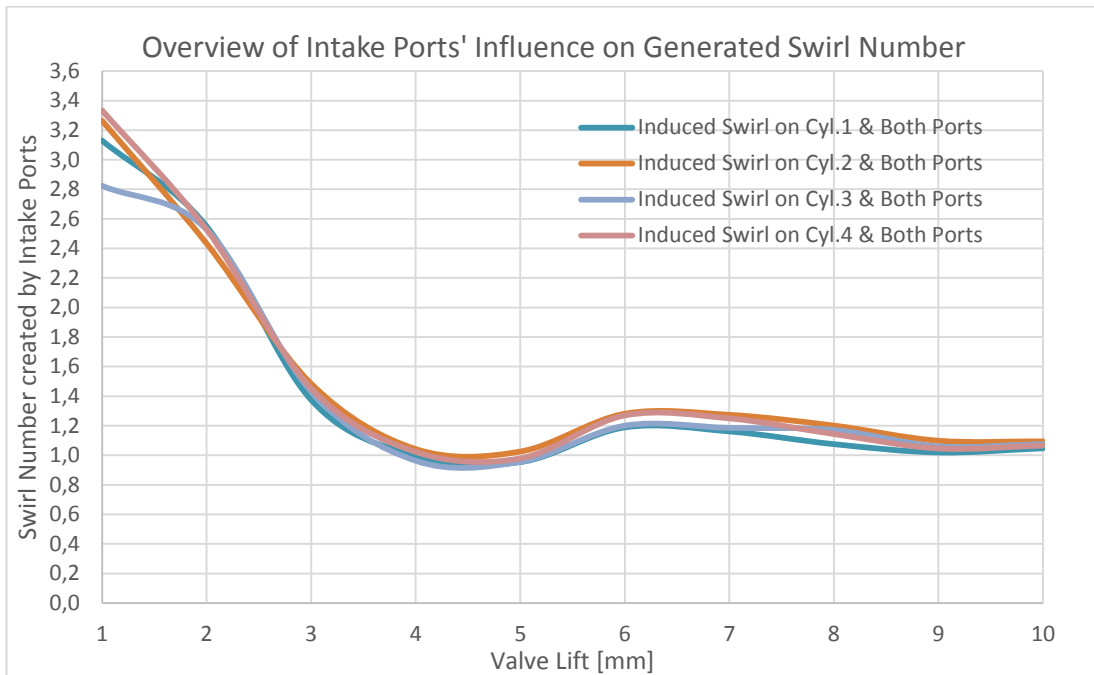


Figure 4. 5: Swirl generation of the both of intake ports.

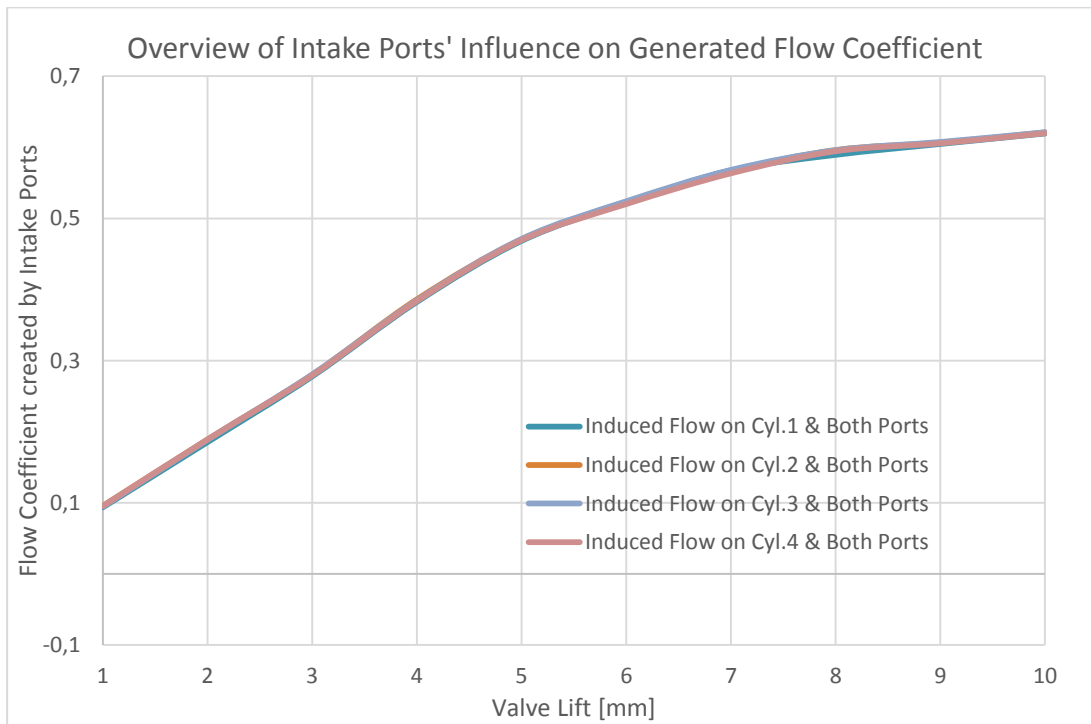


Figure 4. 6: Flow performance of the both of intake ports.

The variations of the swirl number and the flow coefficient respectively by the short ports, the long ports and the simultaneously actuated ports are being superposed in one swirl graphic on Figure 4. 7 and one flow coefficient graphic on Figure 4. 8 in order to facilitate the comparison of the effects of each intake port.

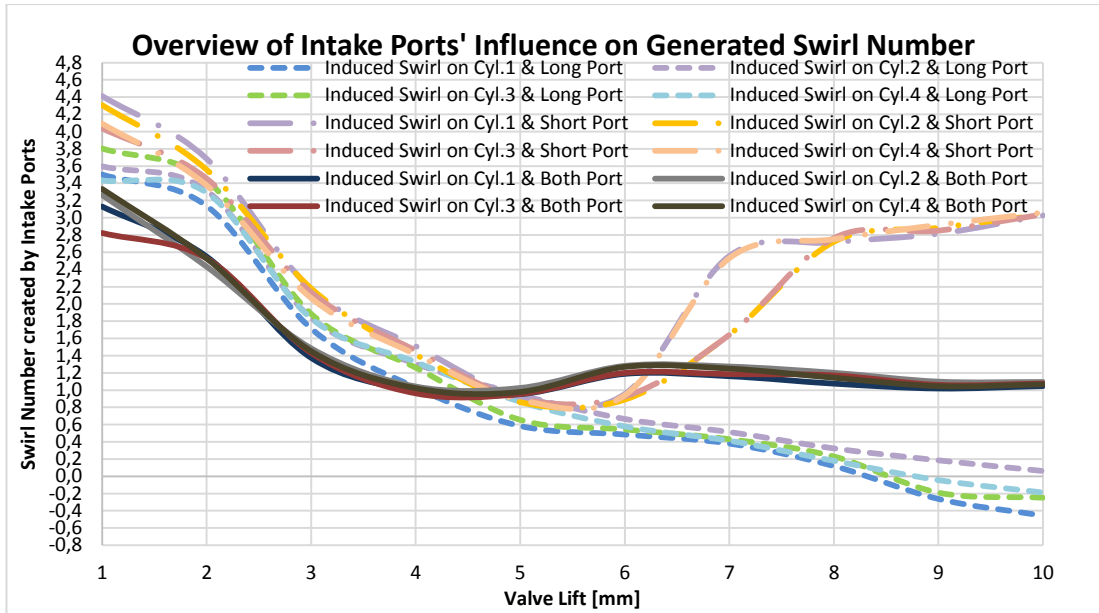


Figure 4. 7: Synopsis of the swirl generation between short and long ports.

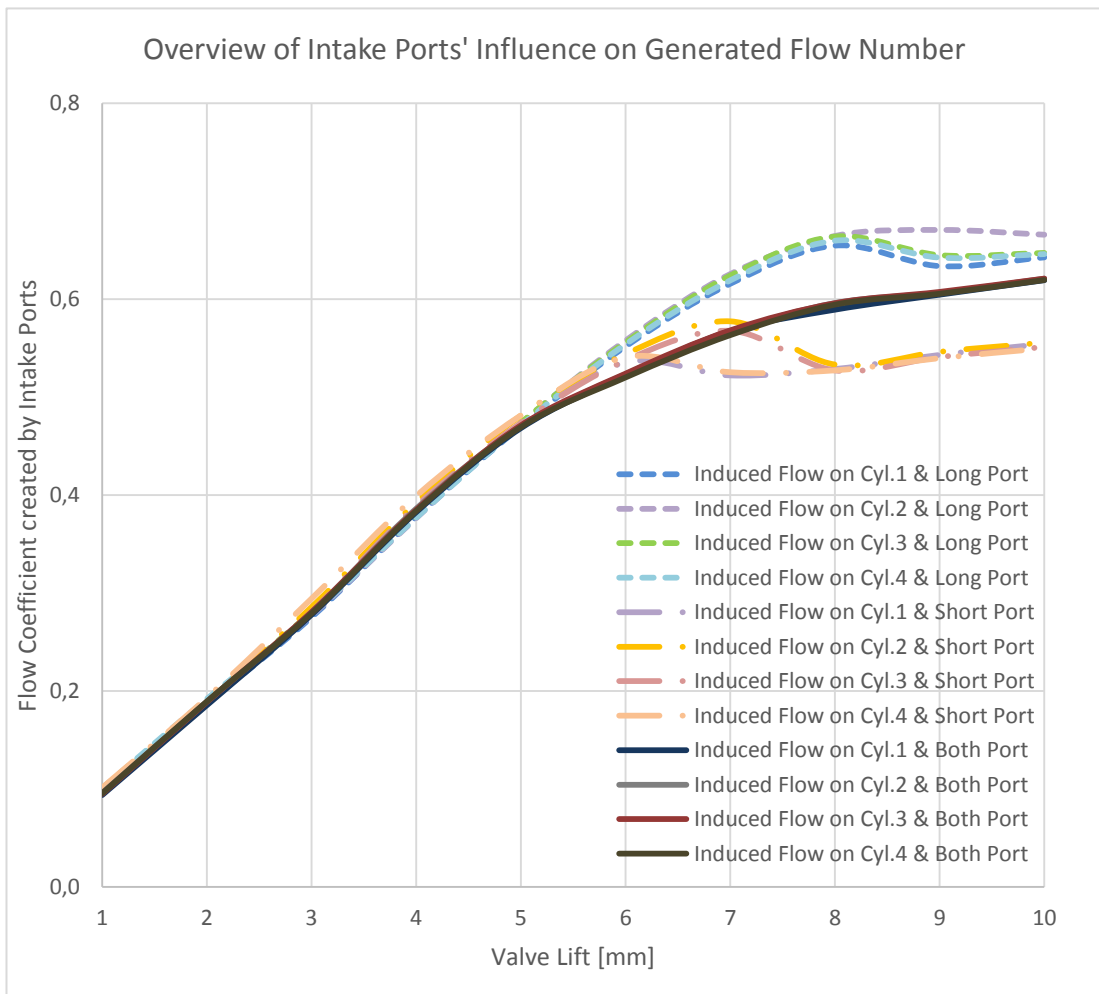


Figure 4. 8: Synopsis of the flow performance between short and long ports.

As seen on Figure 4. 7, the value of the swirl generation at low valve values when both the two valves are opened is below the swirl number generated by each respective intake port. Therefore one can deduce that the swirl generated by straight and helical intake port cancel out each other at low valve lift, then at around 5mm of lift, the long (or tangential) port tend to increase the overall swirl production and finally the swirl number stabilizes beyond 7mm valve lift.

To summarize, one can note that the tangential port has more influence on the overall swirl generation at low valve lifts where the helical ports are more influent at higher valve lifts.

In the following sections, the assessments will be made based on a simultaneous actuation of the intake valves, and the overall swirl ratio generated will be the focus of discussion and evaluation.

4.2 Effects of the Depth of the Concentric Chamfer

To evaluate the effects of the depth of the concentric chamfer, the following cylinder head configuration is used:

- Seat Angle: 45°,
- Concentric Chamfer Depth: 0 [mm] for the first case (referred as Head#14) and 0.30 [mm] for the second case (referred as Head #14bis),
- Concentric Chamfer Angle: 90 ° for the second case as there is no chamfer for the first case study,
- Swirl Chamfer Offset: 1,2 [mm].

To eliminate the casting variations, care has been taken to evaluate the change induced by the c-chamfer depth variation on the same cylinder head for this case study. That is the reason for coding the case studies as Head#14 and Head#14bis, consisting of the same cylinder head.

Figure 4. 9 and Figure 4. 10 summarize the variation of respectively the generated swirl and the induced flow coefficient against valve lift displacements. Induced airflow still obeys the behavior stated above for the simultaneous actuation of the intake valves.

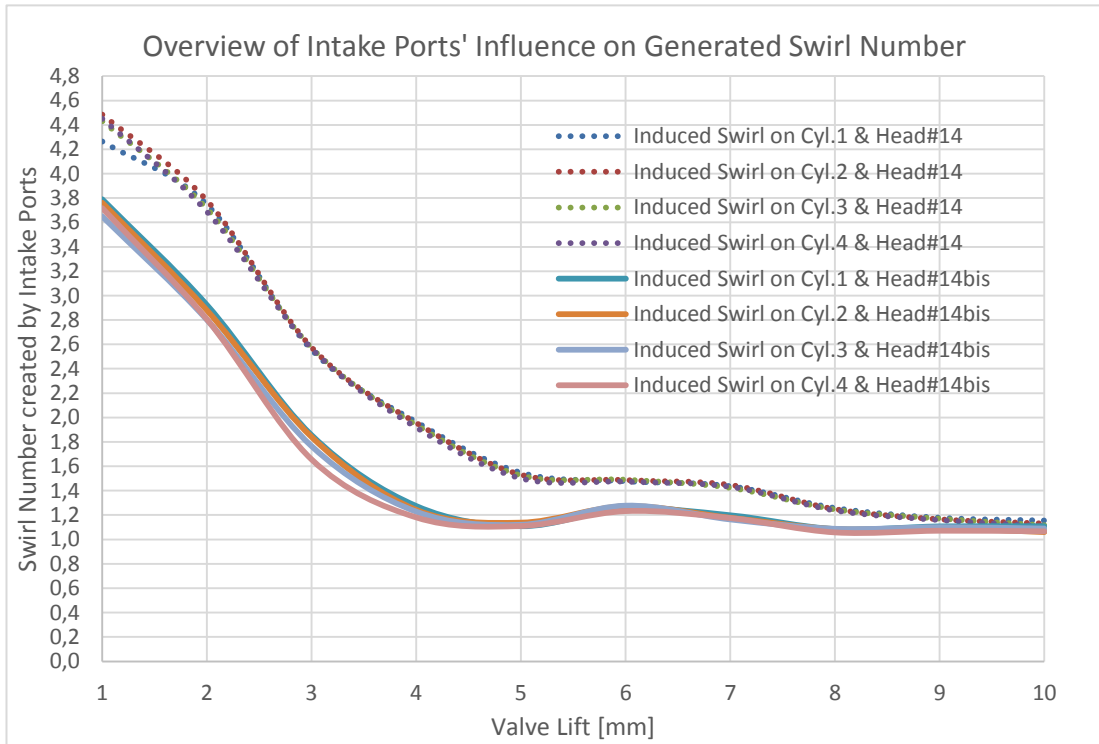


Figure 4. 9: Swirl generation of two different chamfer depths.

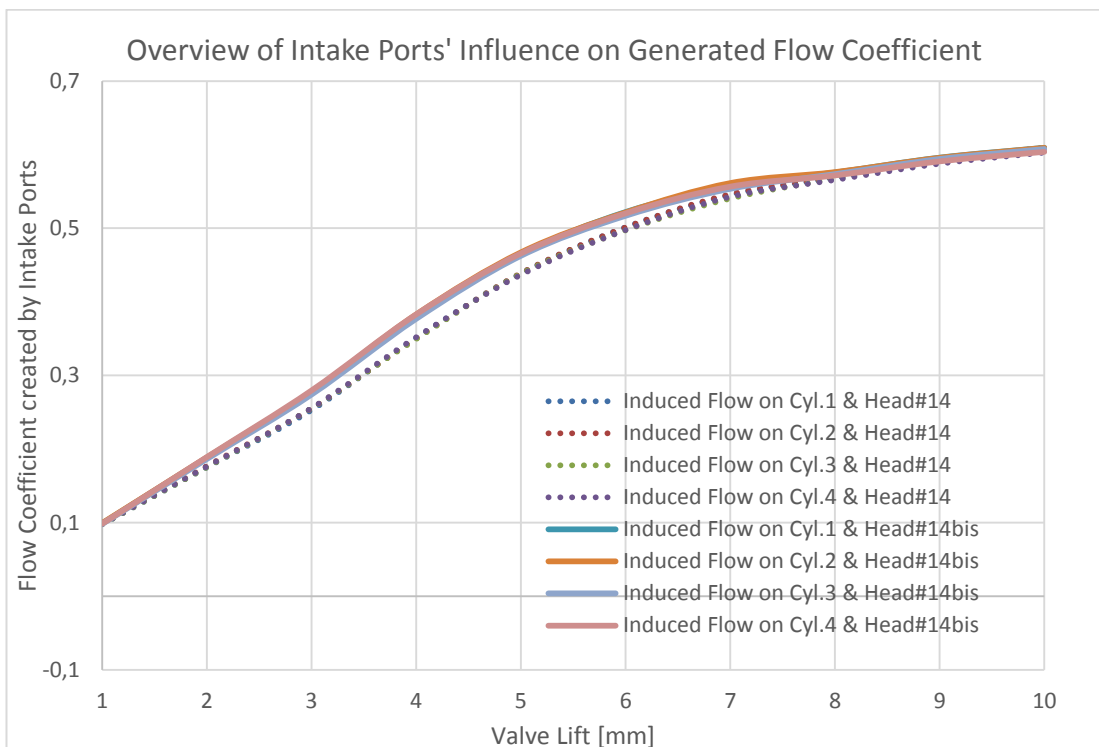


Figure 4. 10: Flow performance induced by two different chamfer depths.

Table 4. 5: Measurement results on two different c-chamfer depths.

BOTH PORTS	Head # 14 [ref_14 (No C-Chamfer)]								Head # 14bis [ref_14bis (0,30mm*45° C-Chamfer)]							
	Swirl Number	Flow Coeff.	Swirl Number	Flow Coeff.	Swirl Number	Flow Coeff.	Swirl Number	Flow Coeff.	Swirl Number	Flow Coeff.	Swirl Number	Flow Coeff.	Swirl Number	Flow Coeff.		
Valve Lift	Cyl.1		Cyl.2		Cyl.3		Cyl.4		Cyl.1		Cyl.2		Cyl.3		Cyl.4	
1	4,264	0,098	4,485	0,099	4,431	0,098	4,451	0,098	3,790	0,099	3,762	0,099	3,649	0,098	3,718	0,098
2	3,746	0,175	3,779	0,177	3,712	0,175	3,688	0,176	2,923	0,188	2,879	0,189	2,801	0,187	2,805	0,189
3	2,556	0,253	2,575	0,255	2,571	0,255	2,566	0,256	1,855	0,277	1,841	0,278	1,765	0,274	1,656	0,280
4	1,963	0,351	1,956	0,350	1,939	0,350	1,918	0,352	1,274	0,379	1,243	0,383	1,228	0,377	1,181	0,383
5	1,548	0,439	1,531	0,439	1,525	0,438	1,501	0,437	1,109	0,465	1,138	0,467	1,120	0,463	1,110	0,466
6	1,478	0,501	1,487	0,501	1,490	0,497	1,474	0,498	1,254	0,522	1,273	0,521	1,277	0,517	1,232	0,520
7	1,437	0,545	1,447	0,546	1,423	0,540	1,431	0,543	1,198	0,557	1,178	0,561	1,164	0,554	1,176	0,557
8	1,258	0,569	1,248	0,569	1,246	0,567	1,237	0,566	1,085	0,576	1,085	0,576	1,087	0,574	1,058	0,572
9	1,178	0,593	1,166	0,592	1,171	0,590	1,159	0,588	1,107	0,596	1,093	0,596	1,100	0,594	1,072	0,591
10	1,155	0,610	1,131	0,608	1,117	0,606	1,109	0,603	1,108	0,609	1,060	0,609	1,089	0,608	1,067	0,604
Swirl Ratio	1,832		1,843		1,817		1,821		1,465		1,446		1,423		1,427	
Overall Swirl Ratio	1,828								1,440							
Flow Coeff.	0,330		0,331		0,328		0,329		0,344		0,346		0,342		0,345	
Overall Flow Coeff.	0,330								0,344							

A drastic change can be observed through Table 4. 5 regarding the generated overall swirl ratio. On a cylinder head configured without C-Chamfer, the value is around 1,83 while it decreases up to 1,44 after implementing a 90 degrees concentric chamfer at 0,30mm depth. An extended measurement is taken on a serie of different cylinder heads in order to have a more accurate assessment on the effect of the c-chamfer depth onto the swirl generation. Measurement results are regrouped on Figure 4. 11 for the swirl ratio and Figure 4. 12 for flow coefficient generations. Measurement results are detailed on Appendix B.

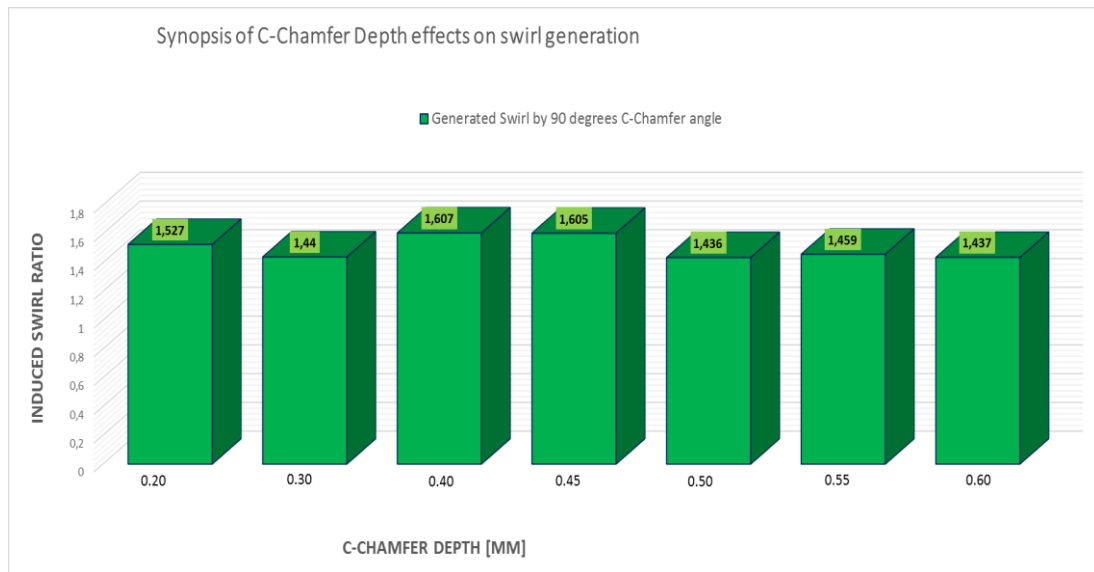


Figure 4. 11: Synopsis of swirl production through different c-chamfer depths.

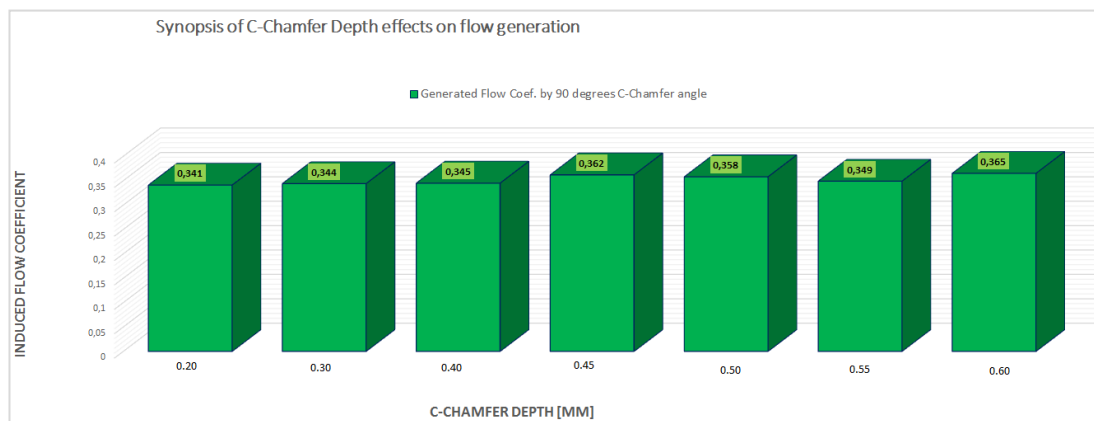


Figure 4. 12: Synopsis of flow performance through different c-chamfer depths.

In the serie of measurements achieved to assess the effect of the c-chamfer depth variation, the variable parameter is set to change between 0.20 mm through 0.70 mm.

As far as precise machining of the cylinder heads is concerned, measuring the offset of the c-chamfer depth is quite difficult even with the help of sophisticated measuring devices such as CMM's (Coordinate Measuring Machines). Therefore, experimental measurements could not be achieved on one specific cylinder head because of that difficulty. Instead, seven cylinder heads have been used to carry out the measurement process. Concentric chamfer depths are therefore set as 0.20mm, 0.30mm, 0.40mm, 0.45mm, 0.50mm, 0.55mm and 0.60mm respectively for the cylinder heads referred as follow: Head#16, Head#14bis, Head#2, Head#11, Head#13, Head#36 and Head#10.

The main drawback of the observation through those seven cylinder heads is that the following assessment would also include the variations induced by the manufacturing process, indeed the casting procedure.

Nevertheless, it is not challenging to note that despite the fluctuation spotted on Figure 4. 11, the swirl ratio production decreases as the c-chamfer depth increases. A special attention will be paid to this issue in the following chapter, where the analysis is based on a different point of view. Reciprocally, the flow coefficient is also adopting a rising trend along with the increase on concentric chamfer depth.

4.3 Effects of the Angle of the Concentric Chamfer

The effect of the concentric chamfer depth on the induced airflow and corresponding swirl generation being considered in the section above, there is also a need to assess the effect of the concentric chamfer angle, which is nothing but a complementary compound of the concentric chamfer depth itself, to the swirl and flow generation. Such an evaluation is addressed through this section of the survey.

To evaluate the influence of the concentric chamfer angle, the following cylinder head configuration is used:

- Seat Angle: 45°,
- Concentric Chamfer Depth: 0.30 mm for the first set of case study, 0.50 mm for the second set and 0.60mm for the third set of case study. The c-chamfer depth is kept at the same level for each different value of the c-chamfer angle.

- Concentric Chamfer Angle: 90° and separately 120° for each respective set of case study, making a lot of six studies in total.
- Swirl Chamfer Offset: 1,2 [mm].

The c-chamfer depth is kept at the same level for each different value of the c-chamfer angle. In contrast with the evaluation of the chamfer depth effect, casting variations cannot be disregarded because each configuration cannot be reproduced twice on the same cylinder head. The cylinder heads configurations used throughout this investigation are summarized in Table ... and the experimental measurement results are given in Appendix B, with respect to the reference given to the cylinder heads.

Table 4. 6: Cylinder head configurations illustrating c-chamfer angle variations.

C-CHAMFER DEPTH [mm]	C-CHAMFER ANGLE [°]	Head No: (Reference #)
0,6	90	10 (Retest_10)
0,6	120	1
0,5	90	31
0,5	120	44
0,3	90	14bis
0,3	120	43

Figure 4. 13 and Figure 4. 14 summarize the variation of respectively the generated swirl and the induced flow coefficient against valve lift displacements, given a chamfer depth of 0.30mm. Induced airflow still obeys the behavior stated above for the simultaneous actuation of the intake valves. Numerical measurement results are grouped through Table 4. 7 with 90° concentric chamfer angle configuration for Head #14bis and with 120° concentric chamfer angle configuration for Head#43.

Table 4. 7: Measurement results on two different c-chamfer angles.

BOTH PORTS	Head # 14_bis (0,30mm*90°)								Head # 43 (0,30mm*120°)							
	Swirl Number	Flow Coeff.	Swirl Number	Flow Coeff.	Swirl Number	Flow Coeff.	Swirl Number	Flow Coeff.	Swirl Number	Flow Coeff.	Swirl Number	Flow Coeff.	Swirl Number	Flow Coeff.		
Valve Lift	Cyl.1		Cyl.2		Cyl.3		Cyl.4		Cyl.1		Cyl.2		Cyl.3		Cyl.4	
1	3,790	0,099	3,762	0,099	3,649	0,098	3,718	0,098	4,127	0,097	3,696	0,098	3,888	0,099	3,829	0,099
2	2,923	0,188	2,879	0,189	2,801	0,187	2,805	0,189	3,186	0,184	2,512	0,185	3,187	0,185	3,162	0,187
3	1,855	0,277	1,841	0,278	1,765	0,274	1,656	0,280	2,185	0,271	2,145	0,272	2,100	0,273	2,116	0,274
4	1,274	0,379	1,243	0,383	1,228	0,377	1,181	0,383	1,571	0,370	1,551	0,369	1,499	0,368	1,494	0,372
5	1,109	0,465	1,138	0,467	1,120	0,463	1,110	0,466	1,271	0,457	1,279	0,456	1,267	0,459	1,264	0,457
6	1,254	0,522	1,273	0,521	1,277	0,517	1,232	0,520	1,362	0,513	1,338	0,511	1,368	0,514	1,338	0,513
7	1,198	0,557	1,178	0,561	1,164	0,554	1,176	0,557	1,300	0,555	1,297	0,555	1,311	0,560	1,290	0,558
8	1,085	0,576	1,085	0,576	1,087	0,574	1,058	0,572	1,135	0,573	1,131	0,578	1,141	0,583	1,183	0,583
9	1,107	0,596	1,093	0,596	1,100	0,594	1,072	0,591	1,119	0,592	1,095	0,597	1,090	0,599	1,107	0,600
10	1,108	0,609	1,060	0,609	1,089	0,608	1,067	0,604	1,091	0,606	1,076	0,613	1,087	0,615	1,091	0,616
Swirl Ratio	1,465		1,446		1,423		1,427		1,621		1,599		1,617		1,598	
Overall Swirl Ratio	1,440								1,609							
Flow Coeff.	0,344		0,346		0,342		0,345		0,340		0,340		0,342		0,343	
Overall Flow Coeff.	0,344								0,341							

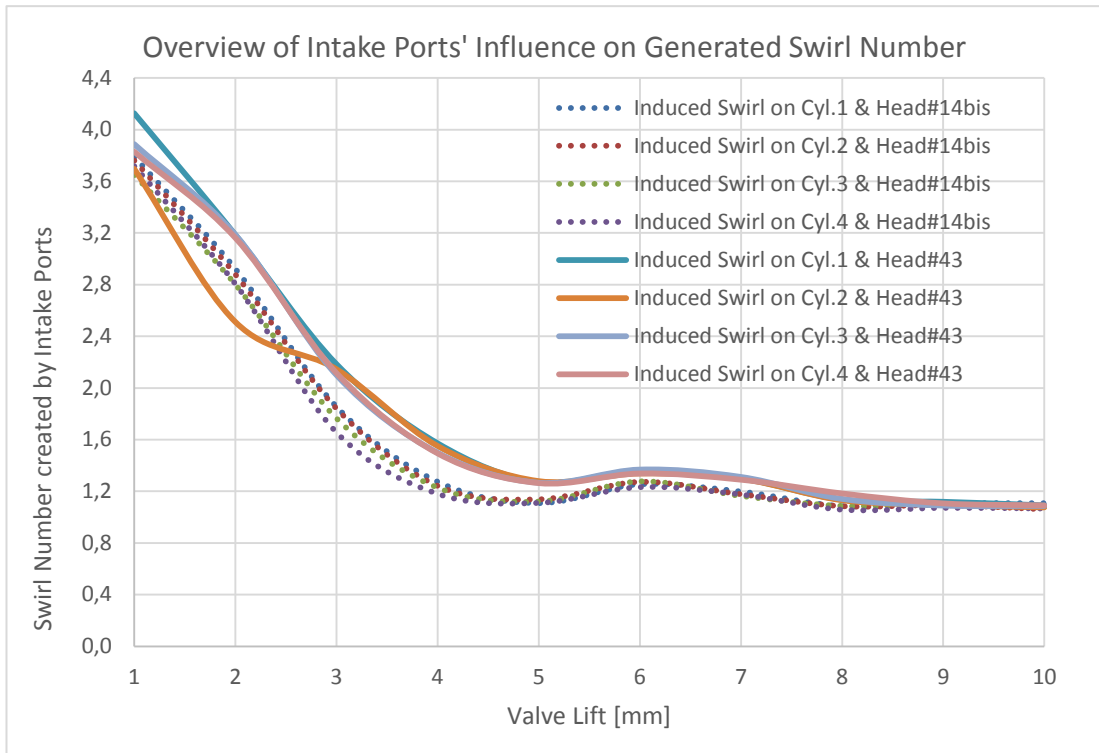


Figure 4. 13: Swirl generation of two different chamfer angles.

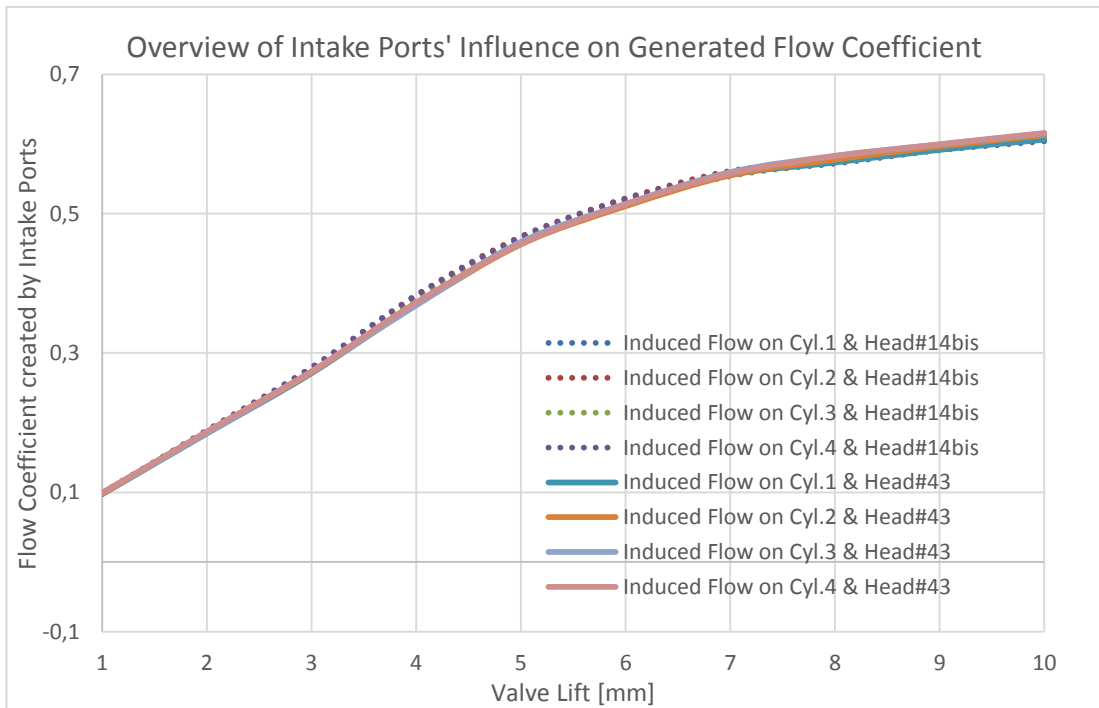


Figure 4. 14: Flow performance induced by two different chamfer angles.

As noted on Table 4. 7, there is a swirl production increase with the increase of the chamfer angle (from 1,440 to 1,609 overall swirl ratio). However, the flow is slightly affected by the chamfer angle (from 0.344 to 0.341 overall flow coefficient). An extended serie of measurements is also conducted with different cylinder heads, as defined on Table 4. 6, in order to evaluate the effect of the chamfer angle with specific depths on the overall flow and turbulent motion. Results of swirl generation and flow coefficients are represented respectively in Figure 4. 15 and Figure 4. 16 for the three specific case studies. Moreover, Figure 4. 13 demonstrates the impact of manufacturing process which leads to inconsistency between cylinder to cylinder swirl productions.

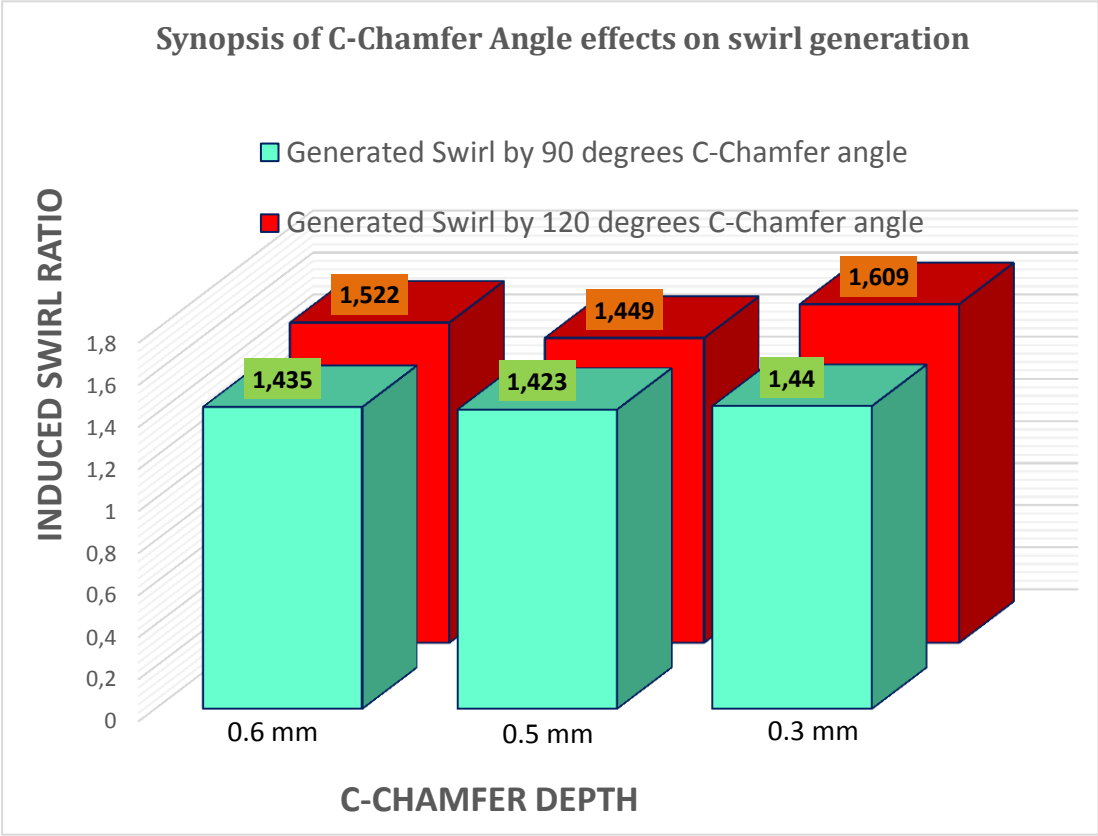


Figure 4. 15: Synopsis of c-chamfer angle effects on swirl generation.

From Figure 4. 15, it is quite evident to deduct that for the same value of concentric chamfer depth, an increase in the overall swirl ratio production is observed.

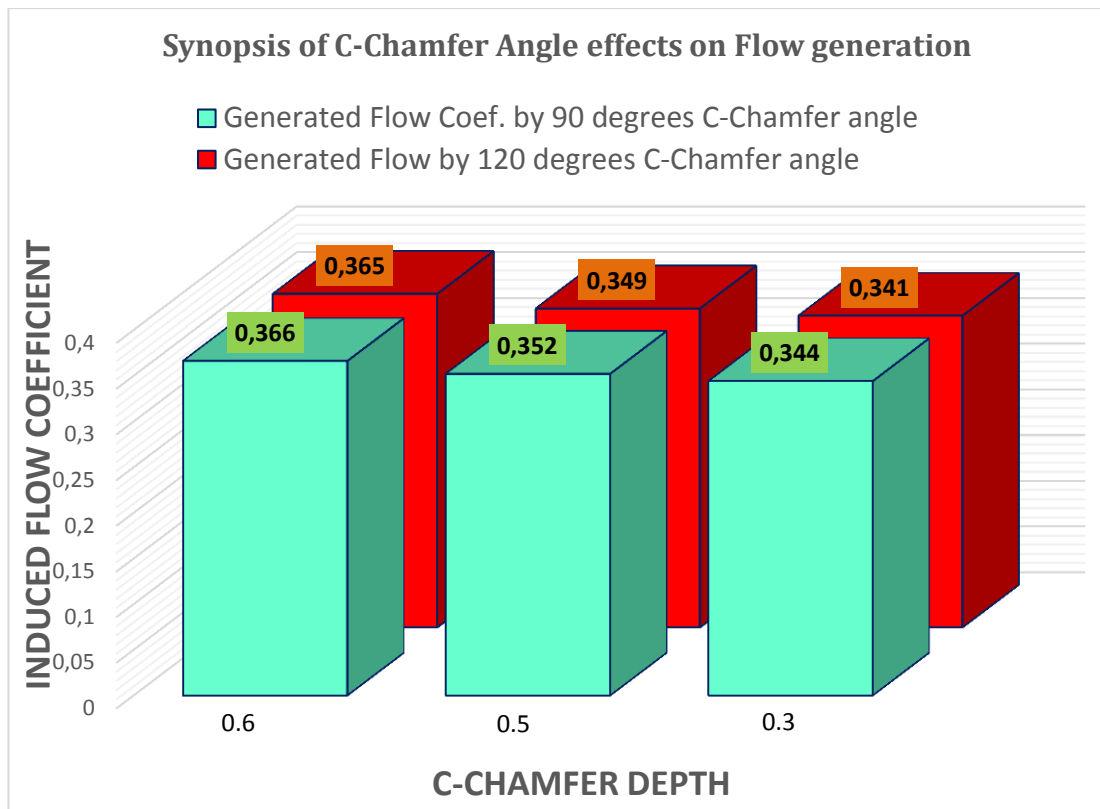


Figure 4. 16: Synopsis of c-chamfer angle effects on flow performance.

In contrast with the swirl ratio increase with the concentric chamfer angle increase, Figure 4. 16 shows that the flow coefficient decreases while the c-chamfer angle increase. Yet the impact of the angle variation on the flow coefficient is quite small compared to its impact on swirl ratio generation.

4.4 Effects of the Swirl Chamfer Offset

The effect of the concentric chamfer depth and its corresponding angle on the induced airflow and corresponding swirl generation have been addressed in the sections above. This following discussion therefore will focus on the swirl ratio and flow coefficient variation caused by the offset value of the swirl chamfer.

To achieve this assessment, the following cylinder head configuration is used:

- Seat Angle: 45°,
- Concentric Chamfer Depth: 0 mm as the effect of the concentric chamfer is dismissed.
- Concentric Chamfer Angle: 0° as well due to the fact of omitting any concentric chamfer machining.

The orientation of the swirl chamfer during its machining is mentioned on Figure 3. 4 in Chapter 3. This information is just recalled in order to have a better insight of the geometrical configuration on the cylinder head.

Similarly with the evaluation of the chamfer angle effect, casting variations cannot be disregarded for the same reason that each configuration cannot be reproduced twice on the same cylinder head. It is therefore preferred to machine different cylinder heads with specific swirl chamfer offset values. The cylinder head configurations used throughout this investigation are summarized in Figure 4. 8 and the experimental measurement datasets are given in Appendix B, with respect to the reference given to the cylinder heads.

Table 4. 8: Cylinder head configurations illustrating s-chamfer offset variations.

S-CHAMFER OFFSET [mm]	C-CHAMFER [mm]*[°]	Head No: (Reference #)
1,2	0*0	9
1,2	0*0	14
0,8	0*0	41
0,8	0*0	42

Results of the measurements taken from the cylinder heads referred as #09 and #41 are grouped in Table 4. 9 below. The following figures, respectively Figure 4. 17 and Figure 4. 18 indeed represent the induced swirl ratio and the corresponding flow coefficient generated along with the intake valve displacement varying from 0mm through 10mm.

Table 4. 9: Measurement results on two different s-chamfer offsets.

BOTH PORTS	Head # 09 (1,20mm Swirl OFFSET)								Head # 41 (0,80mm Swirl OFFSET)							
	Swirl Number	Flow Coeff.	Swirl Number	Flow Coeff.	Swirl Number	Flow Coeff.	Swirl Number	Flow Coeff.	Swirl Number	Flow Coeff.	Swirl Number	Flow Coeff.	Swirl Number	Flow Coeff.		
Valve Lift	Cyl.1		Cyl.2		Cyl.3		Cyl.4		Cyl.1		Cyl.2		Cyl.3		Cyl.4	
1	4,607	0,095	4,636	0,094	4,652	0,095	4,525	0,093	4,103	0,098	4,112	0,098	3,964	0,098	4,199	0,097
2	3,781	0,171	3,859	0,170	3,861	0,169	3,748	0,167	3,232	0,179	3,225	0,181	3,092	0,182	3,213	0,178
3	2,582	0,248	2,602	0,251	2,589	0,249	2,509	0,247	2,268	0,265	2,288	0,264	2,225	0,264	2,267	0,264
4	1,967	0,349	1,964	0,347	1,951	0,348	1,863	0,344	1,591	0,361	1,621	0,361	1,592	0,362	1,632	0,360
5	1,531	0,437	1,551	0,437	1,527	0,438	1,457	0,436	1,262	0,448	1,284	0,448	1,283	0,448	1,286	0,446
6	1,482	0,500	1,518	0,497	1,456	0,499	1,428	0,498	1,345	0,507	1,354	0,507	1,369	0,505	1,347	0,504
7	1,441	0,550	1,472	0,546	1,417	0,548	1,406	0,545	1,331	0,549	1,338	0,551	1,342	0,548	1,310	0,549
8	1,367	0,583	1,408	0,578	1,393	0,583	1,364	0,585	1,161	0,570	1,238	0,574	1,282	0,578	1,238	0,579
9	1,211	0,601	1,220	0,597	1,209	0,601	1,175	0,597	1,128	0,591	1,156	0,593	1,138	0,593	1,095	0,594
10	1,160	0,619	1,161	0,618	1,142	0,618	1,139	0,615	1,093	0,607	1,109	0,608	1,044	0,607	0,990	0,605
Swirl Ratio	1,841		1,873		1,821		1,789		1,654		1,665		1,659		1,642	
Overall Swirl Ratio	1,831								1,655							
Flow Coeff.	0,349		0,347		0,348		0,345		0,335		0,336		0,336		0,333	
Overall Flow Coeff.	0,347								0,335							

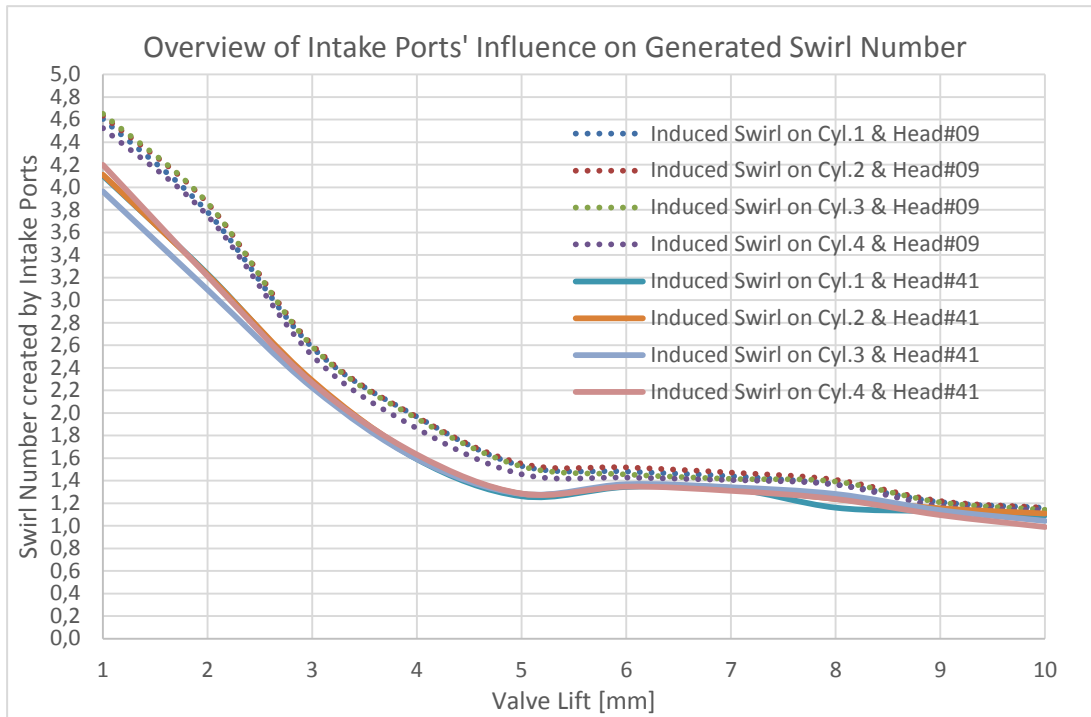


Figure 4. 17: Swirl generation of two different s-chamfer offsets.

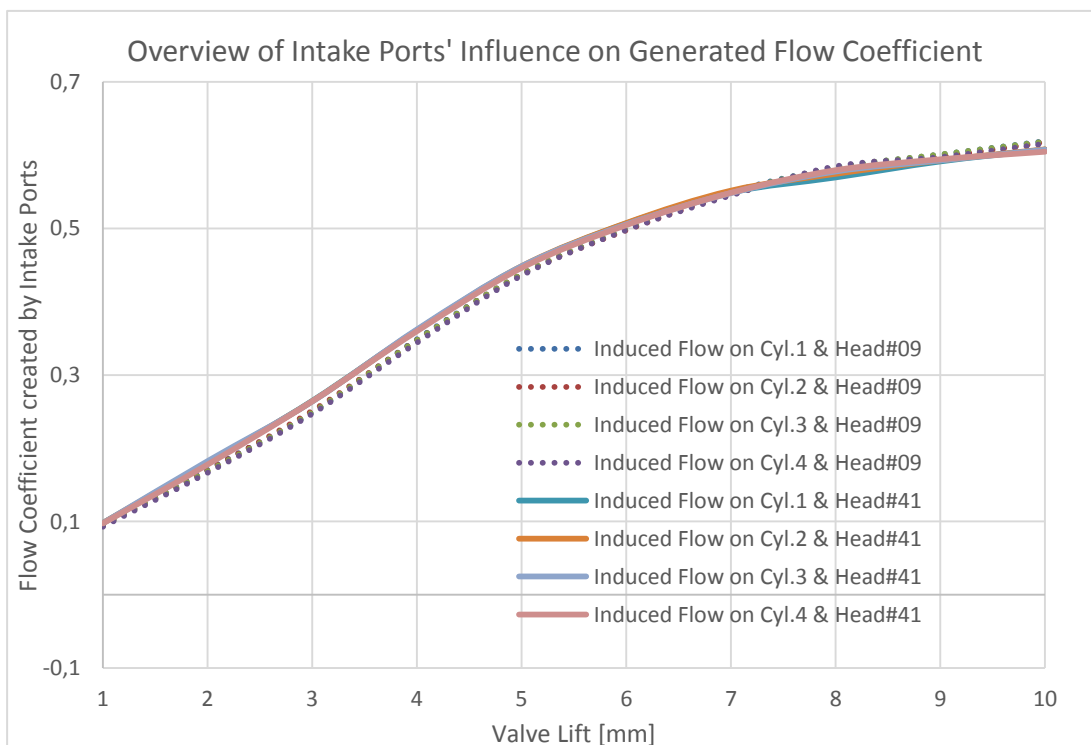


Figure 4. 18: Flow performance induced by two different s-chamfer offsets.

It is clearly seen from Figure 4. 17 that the swirl ratio generated by a single swirl chamfer rises as the offset value of the s-chamfer increases. Generally, all over the valve lifts, the turbulent motion produced by a 1.2 mm swirl chamfer offset is greater than that produced by a 0.8mm swirl chamfer. A similar measurement has been carried out on two different cylinder heads of respectively 0.8mm and 1.2mm swirl offset configuration, with no concentric chamfer, to confirm this effect. Those cylinder heads are coded Head#14 and Head#42 and the measurement results are given on Appendix B while a synopsis of the results on swirl generation and flow coefficients are given through Figure 4. 19 and Figure 4. 20.

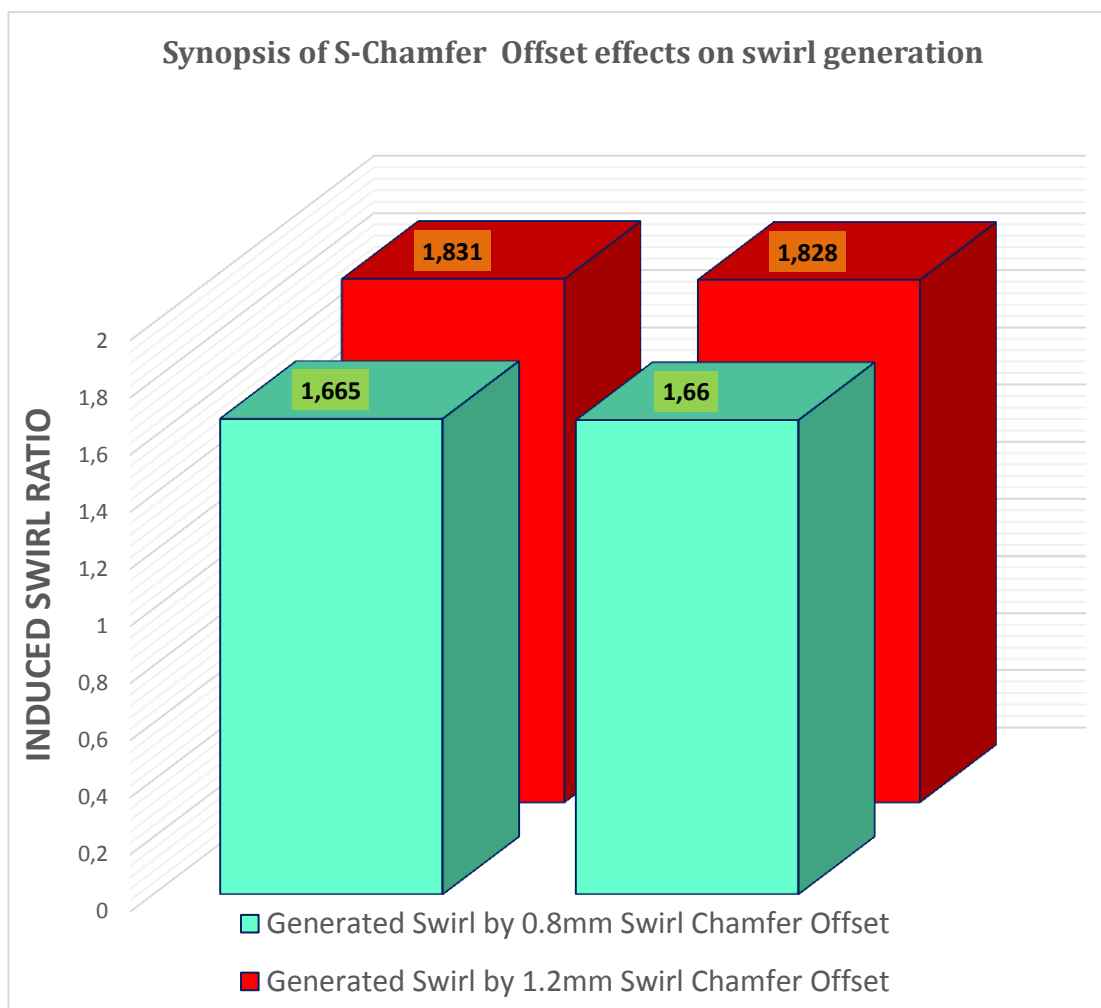


Figure 4. 19: Synopsis of s-chamfer offset effects on swirl generation.

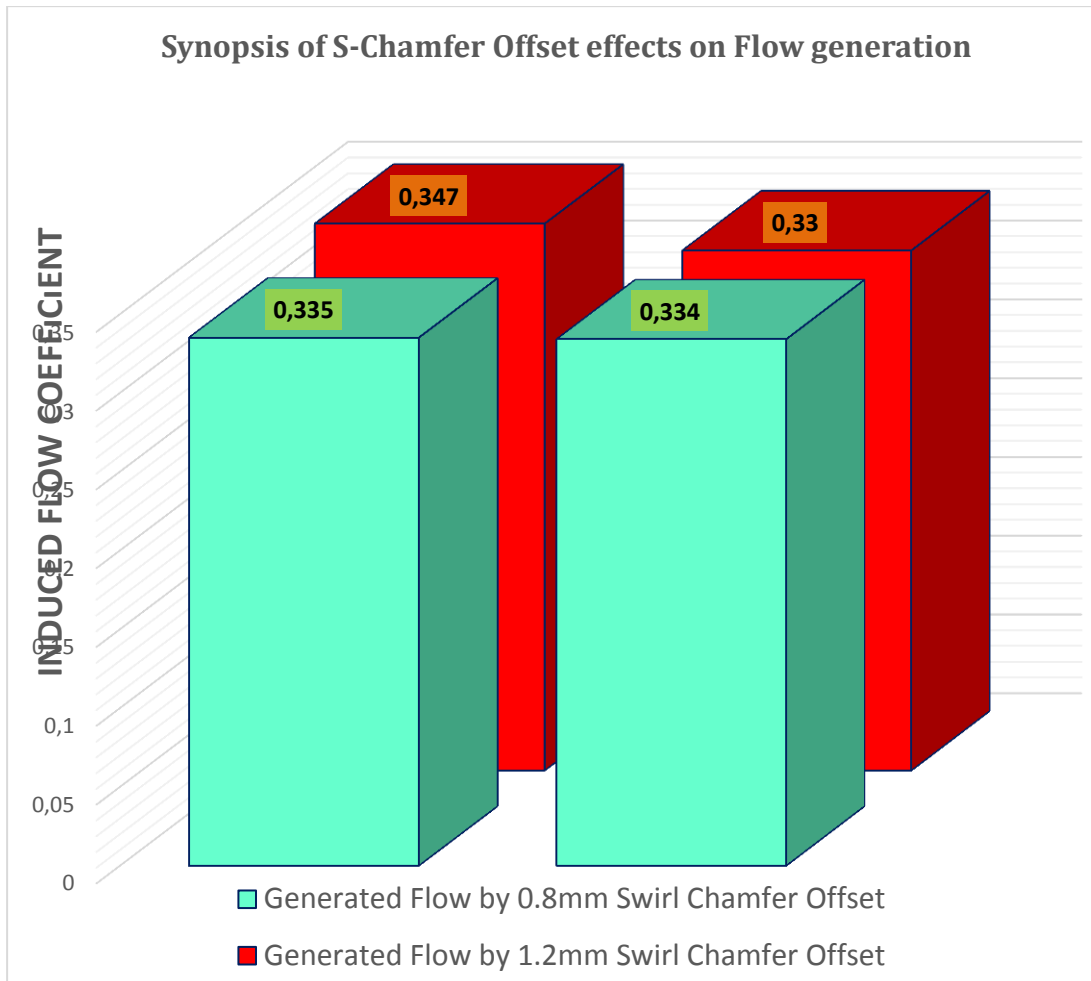


Figure 4. 20: Synopsis of s-chamfer offset effects on flow performance.

From Figure 4. 19 above, one can see that the swirl value is indeed increasing along with the value of the swirl chamfer offset. However, Figure 4. 20 shows that the flow coefficient decreases as the swirl chamfer offset increases. This flow coefficient behavior is coherent with each flow characteristic analysis conducted so far.

5. CONCLUDING DISCUSSIONS

The effects of each single intake port on the swirl number variation and the overall swirl ratio production have been investigated and reported on one hand as the tangential (or long or straight) port generating a swirl number value continuously decreasing with respect to the increasing valve lift. On the other hand, the helical (or short) intake port has a higher swirl number and relatively a higher overall swirl ratio production over the valve lift displacement compared to the tangential port performance. The investigation of the effects of the two type of intake ports being simultaneously actuated shows that the tangential intake port dominates the overall flow at low valve lifts while the helical ports becomes more influent at lift values close to the maximum valve lift displacement.

In addition, it has been seen through all the investigations that the increase in swirl number yield a decrease in the flow coefficient variation.

Furthermore, experimental measurements demonstrates that the concentric chamfer depth has a detractive effect on the swirl ratio generation while the concentric chamfer angle has an increasing effect on the swirl ratio production. Besides, the swirl chamfer offset also raises the swirl ratio production of the cylinder heads.

The respective influence of each parameter onto the swirl ratio production and the flow characteristics are deducted from the experiments conducted in the previous sections, but the interactions of each of those parameters will be addressed on the following section.

5.1 Combined Effects of the C-chamfer Depth, Angle and Swirl Chamfer Offset

To perform an accurate tuning of the swirl production on cylinder heads of internal combustion engines, one needs to also investigate the interactions of these parameters on the overall swirl and flow coefficient production so as to predict the swirl response.

Several measurements are conducted on the cylinder head, involving different combinations of the concentric chamfer depth and its angle, along with different values of the swirl chamfer offset. The purpose of measuring the swirl ratio and the corresponding flow coefficient on these combinations is to assess the effect of each parameter while combined with the others. Results of these experiments are grouped in Appendix B. Those results are then used in a statistical analysis software (Minitab) to evaluate the effects of their interactions on the overall swirl generation in the scope of in-depth statistical analysis. The output of the analysis is shown on Figure 5. 1 for the swirl generation and Figure 5. 2 for the flow coefficient.

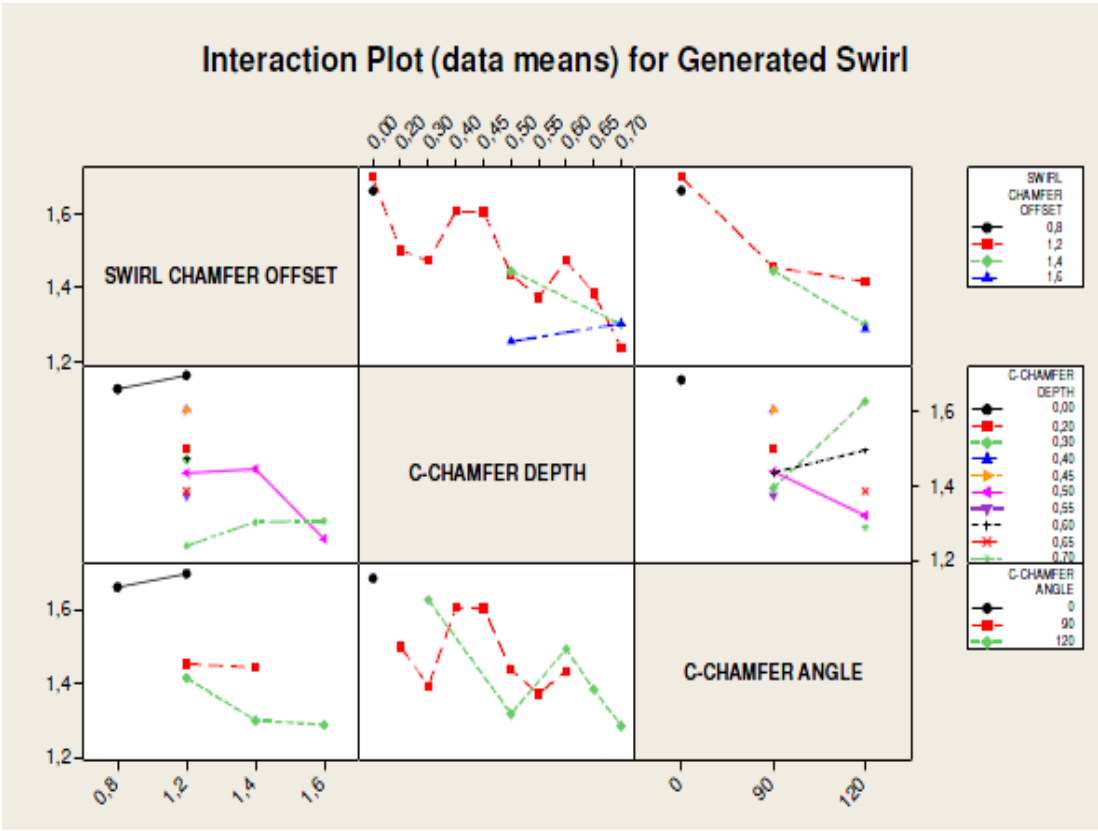


Figure 5. 1: Interaction graph between the chamfers - effects on swirl generation.

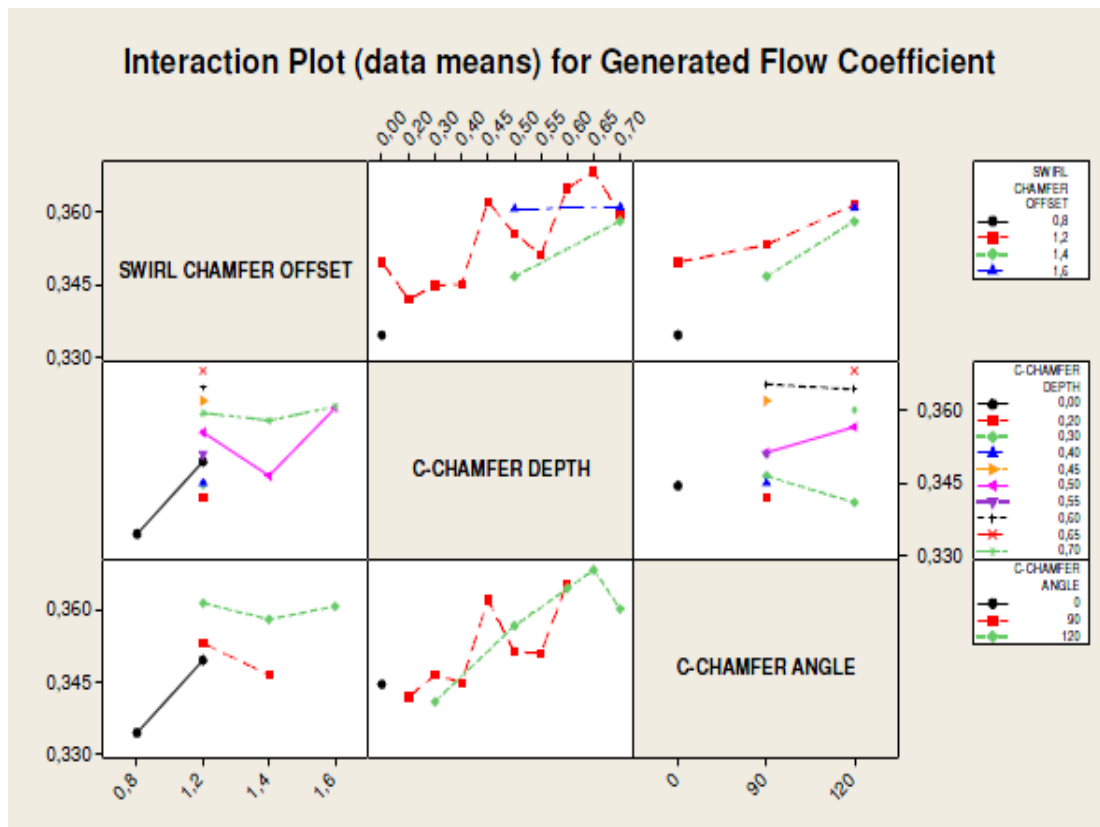


Figure 5. 2: Interaction graph between the chamfers - effects on flow performance.

At a first look, it is seen that fluctuations are present on the interaction graph. These fluctuations are induced by the casting variations. Indeed, the cavities forming the intake ports are produced by means of sand cores (solid volume), and with the molten metal travelling along the casting cavities between the mold and the cores, the intake cores are exposed to high temperature (yielding dilatation) and buoyancy. This process inevitably induces some deformations at the core surfaces, or even worse a core floatation during the passage of the molten metal. As a result, the effect of these manufacturing parameters are illustrated as fluctuations on the swirl production.

Nevertheless, the swirl chamfer offset increases the overall swirl ratio generation independently of the casting variations. Similarly, the c-chamfer angle also increases the overall swirl ratio production while the c-chamfer depth decreases the swirl production.

Compromise between swirl chamfer offset and the c-chamfer depth can be suggested to obtain a specific value of swirl number as required for the combustion performance.

5.2 Limitations of the Experimental Investigation

The measurement procedure used throughout this investigation is a steady-state measurement procedure. As described in previous sections, this procedure gives only a rough information about the flow through the intake ports without considering the effect of the piston bowl geometry. This measurement procedure is therefore very limited since it cannot give an insight on the flow mechanism within the combustion chamber after the intake valve closures. A more sophisticated experimental bench such as PIV or LDV measurement bench is required to achieve this, and the time constraint restricts such an investigation results to be presented in this thesis.

In addition, the swirl chamfer offset, its depth, the concentric chamfer depth and its angle could be more accurately investigated under unsteady conditions, involving also the firing processes.

Furthermore, with as simplified measurement as steady-state measurements, fluctuations are still affecting the results because of the casting variations.

One should also recall the errors induced by the numerical integration method. Although the remainder diminishes in a range of 10^4 (equation (2. 27)), it still affects the absolute result of the swirl generation and intake ports' performance.

One more parameter to consider is also the assumption of the swirl axis. Indeed, the in-flowing air is considered rotating with a coaxial axis with respect to the combustion chamber axis, which sometimes does not coincide. Therefore, the paddle speed might be limited in term of accuracy in some cases.

Last but not the least, the intake valve opening and closure time were assumed to occur between the piston travel between the dead centers (from TDC through BDC), therefore the valve overlap phenomenon occurring when both the intake and exhaust valves are opened is disregarded, yielding to a deviation from the physical state of the intake process

5.3 Recommendations for Future Studies

As observed throughout this survey, the measured flow and the consequent swirl ratio production are highly affected by the casting variations during the

manufacturing process. Studying at a closer scale of the effect of the casting processes onto the flow performance can be suggested as a further investigation.

Additionally, other machining parameters such as shroud diameters, curvature of the tangential (or straight) intake ports and the basic geometries of the intake ports are also influencing the overall characteristic of the flow. It might also be possible to deep dive the interactions between these afore-mentioned parameters with appropriate measurement rig and dedicated works.

REFERENCES

- [1] <http://www.merriam-webster.com/dictionary/movement> (n.d.), retrieved on 15.12.2013.
- [2] **Raux, C.** (2010). The potential for CO2 Emissions trading in transport: the case of personal vehicles and freight. *Energy Efficiency*: Vol. 3, no. 2, pp. 133-148.
- [3] **Sims, R. E. H., Rogner, H., Gregory, K.** (2003). Carbon emission and mitigation cost comparisons between fossil fuel, nuclear and renewable energy resources for electricity generation. *Energy Policy*, 31, 1315-1326.
- [4] http://ww1.prweb.com/prfiles/2012/08/07/9776089/technology_improvements_piechart.jpg (n.d.), retrieved on 03.01.2014.
- [5] http://en.wikipedia.org/wiki/European_emission_standards (n.d.), retrieved on 03.01.2014.
- [6] **Adolph, D., Rezaei, R., Pischinger, S., Adomeit, P. et al.** (2009). Gas Exchange Optimization and the Impact on Emission Reduction for HSDI Diesel Engines. *Society of Automotive Engineers, Technical Paper no: 2009-01-0653*, doi:10.4271/2009-01-0653.
- [7] <http://web.itu.edu.tr/~sorusbay/ICE/ICE.html> (n.d.), retrieved on 04.01.2014.
- [8] **Heuvel, B. V. D.,** (1998). *In-cylinder flow analysis for production-type internal combustion engines* (PhD Thesis). Retrieved from <http://alexandria.tue.nl/extra2/9803414.pdf>
- [9] **Wilson, B.M.,** (2009). *Demonstration of a Completely Described Swirling Jet Experiment Used for Numerical Validation*, (PhD Thesis), pp. 12-22, Utah State University.
- [10] **Heim, D. M., Ghandhi, J. B.,** (2011), Investigation of swirl meter performance, *Proceedings of the Institution of Mechanical Engineers, Part D: Journal of Automobile Engineering*, Vol. 225, pp. 1068.
- [11] **Khalid, A., Manshoor, B.** (2012), Effect of High Swirl Velocity on Mixture Formation and Combustion Process of Diesel Spray, *Applied Mechanics and Materials*, Vols. 229-231, pp. 695 – 699.
- [12] <https://www.airflowresearch.com/performance.php> (n.d.), retrieved on 04.02.2014.

- [13] **Frenzel, F., Grothey, H., Habersetzer, C., Hiatt, M., Hogrefe, W., et al.** (2011). *Industrial Flow Measurement Basics and Practice*, Chap. 2, (pp. 29-165), ABB Automation Products GmbH.
- [14] **Taylor, R. A.**, (1963), *Investigation on the Intake Induced Air Swirl of a Stratified Charge Engine*. (PhD Thesis), pp. 13 – 18, Pennsylvania State University.
- [15] **Acroumanis, C., Hu, Z. And Whitelaw, J. H.** (1994), Droplet Velocity Measurements in a Four-Cylinder Optical DI Diesel Engine, *International Symposium COMODIA 94*, p. 206.
- [16] **Moreau, J.**, (2003), *Interaction Entre un Jet de Tourbillon Compressé – Etude Experimentale de l’Aerodynamique et du Mélange*, (PhD Thesis), pp. 59–66, retrieved from <http://hal.archives-ouvertes.fr/docs/00/04/72/10/PDF/tel-00007174.pdf>.
- [17] **Laurant, Y., Michard, M., Slama, G. And Rey, P.**, (2007), Caractérisation spatio-temporelle des tourbillons générés proches de la soupape d’un moteur à combustion interne, *18ème Congrès Français de Mécanique*, Grenoble, FR, August 27-31.
- [18] **Oishi, Y. and Watanabe Y.**, (1994), Prediction of Intake Swirl Applying CFD Technique, *International Symposium COMODIA 94*, p. 325.
- [19] **Ramajo, D. E. and Nigro, N.M.**, (2008), Numerical and Experimental In-Cylinder Flow Study in a 4-Valve Spark Ignition Engine, *Mecanica Computacional*, Vol. XXVII, pp. 181-205., San Luis, AR, November 10-13.
- [20] **Jovanovic, Z., Masonicic, Z.**, (2012), The Effect of Turbulence Model Variation on Flame Propagation in a Particular 4-Valve Engine Combustion Chamber, *Proceedings of the Sixth Global Conference on Power Control and Optimization*, p. 405, RS.
- [21] **Gill, A., Gutheil, E. And Warnatz, J.**, (1994), Numerical Investigation of the Turbulent Combustion in a Direct-Injection Stratified Charge Engine with Emphasis on Pollutant Formation, *International Symposium COMODIA 94*, pp. 583-588.
- [22] **Rabety, T.** (2013). Personal Communication with Ford Otosan CAE Department
- [23] **Heywood, J. B.**, (1988), *Internal Combustion Engine Fundamentals*, Chap. 8, pp. 326-365, ISBN: 0-07-028637-X, McGraw Hills, USA.
- [24] **Kheyrollahi, J., Keshavarz, M., Jazayeri, S. A., Pourfallah, M.**, (2010), Optimization on Intake Port Shape in a DI Diesel Engine Using CFD Flow Simulation, *International Council on Combustion Engines (CIMAC)Congress*,NO.

- [25] **Thien, G.**, (1965), *Port Development – Flow Test Bench*, Memo 618, pp. 8 – 19, AVL.
- [26] **SF-300/600FC Flowbench Operator’s Manual** (n.d.)
- [27] **Wotton, C. R. N.**, (1993), *Ricardo Steady State Flowbench Port Performance Measurement and Analysis Techniques*, DP93/0704 Restricted Document, pp. 2 - 6.
- [28] **Pouille, J.**, (n.d.), *Moteurs Diesel d’Automobiles – Conception et mise au point*, Direction de la Mécanique-Renault, pp. 1 - 24.
- [29] **Haupais, A.**, (n.d.), *Combustion dans les moteurs Diesel*, Centre de Recherches en Machines Thermiques (CRMT), pp. 1 – 33.
- [30] **Ricardo Consulting Engineers, Ltd.**, (2011), Personal Communication.
- [31] **Sarshari, E.** (2011), Effects of Inlet Port Design Factors on Combustion Characteristics and Emission Levels of Diesel Engines, *International Journal of Automotive Engineering*, Vol. 1, no: 2, pp: 31-35.
- [32] <http://mathfaculty.fullerton.edu/mathews/n2003/simpsonsrulemod.html> (n.d.), retrieved on 04.02.2014
- [33] **Sabale, S. K., Sanap, S. B.**, (2013), Design and Analysis of Intake Port of Diesel Engine for Target Value of Swirl, *American Journal of Mechanical Engineering*, Vol. 1, no: 5, pp: 138-142, doi:10.12691/ajme-1-5-6.
- [34] **Taylor, C. F.**, (1985), *Internal Combustion Engine in Theory and Practice, 2nd Edition*, pp: 476-481.
- [35] **Challen, B., Baranescu, R.**, (1999), *Diesel Engine Reference Book, 2nd Edition*, pp: 201 – 211.
- [36] **Bettes, H.**, (2010), *Engine Airflow*, Penguin Group, USA, pp: 17 - 50.

APPENDICES

APPENDIX A: Swirl and Flow Coefficients Calculation Formula Code

APPENDIX B: Results of Case studies

APPENDIX C : Intake Valve lift Vs. Crankshaft Angle Variation

APPENDIX D : Emission restrictions and data collection sheets

APPENDIX A

% symbols express the comments and further explanations (such as SI units when necessary) given through the calculation sheet. Code was written in MATLAB as mentioned on the core of the thesis.

```
clear; clc;
format short;
Do=0.0381% Orifice Diameter [m]
Dp=0.1016% Pipe Diameter [m]
g=9.80665 % attraction of gravity [N/m^2]
S=0.0946% Engine stroke [m]
B=0.086% Cylinder bore [m]
CR=0.155% Con rod length [m]
ISD=0.0278% effective diameter of a single intake valve.
VN=2% Considering two intake valves
isd=ISD*sqrt(VN)% Effective Inner Seat Diameter for intake (assuming 2 valves per
combustion chamber) [m]
Vh=S.*pi.*(B.^2)./4% Volume displacement of each cylinder [m^3]
Tatm=294.3% Temperature of atmosphere [K]
Patm=100200% Pressure of atmosphere [Pa]
Rair=287.1 % Specific gas constant for air [J/(kg.K)]
rhoa=Patm./(Rair.*Tatm)% atmospheric density of dry air [kg/m^3]
Cd=0.6013% Discharge coefficient of the measurement pipe [non-dimensional]
Ao=pi.*(Do.^2)./4 % Orifice Area
rm=(Do./Dp).^2 % Diameter ratio
c1=Cd.*Ao./(1-(rm.^2)) % Orifice flow coefficient of the measuring device
rl=S./(2*CR)% Crank Ratio (Eccentricity of con-rod(radius)/con-rod length)
gamma=1.41% ratio of specific heats
i=1:1:10; % number of valve lift increments through the measurement
P2prim=[500.2 500.2 254.7 256.0 255.8 255.4 255.8 256.7 255.1 254.9]; % Pressure
drop across ports [mm H2O]*MANUAL INPUT***
P2=P2prim.*g% Pressure drop across ports [Pa]
rhom=rhoa.*(Patm-P2)./(Patm)% air density through inlet ports [kg/m^3]
rho=rhoa.*(((Patm-P2)./Patm).^1/gamma)% air density through inlet ports assuming
compressible fluid [kg/m^3]
rhomean=(rhoa+rho)/2% mean density of dry air throughout measurement [kg/m^3]
V0=sqrt(2.*P2./rhomean)% Velocity head [m/s]
tmf=(pi*(isd^2)/4).*rho.*V0% mass flow at inlet ports [kg/s]
P3prim=[13.5 50.3 56.1 107.3 162.9 202.3 239.1 258.8 276.8 291.1]% Pressure drop
across orifice [mm H2O]*MANUAL INPUT***
P3=P3prim.*g% Pressure drop across orifice [Pa]
mf=c1.*sqrt(2.*rhom.*P3) % mass flow at orifice [kg/s]
nf=mf./(2*rho*Vh)% Fictitious engine speed [m/s]
Vs=[36.9 55.4 38.0 37.2 39.2 50.3 55.1 49.0 49.5 50.4]% vane speed (okunan deđer)
[rev/s]*MANUAL INPUT***
sr=Vs./nf % Swirl number per valve lift
fcc=mf./tmf % Flow coefficient per valve lift
alpha=0:15:180% Cranck Angle Value through the intake stroke
```

```

vlr=[0 0.03677 0.07495 0.11809 0.15132 0.17536 0.18950 0.19445 0.18950 0.17536
0.15132 0.11809 0] % Valve lift ratio over the seat diameter (obtained from the cam
profile of the engine) [DIMENSIONLESS]
lift=vlr.*isd.*1000 %Real valve lift displacement [mm]
lift_rounded=round(lift)%Rounded valve lift displacement [mm] to be used for the
interpolation
a=alpha.*pi./180%Cranck angle through the valve lift in radian [rad]
h=lift%Real Valve lift displacement values on a gap of 15 degrees Crank Angle
cc=0.5*pi*(1+(rl.*cos(a)./(sqrt(1-((rl.*sin(a)).^2))))).*sin(a);%Ratio of the actual
piston velocity over the mean piston velocity
cc;
%
%*****INTERPOLATION OF THE VALUES ON MEASUREMENT
POINTS*****
%
%SRR matrix 1x13 matrix in dimensions
%sr matrix 1X10 matrix in dimensions
SRR=1:1:length(alpha);
SRR(1)=0;
SRR(13)=0;
for j=2:1:12;
    SRR(j)=(((sr(lift_rounded(j)))-(sr(lift_rounded(j)+1))))./((lift_rounded(j))-
((lift_rounded(j)+1))).*(h(j)-(lift_rounded(j)))+(sr(lift_rounded(j)));
end
SRR%Swirl coefficient to be used for interpolation
FCCR=1:1:length(alpha);
FCCR(1)=0;
FCCR(13)=0;
for k=2:1:12;
    FCCR(k)=(((fcc(lift_rounded(k)))-(fcc((lift_rounded(k)+1))))./((lift_rounded(k))-
((lift_rounded(k)+1))).*(h(k)-(lift_rounded(k)))+(fcc(lift_rounded(k)));
end
FCCR%Flow coefficient to be used for interpolation
ys=SRR.*(cc.^2);
ys%DIMENSIONLESS SWIRL COEFFICIENT PER CRANK ANGLE
INTERVAL
yf=1:1:length(alpha);
yf(1)=0;
yf(13)=0;
for q=2:1:12;
    yf(q)=(cc(q).^3)./(FCCR(q).^2);
end
yf%DIMENSIONLESS FLOW COEFFICIENT PER CRANK ANGLE INTERVAL
%
% INTEGRAL METHOD FOR OVERALL SWIRL
CALCULATION*****
%
for n=1:1:length(alpha);
    for n1=2:2:length(alpha);

```

```

    x(n1)=ys(n1);
end
S1=sum(x);%pair
for n2=1:2:length(alpha);
    xx(n2)=ys(n2);
end
S2=sum(xx);%impair
end
S1;
S2;
SRM=(1/36).*(ys(1)+(ys(length(alpha)))+(2.*S1)+(4.*S2))% alpha in RADIAN
SRMR=SRM.*B./S;
SRMR%***OVERALL REDUCED SWIRL RATIO COEFFICIENT***
%
%INTEGRAL METHOD FOR OVERALL FLOW COEFFICIENT
CALCULATION*****
%
for z=1:1:length(alpha);
    for z1=2:2:length(alpha);
        x1(z1)=yf(z1);
    end
    SS1=sum(x1);%pair
    for z2=1:2:length(alpha);
        xx1(z2)=yf(z2);
    end
    SS2=sum(xx1);%impair
end
SS1;
SS2;
FCM=1/(sqrt((yf(1)+yf(length(alpha)))+(4*SS1)+(2*SS2))/36));%***OVERALL
FLOW COEFFICIENT***
FCM

```

Do = 0.0381
 Dp = 0.1016
 g = 9.8066
 S = 0.0946
 B = 0.0860
 CR = 0.1550
 ISD = 0.0278
 VN = 2
 isd = 0.0393
 Vh = 5.4951e-04
 Tatm = 294.3000
 Patm = 100200
 Rair = 287.1000
 rhoa = 1.1859
 Cd = 0.6013
 Ao = 0.0011
 rm = 0.1406
 c1 = 6.9937e-04
 rl = 0.3052
 gamma = 1.4100

P2 = 1.0e+03 *
 Columns 1 through 7
 4.9053 4.9053 2.4978 2.5105 2.5085 2.5046 2.5085
 Columns 8 through 10
 2.5174 2.5017 2.4997

rhom =
 Columns 1 through 7
 1.1278 1.1278 1.1563 1.1562 1.1562 1.1562 1.1562
 Columns 8 through 10
 1.1561 1.1563 1.1563

rho =
 Columns 1 through 7
 1.1444 1.1444 1.1648 1.1647 1.1648 1.1648 1.1648
 Columns 8 through 10
 1.1647 1.1648 1.1648

rhomean =
 Columns 1 through 7
 1.1652 1.1652 1.1754 1.1753 1.1753 1.1753 1.1753
 Columns 8 through 10
 1.1753 1.1754 1.1754

V0 =
Columns 1 through 7
91.7605 91.7605 65.1933 65.3609 65.3352 65.2836 65.3352
Columns 8 through 10
65.4510 65.2449 65.2191

tmf =
Columns 1 through 7
0.1275 0.1275 0.0922 0.0924 0.0924 0.0923 0.0924
Columns 8 through 10
0.0925 0.0923 0.0922

P3prim =
Columns 1 through 7
13.5000 50.3000 56.1000 107.3000 162.9000 202.3000 239.1000
Columns 8 through 10
258.8000 276.8000 291.1000

P3 =
1.0e+03 *
Columns 1 through 7
0.1324 0.4933 0.5502 1.0523 1.5975 1.9839 2.3448
Columns 8 through 10
2.5380 2.7145 2.8547

mf =
Columns 1 through 7
0.0121 0.0233 0.0249 0.0345 0.0425 0.0474 0.0515
Columns 8 through 10
0.0536 0.0554 0.0568

nf =
Columns 1 through 7
9.6090 18.5479 19.4861 26.9498 33.2059 37.0040 40.2295
Columns 8 through 10
41.8548 43.2844 44.3882

Vs =
Columns 1 through 7
36.9000 55.4000 38.0000 37.2000 39.2000 50.3000 55.1000
Columns 8 through 10
49.0000 49.5000 50.4000

sr =
Columns 1 through 7
3.8401 2.9869 1.9501 1.3803 1.1805 1.3593 1.3696
Columns 8 through 10
1.1707 1.1436 1.1354

fcc =
Columns 1 through 7
0.0948 0.1830 0.2706 0.3733 0.4601 0.5131 0.5574
Columns 8 through 10
0.5789 0.6006 0.6162

alpha =
0 15 30 45 60 75 90 105 120 135 150 165 180

vlr =
Columns 1 through 7
0 0.0368 0.0750 0.1181 0.1513 0.1754 0.1895
Columns 8 through 13
0.1945 0.1895 0.1754 0.1513 0.1181 0

lift =
Columns 1 through 7
0 1.4456 2.9467 4.6427 5.9492 6.8943 7.4502
Columns 8 through 13
7.6448 7.4502 6.8943 5.9492 4.6427 0

lift_rounded =
0 1 3 5 6 7 7 8 7 7 6 5 0

a =
Columns 1 through 7
0 0.2618 0.5236 0.7854 1.0472 1.3090 1.5708
Columns 8 through 13
1.8326 2.0944 2.3562 2.6180 2.8798 3.1416

h =
Columns 1 through 7
0 1.4456 2.9467 4.6427 5.9492 6.8943 7.4502
Columns 8 through 13
7.6448 7.4502 6.8943 5.9492 4.6427 0

cc =
 Columns 1 through 7
 0 0.5268 0.9954 1.3562 1.5756 1.6427 1.5708
 Columns 8 through 13
 1.3919 1.1451 0.8653 0.5754 0.2863 0.0000

SRR =
 Columns 1 through 7
 0 3.4599 1.9805 1.1166 1.3588 1.3907 1.2801
 Columns 8 through 13
 1.1803 1.2801 1.3907 1.3588 1.1166 0

FCCR =
 Columns 1 through 7
 0 0.1341 0.2651 0.4412 0.5109 0.5552 0.5671
 Columns 8 through 13
 0.5712 0.5671 0.5552 0.5109 0.4412 0

ys =
 Columns 1 through 7
 0 0.9601 1.9624 2.0537 3.3731 3.7526 3.1585
 Columns 8 through 13
 2.2867 1.6786 1.0412 0.4498 0.0916 0

yf =
 Columns 1 through 7
 0 8.1278 14.0325 12.8157 14.9845 14.3819 12.0509
 Columns 8 through 13
 8.2634 4.6691 2.1019 0.7298 0.1206 0

SRM = 1.7461

SRMR = 1.5874

FCM = 0.3610

Published with MATLAB® R2012b

APPENDIX B

Results of case studies.

Table B. 1: Overall swirl ratio and integrated mean flow coefficient response.

HEAD NUMBER	C-CHAMFER DEPTH [mm]	C-CHAMFER ANGLE [°]	S-CHAMFER OFFSET [mm]	Generated Swirl [-]	Generated Flow Coeff. [-]
1 (meas. Set 1)	0,6	120	1,2	1,485	0,363
1 (meas. Set 2)	0,6	120	1,2	1,479	0,365
1 (meas. Set 3)	0,6	120	1,2	1,522	0,365
2	0,4	90	1,2	1,607	0,345
3	0,65	120	1,2	1,385	0,37
4	0	0	1,2	1,412	0,368
5	0,65	120	1,2	1,335	0,372
6	0,65	120	1,2	1,4	0,366
7	0,65	120	1,2	1,42	0,365
8	0	0	1,2	1,723	0,353
9	0	0	1,2	1,831	0,347
10	0,6	90	1,2	1,437	0,365
11	0,45	90	1,2	1,605	0,362
12	0,5	90	1,2	1,552	0,363
13	0,5	90	1,2	1,436	0,358
14	0	0	1,2	1,828	0,33
14_bis	0,3	90	1,2	1,44	0,344
15	0,3	90	1,2	1,347	0,349
16	0,2	90	1,2	1,527	0,341
17	0,2	90	1,2	1,475	0,343
20	0,5	90	1,4	1,444	0,347
21	0,5	120	1,6	1,261	0,359
23	0,5	120	1,6	1,247	0,362
24	0,7	120	1,4	1,301	0,358
25	0,7	120	1,6	1,321	0,361
27	0,7	120	1,6	1,31	0,359
28	0,7	120	1,6	1,306	0,361
30	0,55	90	1,2	1,287	0,353
31	0,5	90	1,2	1,301	0,352
32	0,7	120	1,2	1,256	0,361
33	0,5	90	1,4	1,475	0,346
34	0,5	90	1,4	1,45	0,347
35	0,5	90	1,4	1,41	0,346

Table B. 1 (continued): Overall swirl ratio and integrated mean flow coefficient response.

HEAD NUMBER	C-CHAMFER DEPTH [mm]	C-CHAMFER ANGLE [°]	S-CHAMFER OFFSET [mm]	Generated Swirl [-]	Generated Flow Coeff. [-]
36	0,55	90	1,2	1,459	0,349
38	0,7	120	1,2	1,218	0,358
39	0,7	120	1,6	1,286	0,361
40	0,7	120	1,6	1,294	0,362
41	0	0	0,8	1,665	0,335
42	0	0	0,8	1,66	0,334
43	0,3	120	1,2	1,628	0,341
44	0,5	120	1,2	1,449	0,349

APPENDIX C

Intake Valve lift Vs. Crankshaft Angle Variation.

Assuming the suction stroke occurs between the engine Top Dead Center through Bottom Dead Center yield to consider only the intake valve opening between 0° and 180° hence disregarding the valve overlaps. Therefore, for this calculation, the Intake Valve Opening (IVO) is 0° and Intake Valve Closure (IVC) is 180°

Table C. 1: Intake valve lift displacement.

Engine Crankshaft Angle [°]	Intake Valve Lift Ratio (h_v/d_v) [-]	Dynamic Intake Valve Lift [mm]
0	0	0
15	0,03677	1,4458
30	0,07495	2,9470
45	0,11809	4,6433
60	0,15132	5,9499
75	0,17536	6,8952
90	0,18950	7,4511
105	0,19445	7,6458
120	0,18950	7,4511
135	0,17536	6,8952
150	0,15132	5,9499
165	0,11809	4,6433
180	0	0

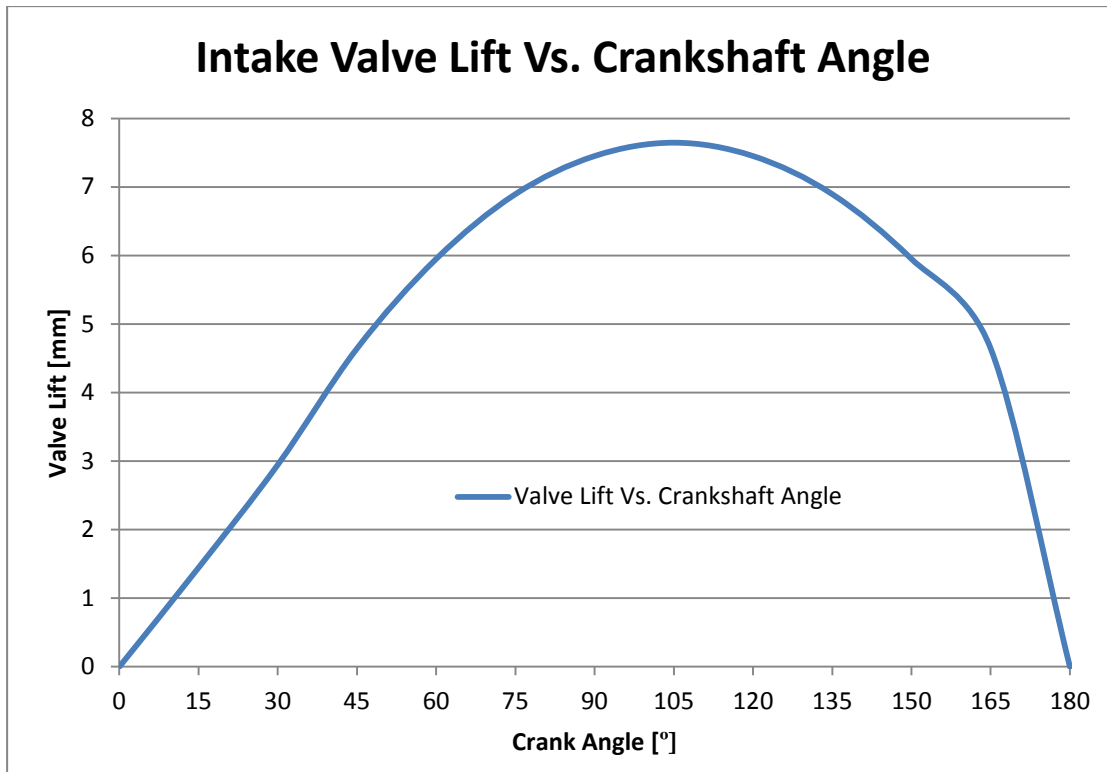


Figure C. 1: Intake valve opening cycle.

APPENDIX D

Tier	Date	CO	THC	NMHC	NO _x	HC+NO _x	PM	P
Diesel								
Euro 1	October 1994	2.72	-	-	-	0.97	0.14	-
Euro 2	January 1998	1.0	-	-	-	0.7	0.08	-
Euro 3	January 2000	0.64	-	-	0.50	0.56	0.05	-
Euro 4	January 2005	0.50	-	-	0.25	0.30	0.025	-
Euro 5	September 2009	0.500	-	-	0.180	0.230	0.005	-
Euro 6	September 2014	0.500	-	-	0.080	0.170	0.005	-
Petrol (Gasoline)								
Euro 1	October 1994	2.72	-	-	-	0.97	-	-
Euro 2	January 1998	2.2	-	-	-	0.5	-	-
Euro 3	January 2000	2.3	0.20	-	0.15	-	-	-
Euro 4	January 2005	1.0	0.10	-	0.08	-	-	-
Euro 5	September 2009	1.000	0.100	0.068	0.060	-	0.005*	-
Euro 6	September 2014	1.000	0.100	0.068	0.060	-	0.005*	-
* Applies only to vehicles with direct injection engines								

Figure D. 1: European emission standards for light commercial vehicles ≤ 1305 kg (category N₁-I), [g/km].

Tier	Date	CO	THC	NMHC	NO _x	HC+NO _x	PM	P
Diesel								
Euro 1	October 1994	5.17	-	-	-	1.4	0.19	-
Euro 2	January 1998	1.25	-	-	-	1.0	0.12	-
Euro 3	January 2001	0.80	-	-	0.65	0.72	0.07	-
Euro 4	January 2006	0.63	-	-	0.33	0.39	0.04	-
Euro 5	September 2010	0.630	-	-	0.235	0.295	0.005	-
Euro 6	September 2015	0.630	-	-	0.105	0.195	0.005	-
Petrol (Gasoline)								
Euro 1	October 1994	5.17	-	-	-	1.4	-	-
Euro 2	January 1998	4.0	-	-	-	0.6	-	-
Euro 3	January 2001	4.17	0.25	-	0.18	-	-	-
Euro 4	January 2006	1.81	0.13	-	0.10	-	-	-
Euro 5	September 2010	1.810	0.130	0.090	0.075	-	0.005*	-
Euro 6	September 2015	1.810	0.130	0.090	0.075	-	0.005*	-
* Applies only to vehicles with direct injection engines								

Figure D. 2: European emission standards for light commercial vehicles 1305 kg-1760 kg (category N₁-II), [g/km].

Tier	Date	CO	THC	NMHC	NO _x	HC+NO _x	PM	P
Diesel								
Euro 1	October 1994	6.9	-	-	-	1.7	0.25	-
Euro 2	January 1998	1.5	-	-	-	1.2	0.17	-
Euro 3	January 2001	0.95	-	-	0.78	0.86	0.10	-
Euro 4	January 2006	0.74	-	-	0.39	0.46	0.06	-
Euro 5	September 2010	0.740	-	-	0.280	0.350	0.005	-
Euro 6	September 2015	0.740	-	-	0.125	0.215	0.005	-
Petrol (Gasoline)								
Euro 1	October 1994	6.9	-	-	-	1.7	-	-
Euro 2	January 1998	5.0	-	-	-	0.7	-	-
Euro 3	January 2001	5.22	0.29	-	0.21	-	-	-
Euro 4	January 2006	2.27	0.16	-	0.11	-	-	-
Euro 5	September 2010	2.270	0.160	0.108	0.082	-	0.005*	-
Euro 6	September 2015	2.270	0.160	0.108	0.082	-	0.005*	-
* Applies only to vehicles with direct injection engines								

Figure D. 3: European emission standards for light commercial vehicles > 1760 kg max 3500 kg (category N₁-III & N₂), [g/km].

Operator Entered			
Labview Entered			
Engine Program	<input type="text"/>	Engine Capacity	<input type="text" value="2,2"/>
Cylinder Head Identity No.	<input type="text"/>	Test Request No.	<input type="text"/>
Test File Name	<input type="text"/>	Test Procedure	<input type="text" value="DEFAULT"/>
Test Operator	<input type="text"/>	Date	<input type="text" value="02.12.2013"/>
Bore Diameter	<input type="text" value="86"/>	Requestor Name	<input type="text" value="TRABETY"/>
Stroke	<input type="text" value="94,6"/>	Inlet / Exhaust	<input type="text" value="Inlet"/>
Con-Rod Length	<input type="text" value="155"/>		
Valve Inner Seat Diameter	<input type="text" value="27,8"/>		
Comments	<input type="text"/>		

To Be filled for each flowed cylinder									
Number of Ports Tested		1			1			2	
tank temp C									
baro press	in. Hg								
	bar.								
valve lift	port								
	press drop								
mm	mm H2O								
1,0	500								
2,0	500								
3,0	255								
4,0	255								
5,0	255								
6,0	255								
7,0	255								
8,0	255								
9,0	255								
10,0	255								
VACUUM CHECK									
<input type="text"/>									

Figure D. 4: Data collection excell sheet.

valve lift mm	press drop across port mm H2O	press drop across orifice mm H2O	vane speed rev/sec	density before orifice kg/m3	mass flow kg/sec	port effective area cm2	swirl ratio	flow coefficient
mean swirl ratio								
reduced mean swirl ratio								
mean port flow coefficient								

Figure D. 5: Data output sheet.

CURRICULUM VITAE



Name Surname: Mihantarivelo Tahiry RABETY

Place and Date of Birth: Antsiranana/MADAGASCAR – 25.04.1988

Address: Lot FIE 154TER Ambohimahitsy - ANTANANARIVO
103 - MADAGASCAR

E-Mail: rabetyt@gmail.com

B.Sc.: Istanbul Technical University – Mechanical
Engineering.

Professional Experience and Rewards: Ford Otomotiv Sanayi A.S. (2011 -)